ERDC/CHL TR-07-6

US Army Corps
of Engineers®
Engineer Research and
Development Center

Wave and Beach Processes Modeling for Sabine Pass to Galveston Bay, Texas, Shoreline Erosion Feasibility Study

David B. King Jr.

August 2007

Coastal and Hydraulics Laboratory

ERDC/CHL TR-07-6
August 2007

Wave and Beach Processes Modeling for Sabine Pass to Galveston Bay, Texas, Shoreline Erosion Feasibility Study

David B. King Jr.

Coastal and Hydraulics Laboratory
U.S. Army Engineer Research and Development Center
3909 Halls Ferry Road
Vicksburg, MS 39180-6199

Final report

Prepared for U.S. Army Engineer District, Galveston
2000 Fort Point Road, Galveston, TX 77553

Abstract: This report describes the STWAVE/GENESIS modeling, the SBEACH modeling, and the related technical analysis that the U.S. Army Engineer Research and Development Center's Coastal and Hydraulics Laboratory has provided the U.S. Army Engineer District, Galveston, in support of their feasibility project: "Sabine Pass to Galveston Bay, Texas – Shoreline Erosion Feasibility Study." The main goal of this effort has been to set up and calibrate the numerical models so that they can provide a predictive capability that will be used to objectively evaluate alternative measures for beach restoration/protection projects within the study area. The predictive capabilities address both long-term performance, evaluated using GENESIS, and short-term storm-induced performance, evaluated using SBEACH.

The setup of the GENESIS model proved to be particularly challenging. As had been found by previous researchers, the use of standard procedures led to the model's prediction of an unrealistic net sediment transport direction on Galveston Island. However, a careful analysis of the important forcing functions, particularly the effects of the local wind field, led to the development of an appropriate alternative procedure which produced GENESIS results in agreement with observations.

Contents

Figures and Tables

Figures

Tables

Preface

This report describes engineering studies that were conducted by the U.S. Army Engineer Research and Development Center (ERDC), Coastal and Hydraulics Laboratory (CHL), Vicksburg, MS, for the U.S. Army Engineer District, Galveston (SWG), in support of their study of solutions to shoreline erosion problems along the upper Texas coast between Sabine Pass and San Luis Pass.

The research was conducted principally by Dr. David B. King Jr., Coastal Processes Branch (CPB), with assistance by Mark Gravens, CPB. Significant technical assistance and/or technical review was provided by Mary Claire Allison, Coastal Engineering Branch (CEB), William R. Curtis, CEB, Dr. Andrew Morang, CEB, Dr. Jeffery Waters, CEB, and Michael Tubman, CEB. Additional technical assistance and guidance was provided by Robert Thomas and Lynn Vera of SWG.

This report was principally prepared by Dr. David B. King Jr. Portions of Chapter 2 were written by Dr. Jeffery Waters. Barbara Tracey, CPB, prepared Appendix C.

The study was conducted under the general supervision of William Curtis, CHL, Principal Investigator of Sabine Pass to Galveston Bay, Texas Shoreline Erosion Feasibility Study, Bruce Ebersole, Chief, CPB, Dr. Yen-hsi Chu, Chief, CEB, and Thomas Richardson, Director, CHL.

COL Richard B. Jenkins was Commander and Executive Director of ERDC. Dr. James R. Houston was Director.

Unit Conversion Factors

Multiply	By	To Obtain
cubic feet	0.02831685	cubic meters
cubic yards	0.7645549	cubic meters
feet	0.3048	meters
inches of mercury	33.86	millibars
inches of mercury	3,386	newtons per meter^2
knots	1.852	kilometers per hour
miles (U.S. statute)	1.609	kilometers
miles per hour	1.609	kilometers per hour
yards	0.9144	meters

1 Introduction

The U.S. Army Engineer Research and Development Center (ERDC) Coastal and Hydraulics Laboratory (CHL) has provided the U.S. Army Engineer District, Galveston (SWG) with technical analysis and numerical modeling assistance for five major engineering activities in support of SWG's "Sabine Pass to Galveston Bay, Texas - Shoreline Erosion Feasibility Study." These activities included the development of WIS (***W***ave ***I***nformation ***S***tudy) wave hindcasts for the Gulf of Mexico for the years 1990-1999, ADCIRC (***AD***vanced ***CIRC***ulation) modeling of storm-induced water surface elevations and currents, STWAVE/GENESIS (***ST***eady-state spectral ***WAVE*** model/***GENE***ralized model for ***SI***mulating ***S***horeline change) modeling of longshore sediment transport, SBEACH (***S***torm-induced ***BEA***ch ***CH***ange) modeling of storm-induced beach profile response, and the development of a sediment budget. The WIS hindcasts and the ADCIRC modeling tasks are discussed in Tracy (2002) and Scheffner et al. (2002), respectively. The STWAVE/GENESIS modeling and SBEACH modeling tasks are the subject of this report. These two tasks, which used results from the WIS and ADCIRC efforts, were conducted in close coordination with the development of a sediment budget for the study site (Morang 2006).

Study objectives

The overall goal of the STWAVE/GENESIS and SBEACH modeling effort has been to develop a predictive capability that will be used to objectively evaluate alternative measures for beach restoration/protection projects within the study area. This includes evaluating the relative merits of competing designs and optimizing the selected alternative for storm-damage reduction and environmental restoration. The predictive capabilities address both long-term performance, evaluated using GENESIS, and short-term storm-induced performance, evaluated using SBEACH. The actual selection of sites for restoration work and the evaluation of alternative designs is the subject of future analysis using the study-reach specific tools developed herein.

Products and deliverables

This effort has produced two main products. The first is this document, the final report. The second is a PC computer compact disk (CD)[1] that contains data files needed to run GENESIS and SBEACH for a specific evaluation project, a .dll file needed to modify the GENESIS code, and text files describing the procedure for running GENESIS and SBEACH. The user of this CD is expected to have GENESIS and SBEACH software available and be familiar with their use.

Overview of report

Chapter 2 describes the study area and previous research on sediment transport rates and shoreline change. Chapter 3 describes the models used in this study. Chapters 4, 5, and 6 discuss the methodology used to set up and calibrate the STWAVE and GENESIS models. Chapters 7 and 8 describe the SBEACH setup and calibration procedures. Results and recommendations are discussed in Chapter 9.

[1] CD available from the author.

2 Description of Study Area

Geographic setting

The study site along the upper Texas coast, comprising the coastlines of Jefferson, Chambers, and Galveston Counties, covers a 100-mile (160-km) length of the Gulf of Mexico shoreline from the Texas/Louisiana border at Sabine Pass in the east, to the western end of Galveston Island at San Luis Pass in the southwest (Figure 1). Jefferson County, the easternmost section, from Sabine Pass to the vicinity of the town of High Island, is a mainland beach fronting a Chenier plain, formed from a Pleistocene promontory overlain by Holocene marginal deltaic sediments. This area is characterized by a broad salt marsh with a muddy shoreface substrate, and is a continuation of the type of terrain found further east along the Louisiana coast. West of High Island, the Chenier plain grades into a sandy barrier island terrain of the Bolivar Peninsula and Galveston Island (Fischer et al. 1972; McGowan and Scott 1975; White et al. 1985). Galveston, at the eastern end of Galveston Island, is the only large city within the study area, though several communities and subdivisions exist on Bolivar Peninsula and on west Galveston Island, interspersed with undeveloped areas (Figure 1). The Jefferson County shoreline is almost entirely undeveloped. Access to portions of this coastline is limited since the portion of coastal Highway 87 that runs between High Island and Sea Rim State Park has been abandoned since 1989 due to shoreline erosion.

From east to west, the inlets in the study area include Sabine Pass, Rollover Pass near the eastern end of the Bolivar Peninsula, the Galveston Entrance Channel between the Bolivar Peninsula and Galveston Island, and San Luis Pass (Figures 2 through 6). Sabine Pass and the Galveston Entrance Channel are large jettied entrances that serve major commercial ports. The U.S. Army Corps of Engineers (USACE), SWG, maintains the jetties and navigation channels.

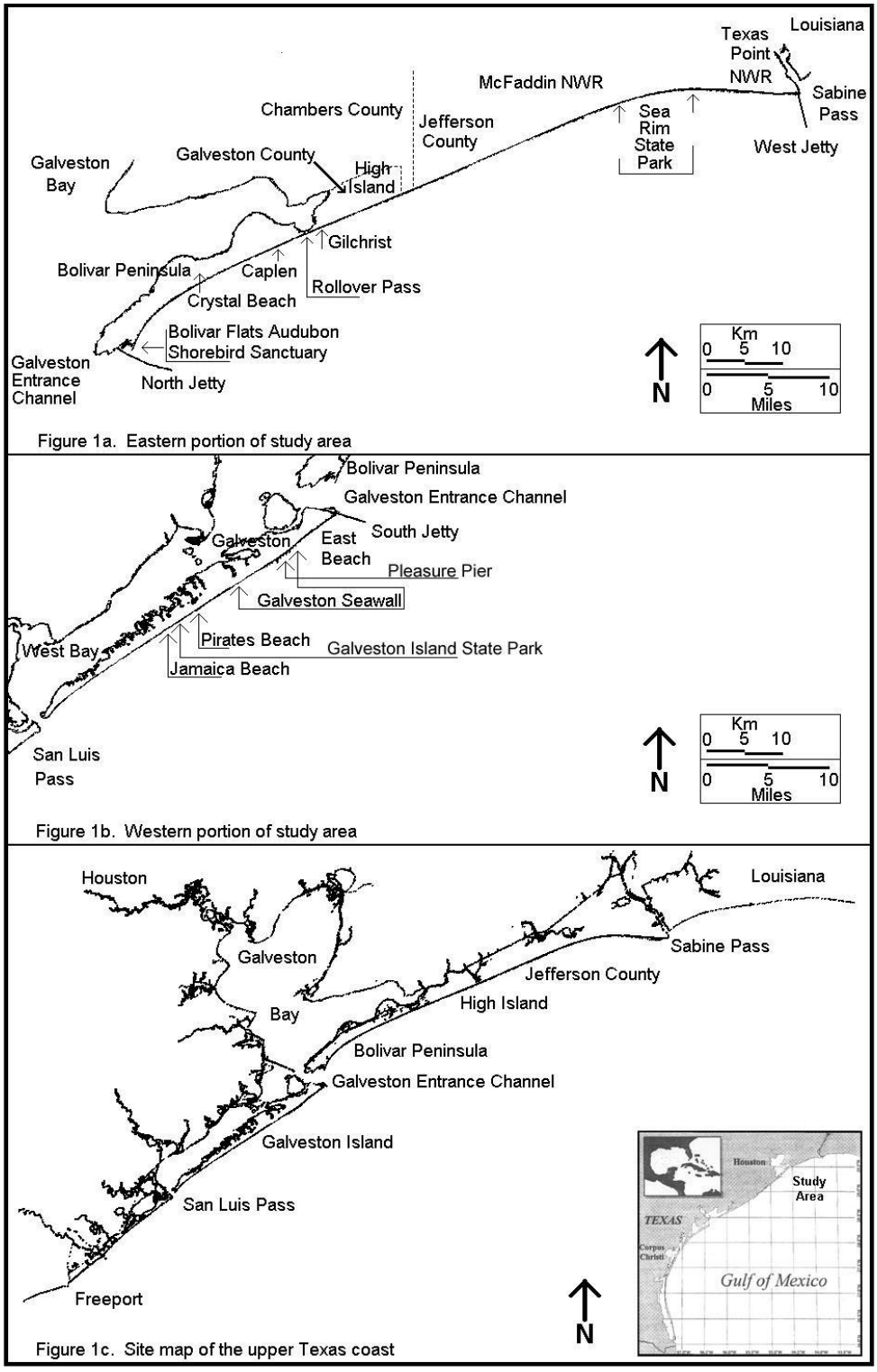

Figure 1. Study area.

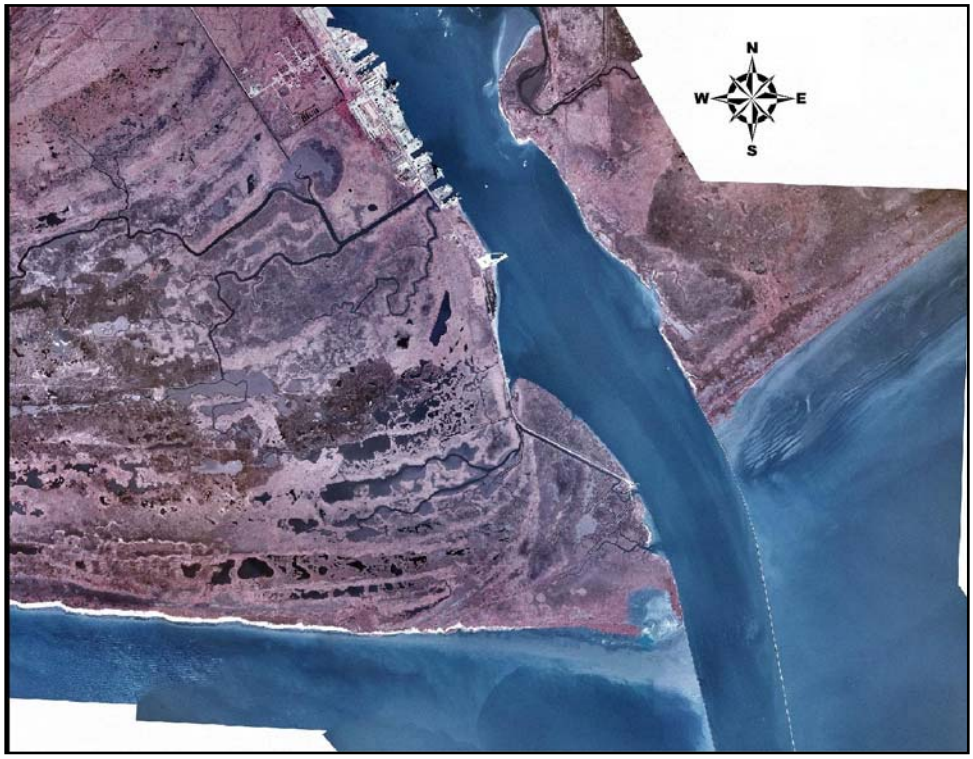

Figure 2. Sabine Pass (2002 photo mosaic courtesy of Texas Bureau of Economic Geology).

Figure 3. Rollover Pass (2002 photo mosaic courtesy of Texas Bureau of Economic Geology).

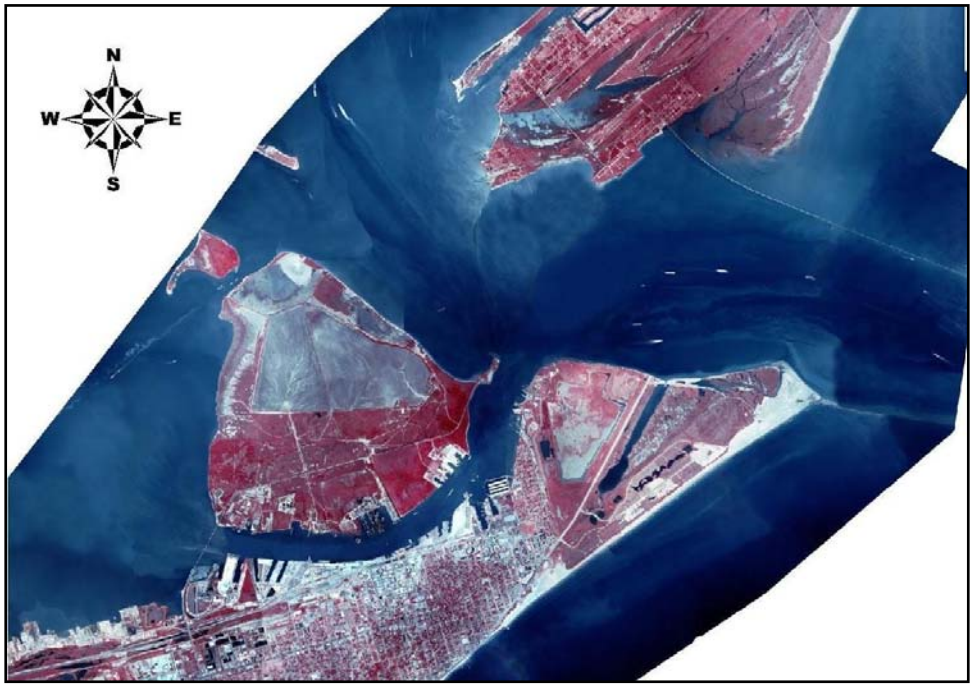

Figure 4. Galveston Entrance Channel, with Galveston at bottom, north and south jetties at right (2005 photo mosaic courtesy of Texas Bureau of Economic Geology).

Figure 5. East Beach and Big Reef. Oblique aerial photo, taken 27 July 2003, looking NW. Galveston Entrance Channel south jetty from foreground to upper center, East Beach at left, Big Reef at right of center, Galveston Entrance Channel at right. Photo courtesy of Texas Government Land Office.

Figure 6. San Luis Pass (1999 photo mosaic courtesy of Texas Bureau of Economic Geology).

Rollover Pass is a non-navigable inlet first constructed in 1954-55 with an initial design depth of 8 ft (2.4 m) and width of 80 ft (24 m). However, before construction was completed the inlet had scoured in spots to a depth of 30 ft (9.1 m) and a width of over 500 ft (150 m). The inlet was closed, then reopened in 1959 with modifications that included a sheet-pile lining along the length of both sides of the channel and a trapezoidal weir across the inlet. Concrete revetments were later constructed to reinforce the sheet-pile walls (USACE 1959; Mason 1981; Bales and Holley 1989). While these modifications have stabilized the inlet, the inlet has continued to be a source of erosion for the adjacent beaches (Prather and Sorensen 1972; Bales and Holley 1989; Parchure, Brown, and McAdory 2000; PIE 2001).

San Luis Pass is a modest sized (Jarrett 1978) downdrift-offset, natural (undredged and unjettied) inlet. While it is a typical non-migratory Texas inlet (Price 1951), the shoals and inlet margins are dynamic. Currently Treasure Beach, a subdivision at the southwest side of the inlet, is

suffering significant erosion. Mason (1981) discusses the inlet's history and stability and suggests that the inlet may be a significant sediment sink, as well as a potential sand source for beach renourishment. The inlet is the subject of a currently ongoing research project by the Bureau of Economic Geology (BEG) of the University of Texas, Austin, as discussed on the website: *http://www.beg.utexas.edu/coastal/texastidalinlets.htm*.

Geologic setting

The modern configuration of the Texas coast is the product of dramatic changes in sediment supply that accompanied late stages of the Holocene sea level rise and the subsequent stillstand. Sea level curves for the Gulf of Mexico indicate that the last low-stand occurred approximately 20,000 BP to 18,000 BP, when sea level was about 350 feet (110 m) below its present position. From that point, a period of rapid sea level rise occurred until 7,000 BP to 6,000 BP, when sea level reached the elevation between -10 and +6 ft (-3 and +2 m). This was followed by a much slower rise to the modern stillstand, which occurred approximately 3,000 BP (Curray 1960; Nelson and Bray 1970; Frazier 1974; Bard et al. 1990; Blum et al. 2001; Otvos 2001). The offshore shoal areas of Sabine and Heald Banks are the remnants of earlier shorelines.

During the period of rapid sea level rise, coastal plain rivers maintained their earlier course and backfilled incised valleys that had developed during the sea level lowstand. A change from a cooler, wetter climate in the early Holocene to a warmer, drier condition significantly decreased the sediment supply of Texas coastal plain rivers. In Texas, only the Rio Grande and Brazos-Colorado River systems, with their large drainage basins, transported sufficient sediment to fully aggrade their upper valleys and develop deltas of moderate size that prograded into the Gulf of Mexico (Morton 1994). In contrast, the Sabine and Trinity Rivers, in the project area, are characterized by elongated drowned river valleys in the form of Sabine Lake and East Galveston Bay. The very limited coarse-grain load in these two rivers is deposited in bay head deltas rather than on the coast. Therefore, the sand on the modern day mainland beaches, spits, and barrier islands in the project area either migrated up the shoreface with the Holocene sea level rise or was eroded from Pleistocene barrier-strand plain deposits exposed on the inner shelf during sea level rise. With the exception of some very minor contribution of coarse-grain material due to the erosion of the Pleistocene promontory, no modern day sand is being delivered to these beaches. This lack of delivery of any coarse-grain

sediment to the project area during the modern stillstand has contributed significantly to shoreline erosion in the area.

The beach between Sea Rim State Park and Sabine Pass (Texas Point National Wildlife Refuge (NWF)) is composed of consolidated mud. Figure 7 shows a typical view of this beach. A thin veneer of sand is thrown up onto the marsh edge by storms, but the shoreface is composed almost entirely of mud. Further west, the Sea Rim State Park area is a sediment transport convergence zone (discussed below), and the beach typically has a substantial veneer of sand. Further west, the McFaddin NWR area is a sediment transport divergence zone, and portions of this area are devoid of sand. The erosion is continuing in this area leading to a continued increase in the exposure of the mud substrate and increasing the frequency of flooding of the interior marshes. Sand veneers gradually thicken to the west, and mud outcrops become less common (Nelson and Bray 1970). Where these veneers exist, subaqueous mud layers are often exposed in the bar troughs, as illustrated schematically in Figure 8 (adapted from Howard 1999).

Figure 7. Inaccessible shoreline at Texas Point. Sabine River location is shown by the vegetation line on the skyline at right. Photo courtesy of Dr. Billy Edge, Texas A&M University.

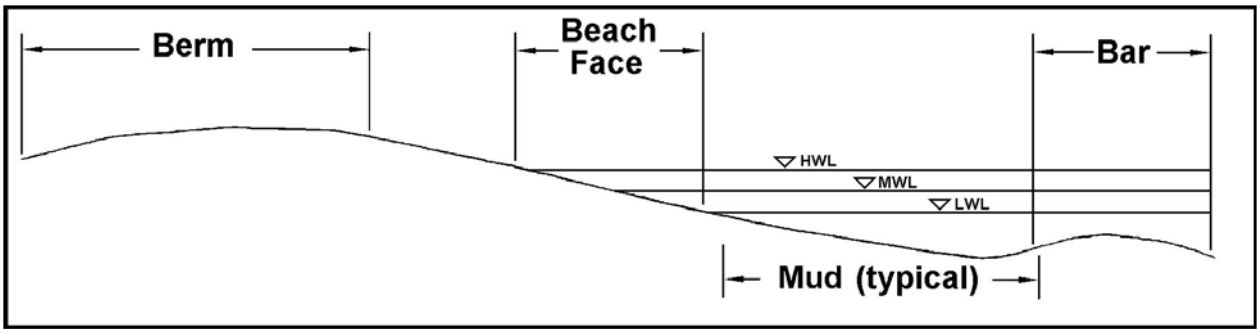

Figure 8. Schematic of typical location of consolidated mud substrate and/or unconsolidated mud ooze occasionally found on beach profiles between Sea Rim State Beach and High Island, adapted from Howard (1999).

West of the High Island/Caplen area, the mud substrate is rarely exposed within the surf zone. Beach face corings in the Gilchrist/Caplen area generally indicate 6 to 10 ft (2-3 m) of sand over the underlying mud. This thickening of the sand surface layer continues west to Galveston Island as shown in Figure 9, where surface sand thicknesses range from 10 to 50 ft (3-16 m). However, even on Galveston Island small mud outcrops have been documented (Stern 1948).

Sediment samples were collected and analyzed for this study by the Ocean and Hydraulic Engineering Program of Texas A&M University (TAMU), under the direction of Dr. Billy Edge. Samples were collected on the berm, at the water's edge, and at wading depths throughout the study area. Of 103 samples collected between Sabine Pass and the Galveston Entrance Channel, the median grain sizes range from 0.0854 to 0.230 mm, with an average value of 0.167 mm. Of 72 samples collected on Galveston Island, median grain sizes range from 0.104 to 0.154 mm, with an average value of 0.129 mm. Consolidated mud samples were not included in this analysis. Coarser material (typically shells, shell fragments, and caliche nodules) was also excluded. Aside from the prevalence of fine-grained sediments (mud) along Texas Point, there is little trend in the median grain sizes throughout the study area (Magouirk 1981; Edge 2000). These results are similar to those in previous sediment analyses (Bullard 1942; Stern 1948; Richardson 1948; Bridges 1959; Van Andel and Poole 1960; Crocker 1963; Nelson and Bray 1970; Howard 1999).

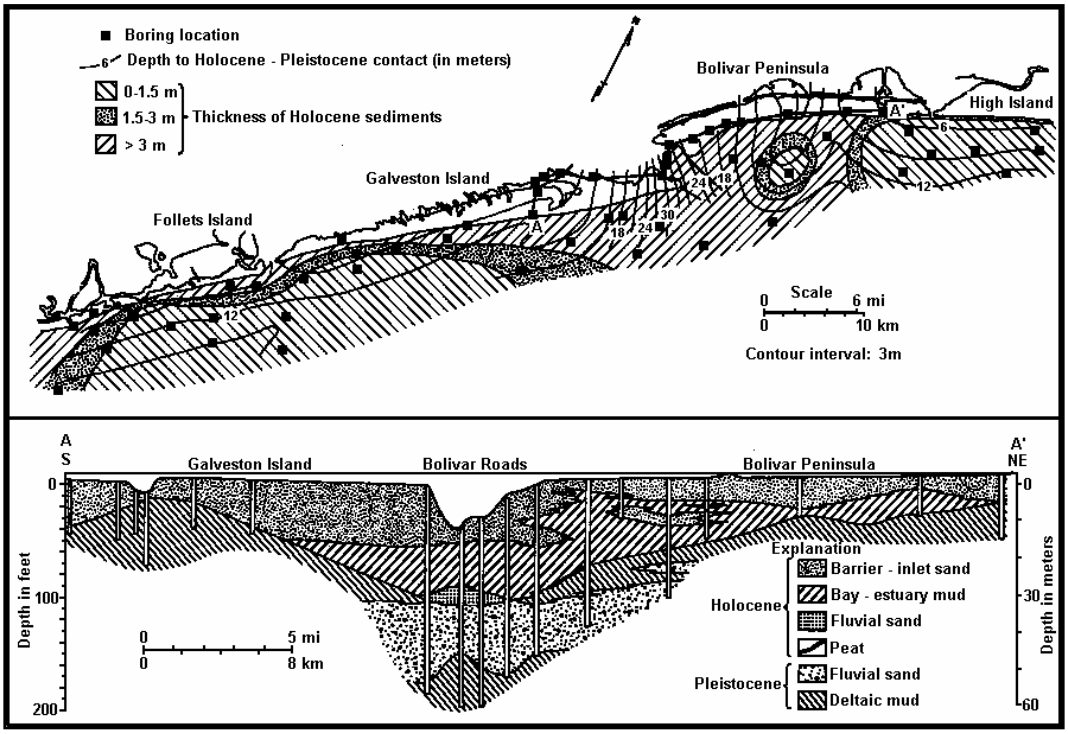

Figure 9. Isopach map of Holocene sediments (top) and strike section of Holocene sediments and subsea depth of the Holocene-Pleistocene unconformity, from White et al. (1985).

Offshore, sandy muds and muds predominate in the inner shelf region. However, offshore banks (Sabine Bank and Heald Bank; locations discussed in Chapter 5) contain significant quantities of beach quality sand (Morton, Gibeaut, and Gutierrez 1995).

Sediment transport rates from previous studies

Numerous studies (e.g., Carothers and Innis 1960; USACE 1971; Fisher et al. 1972; Mathewson 1987; Benton and Bolleter 1987) are in agreement that the typical yearly net longshore sediment transport is to the southwest along most or all of the coastline between Sabine Pass and San Luis Pass. The only reversals of direction that are occasionally mentioned are at Sea Rim State Beach (e.g., Mason 1981) and next to the Galveston Entrance Channel south jetty (East Beach) (e.g., Hall 1976). Transport rate values reported in the literature are shown in Table 1. In the Data/Method column in this table, "LEO" (***L***ittoral ***E***nvironmental ***O***bservations) refers to data collected using standardized visual surf zone observations (Schneider 1981; Thomas 1994). "SPM" refers to a group of related methods of calculating longshore transport rates from wave data discussed in the ***S***hore ***P***rotection ***M***anual (USACE 1984). "B&G" refers to a Bruun and Gerritsen (1958) stability analysis.

Table 1. Sediment transport rates reported in the literature.

Author	Transport Rate m^3/yr		Data Yrs	Data / Method	Incl Wind
	Net	Net Direction			
Sea Rim State Beach					
Mason (1981)	27,000	NE	1975, 1977	LEO, SPM	No
USACE (1983)	54,000	SW	10 yr	LEO, SPM	Yes
High Island					
USACE (1983)	78,000	SW	10 yr	LEO, SPM	Yes
Gilchrist / Rollover Pass					
USACE (1959)	153,000				
Prather and Sorensen (1972)	58,000	SW		B&G	Yes
Hall (1976)	41,000	SW	1975	LEO, SPM	No
Mason (1981)	44,000	SW	1975, 1977	LEO, SPM	No
Bales and Holley (1989)	185,000 – 221,000	SW	1956-1984	Fillet	
Crystal Beach					
USACE (1983)	75,000	SW	10 yr	LEO, SPM	Yes
Galveston Entrance Channel					
Mason (1981)	59,000	SW	1975, 1977	LEO, SPM	No
USACE (1983)	36,000	SW	10 yr	LEO, SPM	Yes
12th St., Galveston					
USACE (1983)	23,000	SW	10 yr	LEO, SPM	Yes
Bermuda Beach					
Hall (1976)	116,000	SW	1975	LEO, SPM	No
Mason (1981)	303,000	SW	1975	LEO, SPM	No
USACE (1983)	44,000	SW	10 yr	LEO, SPM	Yes
Galveston Island State Beach					
Hall (1976)	66,000	SW	1975	LEO, SPM	No
Sea Isle					
Hall (1976)	103,000	SW	1975	LEO, SPM	No
Mason (1981)	178,000	SW	1975	LEO, SPM	No
USACE (1983)	16,000	SW	10 yr	LEO, SPM	Yes
East Side of San Luis Pass					
USACE (1983)	20,000	SW	10 yr	LEO, SPM	Yes

Within the study area, the most unambiguous example of southwesterly transport is at the west end of the Galveston Seawall (Figure 10). In this figure, land is shown in white, water in light blue, and the extent of shoreline change in yellow. The four shorelines shown are discussed below. The annual erosion rate in this area is on the order of 6 to 9 ft/yr (2-3 m/yr). When this portion of the seawall was constructed in 1963, the shoreline was in the vicinity of the edge of the seawall. If the net transport of sand were to the northeast at this location, the end of the seawall would be expected to act like a groin and have a fillet of sand against the end of the wall. It is difficult to envision any natural process other than southwesterly net transport that would cause this shoreline configuration.

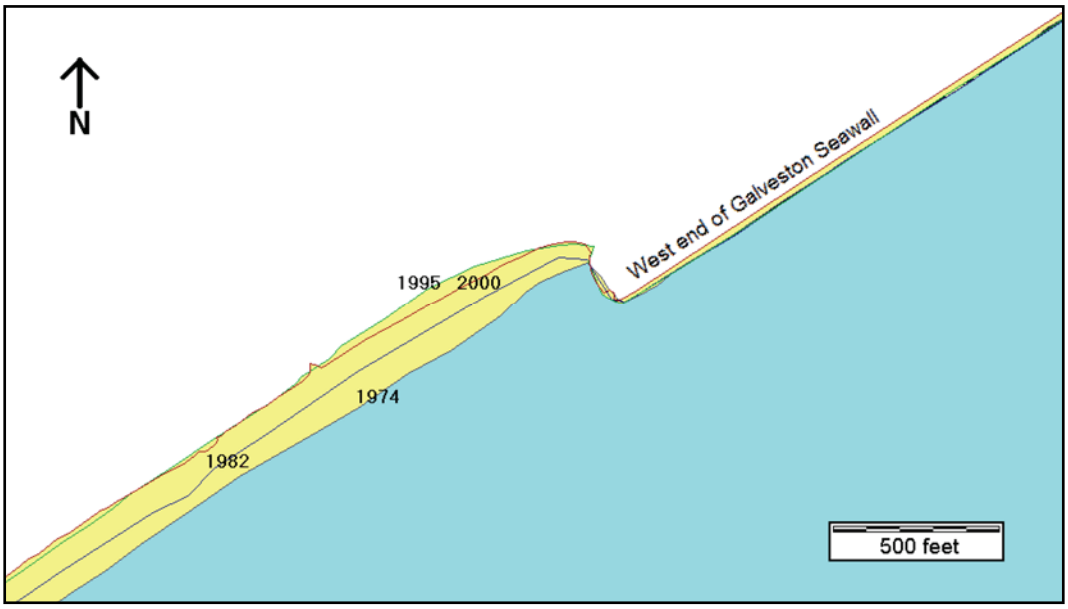

Figure 10. Historical shoreline positions (1974 in gray, 1982 in blue, 1995 in green, and 2000 in red) in the vicinity of the west end of the Galveston Seawall.

Historical shoreline change rates

Several investigations have produced shoreline change rates for the study area, as shown in Figures 11 and 12. In these figures, positive change rates indicate accretion, negative indicate erosion. To convert change rates to meters per year, multiply the data by 0.3048. Other estimates of shoreline change rates (not shown in Figures 11 and 12) have been made for limited stretches of the study area, typically in the Rollover Pass area (USACE 1959, 1983; Benton and Bolleter 1987; and Bales and Holley 1989).

Data sources

In Figures 11 and 12, the bar graph data labeled S&S 1882-1963 show Seelig and Sorensen (1973) shoreline change rate estimates. To address certain legal issues, the National Ocean Survey (NOS) of the National Oceanographic and Atmospheric Administration (NOAA) used the earliest available surveys to establish 226 turning points along the coast of Texas to describe the location of the mean low water line as close in time as possible to the 1845 date that the Republic of Texas entered the Union. Seelig and Sorensen (1973) calculated the distances from these points to the mean low water line on the most current topographic charts and divided by the intervening years to estimate the average annual shoreline change rates. Within the study area, dates for the early surveys ranged from 1850 to 1882, with 1882 being the most common. Study area dates for their most recent surveys ranged from 1957 to 1966, with 1963 being the most common. Sixty-nine of the 226 Texas coastal turning points are within the study area; however, they are not evenly distributed along the coast. For presentation in Figures 11 and 12, the Seelig and Sorensen (1973) rates were interpolated to BEG change rate locations (described below).

BEG has published a series of shoreline change rate estimates, all using the same stations. In Figure 11, the M 1882-1974, P&M 1974-1982, and M 1974-1996 bar graph labels refer to average annual shoreline change rates over the listed intervals using data from Morton (1975), Paine and Morton (1989), and Morton (1997), respectively. The Figure 12 data sources are the same except that M 1882-1974 refers to Morton (1974). For these studies, 62 stations were established along the coast from Sabine Pass to the Galveston Entrance Channel, and 31 were established along Galveston Island; each being spaced 5,000 ft (1,524 m) apart. In these reports, shoreline position data were obtained from surveys, topographic charts, 1974 and 1982 aerial photographs, and a 1996 GPS beach survey. These data were used to determine changes over time in the positions of the wet/dry line, the high water line, the berm crest, the vegetation line, the crest of the washover terrace and/or the coastal structures line, depending upon the location and data source. Discussion of the use of these various shoreline indices is presented in Morton (1979).

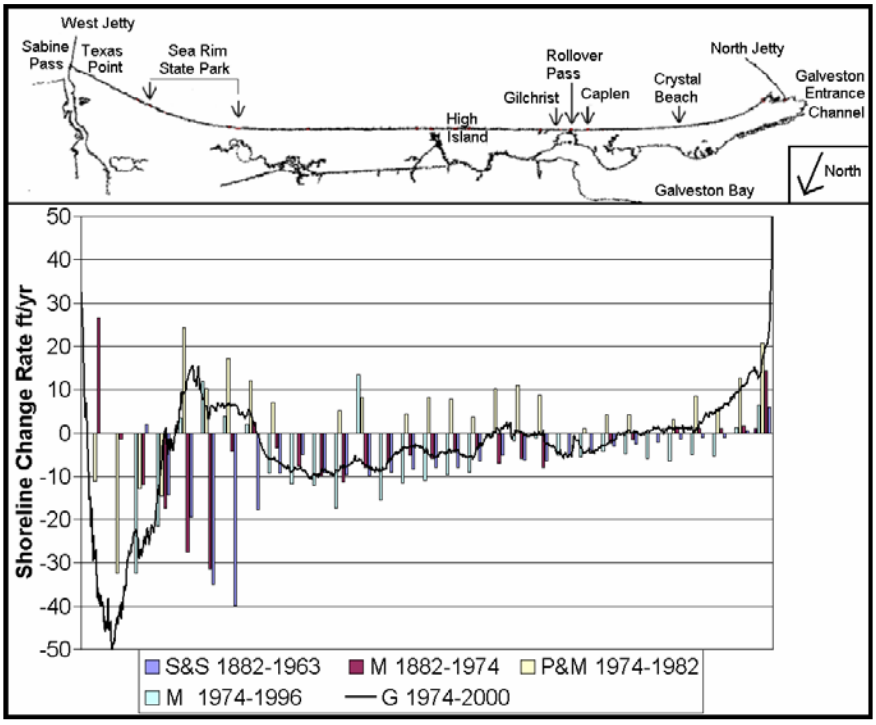

Figure 11. Historical shoreline change along High Island (Jefferson County and Bolivar Peninsula).

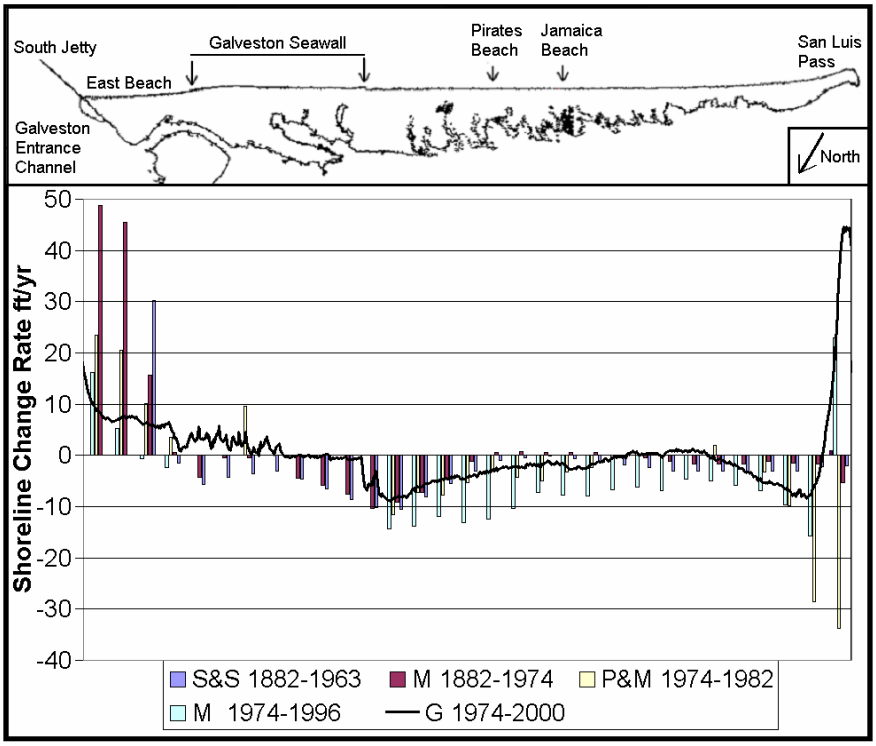

Figure 12. Historical shoreline change along Galveston Island.

As part of the current study, BEG, under the direction of Dr. James Gibeaut, provided ERDC with reanalyzed shoreline change data (Gibeaut et al. 2002) using the 1974 and 1982 aerial photographs, 1995 digital aerial photographs, and 2000 LIDAR surveys (Table 2). The 1974 and 1982 photographs were digitally scanned and ortho-rectified typically using 30 to 60 ground control points per image. Shoreline change rates, established at 50-meter intervals (rather than the earlier 5,000-ft intervals), were calculated using a linear regression analysis involving all four shorelines. These rates are shown as the black line, labeled G 1974-2000, in Figures 11 and 12.

Table 2. Sources for BEG shoreline data.

Date & Time	Type	Scale	Area
9/5/1974	Black&White	1:24,000	Sabine Pass to 5 mi west
6/28/1974	Black&White	1:24,000	5 mi west of Sabine Pass to San Luis Pass
7/9/1982	Color Infrared	1:24,000	Sabine Pass to Galveston Entrance Channel
6/10/1982	Color Infrared	1:24,000	Galveston Entrance Channel to San Luis Pass
1-2/1995, 1-2/1996	Color Infrared	1:40,000 photos, 1:12,000 DOQQ's	Sabine Pass to San Luis Pass
5/23-24/2000	LIDAR topography and intensity	N/A	Sabine Pass to San Luis Pass

Differences in change rates

Figures 11 and 12 show considerable differences in the shoreline change rates obtained from different studies. These differences are due a combination of factors: differences in the definitions of shorelines, errors in the data and data analysis, and natural variations in the rates of shoreline change at different times in the past. For example, recent trends indicate that Texas Point is experiencing the largest erosion rates - up to 40 to 50 ft/yr (12-15 m/yr) - within the study area, and adjacent Sea Rim State Park is accreting. However, shoreline change rates that use early shorelines from the late 1800s show little or no erosion at Texas Point and strong erosion at Sea Rim State Park (Figure 11). Another example of variation of shoreline change rates over time is that accretion was much

greater on East Beach shortly after the south jetty was constructed (Figure 12).

One factor that would influence the variation in these change rates is that this section of coastline has experienced a below average number of hurricanes and severe storms in the past 20 to 30 years relative to earlier in the 20th century. This area experienced ten Category 3 and 4 hurricanes (Saffir-Simpson Scale) between the Great Galveston Hurricane of 1900 and Hurricane Carla in 1961; however, it has only experienced two major hurricanes since then (Hurricanes Celia in 1970 and Alicia in 1983, both Category 3) (plus Hurricane Rita in 2005, Category 3 at landfall).

Thus, while none or any of these historical change rates may be reflective of future shoreline changes, for model calibration purposes (comparing historical change rates to model outputs using historical wave data), the most emphasis was placed upon comparisons with the Gibeaut data because of the greater rigor with which it was calculated.

Interpretation of recent historic change rates

The area immediately west of the Sabine jetty (within the first half mile (one km)) (Figure 12) is accreting due to the sheltering effects of the jetty. Further west, the area of Texas Point, a consolidated mud shoreline, is experiencing the greatest erosion within the study area of up to 40 to 50 ft/yr (12-15 m/yr). As the mud on the shoreface is mobilized by the waves, it is removed from the system (see discussion in Chapter 3). The small amount of sand that is winnowed from this area is transported westward and deposited in the accreting area of Sea Rim State Beach. Sea Rim is accreting due to its concave shoreline shape and due the fact that it is a convergence zone, with sand being supplied from both directions (Chapter 9). The area between Sea Rim State Beach and High Island has suffered continuing erosion that led to the closure and loss of State Highway 87 in 1989. This area of erosion generally extends west past Rollover Pass, which exacerbates the erosion by trapping sediment in its flood shoals (Prather and Sorensen 1972; USACE 1983; Bales and Holley 1989; Parchure, Brown, and McAdory 2000). Further west, in the vicinity of Crystal Beach the shoreline is neutral; and near the tip of Bolivar Peninsula, it becomes strongly accretionary as it is highly sheltered by the Galveston Entrance Channel's north jetty.

On Galveston Island, the area of East Beach is strongly accretionary (Figures 4 and 5). Sediment transport in this area is to the east (Chapter 9), and sand is impounded against the south jetty, with some passing through to the bar just inside the jetty (Big Reef) and into the navigation channel (Figure 5). The accretion along the eastern portion of the Galveston Seawall is largely the remnants of the 1995 beachfill that is trapped by the seawall groin field. There is a reversal of transport direction along the Galveston Seawall, and west of there transport is to the west. The center portion of the island is experiencing erosion. Further west, the net transport rate decreases and the beach becomes neutral. At San Luis Pass, the beach is strongly prograding adjacent to the unstructured inlet (Figure 6).

3 Description of Numerical Models

STWAVE/GENESIS

The longshore sediment transport formula used in GENESIS (which is a modified version of the CERC formula; see e.g., Appendix B or Rosati, Walton, and Bodge 2002, section III-2-3) requires wave information at the seaward edge of the surf zone (the breaker line.) Wave data for this study were available in the form of WIS hindcasts (Tracy 2002) several miles offshore in 20 meters of water depth. The numerical model STWAVE was used to transform these offshore waves to a near-breaking depth. Then, the numerical model GENESIS was used to calculate the breaking wave parameters, the longshore sediment transport, and the resulting shoreline change.

STWAVE is a computationally intense, steady-state spectral wave model that uses a two-dimensional uniform rectilinear grid to transform waves from the offshore region to a near-breaking depth (Resio 1987, 1988a, 1988b; Smith 2001). It solves the complete radiative transfer equation (Jonsson 1990) that includes both propagation effects (refraction, shoaling, diffraction, and wave-current interactions) and source-term effects (wave breaking, wind inputs, and nonlinear wave-wave interactions). As input, the model requires some basic configuration data, a uniform rectilinear bathymetry grid, directional wave spectra at the seaward boundary of the grid, and optionally, wind and current data. This study included local windfields within the grid, but not local currents.

GENESIS is a shoreline change model used to simulate longshore sand transport and the resulting cross-shore change in shoreline position (Hanson 1987; Hanson and Kraus 1989; Gravens, Kraus, and Hanson 1991). One of the GENESIS assumptions is that when erosion or accretion occurs, the entire profile shifts landward or seaward, without changing profile shape, so that only one cross-shore point at each grid cell needs to be tracked. Thus, it belongs to a class of models known as one-line models. At each alongshore grid cell, the model uses the transformed wave data supplied by STWAVE to calculate breaking wave heights and angles, and uses this information to calculate the temporally varying local longshore sediment transport rate. Other inputs include configuration data, shoreline positions, and structure locations. GENESIS can predict shoreline

change in a diverse variety of situations involving almost arbitrary numbers, locations, and combinations of groins, jetties, detached breakwaters, seawalls, and beach fills.

The application of GENESIS described in this report is non-standard. The computer code was modified to accept the entire time series of wave parameters as input, rather than computing transport based upon a selected set of representative wave conditions, and was additionally modified to include the effects of a wind-generated longshore surf zone current in the transport relationship (Chapter 6). This treatment was required because the combination of a broad shelf and low waves in the Gulf of Mexico allows local winds to play a more dominant role in shoreline dynamics in this area than on most other beaches around the United States.

SBEACH

SBEACH is an empirically based numerical model for simulating two-dimensional cross-shore beach change (Larson and Kraus 1989, 1991, 1995; Larson, Kraus, and Byrnes 1990; Wise, Smith, and Larson 1996). The model's intended use is for predicting short-term profile response to storms. In contrast to GENESIS, a fundamental assumption of SBEACH is that profile change is produced solely by cross-shore processes, resulting in a redistribution of sediment across the profile with no lateral gain or loss of material. Model inputs include nearshore bathymetry, sediment grain size, and storm-induced waves and water levels.

Modeling of sediment transport on mud beaches

A cohesive sediment is one in which the grains are small enough that the attractive forces between particles (electrostatic forces) are stronger than the force of gravity pulling the sediment to the bed. Mud and fine-grained sediments are generic terms for a cohesive mixture of clay (particles having diameters < 4 μm) and silt (particles having diameters between 4 and 70 μm) possibly mixed with small percentages of sand (particles having diameters > 0.070 mm). A consolidated mud is one that has had the water largely removed through drainage or evaporation and has compacted and stiffened. As described above, the beaches at the far eastern end of the study area in the region of Texas Point are primarily composed of consolidated mud. Further to the west, extending to the vicinity of High Island, the consolidated mud substrate is overlain by sand veneers of varying thicknesses and is only occasionally exposed.

Sediment transport and deposition processes are distinctly different on mud shorelines than on sandy beaches. Once eroded, cohesive sediments are carried in suspension until deposited in a less energetic environment; either in deeper water outside the surf zone or in wave-sheltered areas, such as quiet bays and estuaries (Nairn and Willis 2002), and so, are lost to the littoral system. On sand beaches, the mobilized sand generally stays within the active profile.

Within the surf zone, breaking wave energy is dissipated into turbulent motion. In addition, both within the surf zone and in the areas somewhat further seaward, additional turbulence is generated within the bottom boundary layer due to the wave-induced orbital water motion and nearshore currents. This turbulence acts to suspend sediment off the bottom, and once a particle is suspended, it takes a characteristic amount of time (which is a function of the grain's size) to fall back to the bed. For a sufficiently large amount of turbulent energy and a sufficiently small particle, the particle will not have time to fall back to the bed before more turbulent energy is supplied by the passage of the next wave, and thus it remains in suspension. For the wave conditions characteristic of typical beaches, this condition applies to silts and clays. These size particles do not settle out within the surf zone once they are suspended. This is the primary reason that most of the world's beaches are composed of sediments having diameters greater than 0.10 mm.

In regions that have large supplies of fine grain sediments, the nearshore seabed can be blanketed with thick, unconsolidated, gel-like, mud oozes. These environments can attenuate waves through bottom friction at rates 1 to 2 orders of magnitude greater than sand bottoms (Gade 1959; Tubman and Suhayda 1976; Dalrymple and Liu 1978; Hsiao and Shemdin 1980; Wells and Kemp 1986). There are anecdotal reports of regions off the Louisiana coastline and off Texas Point being safe havens for vessels during storms due to the near-total attenuation of waves (Morgan, Van Lopik, and Nichols 1953; Wells and Kemp 1981; *http://www.wtblock.com/wtblockjr/oilpond.htm*).

In these mud-rich environments, accretion can occur on beaches by poorly understood processes. Morgan, Nichols, and Wright (1958) report up to 300 meters of shoreline accretion in two mud arcs, totaling 7.2 km in length along a western Louisiana shoreline in a few days during the passage of Hurricane Aubrey in 1957. At the same time, other nearby sections of

coastline experienced significant erosion. Studies by Wells and Kemp (1986) in western Louisiana indicate that accretion most frequently occurs during storms, that the process can be very rapid (hours to days) and that much of the accretion is above the mean water line. Huh et al. (1991) report surge deposits of gel-like mud becoming stranded on the upper shoreface during storms. These deposits dried and cracked, occasionally forming mud cobbles which helped armor the shoreline from further attack. PIE (2003) reports evidence of these processes occurring near Sea Rim State Park.

If a consolidated mud beach contains some fraction of sand, this sand will stay within the surf zone and be subject to the same forces that cause longshore and cross-shore transport as occur on sandy beaches. On erosive mud shorelines, if the sand is not removed by longshore transport, its percentage will increase because the fines are being removed, and it will form lenses or veneers over the mud substrate. As these lenses thicken, they help protect the underlying mud from further erosion. Nairn (1992) found that approximately 200 m^3/m of sand cover (measured from the top of the beach out to the 4-m contour) halted the erosion process at a series of sites in the Great Lakes, and half that quantity provided some protection to the underlying cohesive sediment.

In smaller quantities, sand can also act to accelerate the erosion of a mud beach. If the consolidated mud is not covered with a sand veneer, any sand present that is mobilized by wave action will act as a scouring agent along the surface of the bed increasing the amount of fine material going into suspension.

GENESIS is a longshore transport model developed for sandy shorelines. Because of the differences in sandy and mud coastlines, this model was not expected to have strong predictive capabilities for the mud shorelines in the vicinity of Texas point. A few numerical models have been developed that apply specifically to cohesive shoreline erosion (Penner 1993; Nairn, Pinchin, and Philpott 1986; Nairn and Southgate 1993). Unfortunately, these models are not far advanced and rely on a significant degree of empiricism. Because of the lack of understanding of the processes involved, it was not deemed prudent to develop additional model capabilities for this portion of the study area.

4 STWAVE/GENESIS Model Grids

High Island and Galveston Island STWAVE grids

Bathymetry data were needed as input to the STWAVE grids. These data were obtained from the National Ocean Survey (NOS) hydrographic surveys that are available in electronic format from the Geophysical Data System (GEODAS, version 4.0) developed by the National Geophysical Data Center (NGDC). GEODAS is an interactive database management system for use in the assimilation, storage, and retrieval of geophysical data. Bathymetric surveys of the northeast Texas coastal area collected in the 1960s and 1970s provided overall coverage of the study area (Table 3) and were selected as the primary data sets for wave model grid development. Earlier surveys were used to fill gaps in the primary coverage (Table 4).

Horizontal survey datums were converted to the North American Datum of 1983 (NAD83), Universal Transverse Mercator (UTM) Zone 15, meters, coordinate system. Vertical survey datums were converted from mean low water (MLW) to the North American Vertical Datum of 1988 (NAVD88) by adding 0.19 ft (0.058 m) of depth to each sounding, the relationship established at NOAA Tide Station 8771510, located on the Galveston Pleasure Pier (Figure 1B) at Latitude 29° 17.1′ N, Longitude 94° 47.3′ W (UTM 326295.387 Easting, 3240914.357 Northing), as shown in Table 5. The data for this table were obtained from the following NOAA Web page: *http://tidesandcurrents.noaa.gov/benchmarks/benchmarks_old/771510.html#DatumsPage*.

Two STWAVE model grids were established; one for Bolivar Peninsula and Jefferson County (referred to herein as the High Island grid), and one for Galveston Island. The borders of these two-dimensional (2-D) wave model grids are the rectangles shown in Figure 13, along with the bathymetry contours in 5-m intervals, shown in green.

Table 3. Primary bathymetric surveys.

NGDC No.	Survey	Soundings	Date	Datum	Datum Ref	Location
3071075	H08712	14557	1962	MLW	NAD27	Sabine Bank
3071077	H08737	5599	1963	MLW	NAD27	Heald Bank
3071078	H08738	12359	1963	MLW	NAD27	South of Sabine Bank
3071079	H08739	11672	1963	MLW	NAD27	Sabine Bank
3071080	H08767	4214	1962	MLW	NAD27	Sabine Bank
3071082	H08795	16438	1964	MLW	NAD27	Sabine Bank
3071083	H08796	23068	1964	MLW	NAD27	Sabine Bank
3081109	H10011	24894	1982	MLW	NAD27	South of San Luis Pass
3081112	H10021	17787	1982	MLW	NAD27	Approaches San Luis Pass
3091061	H09765	23172	1978	MLW	NAD27	Offshore Gilchrist, Texas
3091062	H09769	10496	1978	MLW	NAD27	Vicinity of High Island
3091063	H09774	20025	1978	MLW	NAD27	Offshore Galveston
3091064	H09775	23060	1978	MLW	NAD27	West of Heald Bank
3091065	H09783	12741	1978	MLW	NAD27	Offshore Galveston
3091066	H09784	23285	1978	MLW	NAD27	Southeast of Galveston
3091071	H09843	50674	1979	MLW	NAD27	Bermuda Beach Offshore
3091072	H09851	18982	1979	MLW	NAD27	Offshore Galveston
3091073	H09885	28453	1980	MLW	NAD27	Southeast of Freeport
03F11447	H08749	5627	1965	MLW	NAD27	Galveston Channel
03F11449	H08751	4589	1962	MLW	NAD27	Galveston Bay Entrance
03F11450	H08752	10001	1963	MLW	NAD27	Texas Outer Coast

Table 4. Secondary bathymetric surveys used to fill gaps in primary coverage.

NGDC No.	Survey	Soundings	Date	Datum	Datum Ref	Location
3071008	H06291	16652	1937	MLW	NAD27	South of Galveston
3071042	H06251	11561	1937	MLW	NAD27	Bolivar Penin to Heald Bank
3071043	H06252	12345	1937	MLW	NAD27	Approaches Galveston Bay
3071044	H06253	10819	1937	MLW	NAD27	Galveston to San Luis Pass
3071045	H06294	4094	1937	MLW	NAD27	Southeast of Sabine Bank
3071091	H06398	11351	1938	MLW	NAD27	Approach Brazos River Ent
03F11469	H05488	8018	1933	MLW	NAD27	San Luis Pass

Table 5. Galveston Pleasure Pier tidal datums referenced to mean lower low water.

Datum	Symbol	Meters	Feet
Highest Observed Water Level (11 Sep 61)		2.829	9.28
Mean Higher High Water	MHHW	0.649	2.13
Mean High Water	MHW	0.578	1.90
Mean Tide Level	MTL	0.364	1.19
Mean Sea Level	MSL	0.359	1.18
North American Vertical Datum-1988	NAVD88	0.209	0.69
National Geodetic Vertical Datum-1929	NGVD29	0.165	0.54
Mean Low Water	MLW	0.151	0.50
Mean Lower Low Water	MLLW	0.000	0.00
Lowest Observed Water Level (12 Feb 85)		-1.463	-4.80

The two STWAVE grids extend offshore approximately to the 60-ft (20-m) contour, a depth where bottom influences on the waves become minimal. Figures 14 and 15 show contour plots of the bathymetric relief within the two grids. The High Island grid extends 302,000 ft (57 miles, 92 km) alongshore and 239,000 ft (45 miles, 73 km) offshore. This grid, covering a 2,600-mi^2 (6,700-km^2) area, is comprised of 88,000 grid cells at a 1,000-ft (304.8-m) spacing. The Galveston grid is only about 40 percent as large (though still larger than the typical STWAVE grid). It extends 159,000 ft (30 miles, 49 km) along the length of the island and 189,000 ft (36 miles, 58 km) offshore. Approximately 31,000 grid cells, at a 1,000-ft (304.8-m) spacing, cover this 1,100-mi^2 (2,800-km^2) area. The offshore direction is 157 deg azimuth for the High Island grid and 147 deg azimuth for the Galveston Island grid.

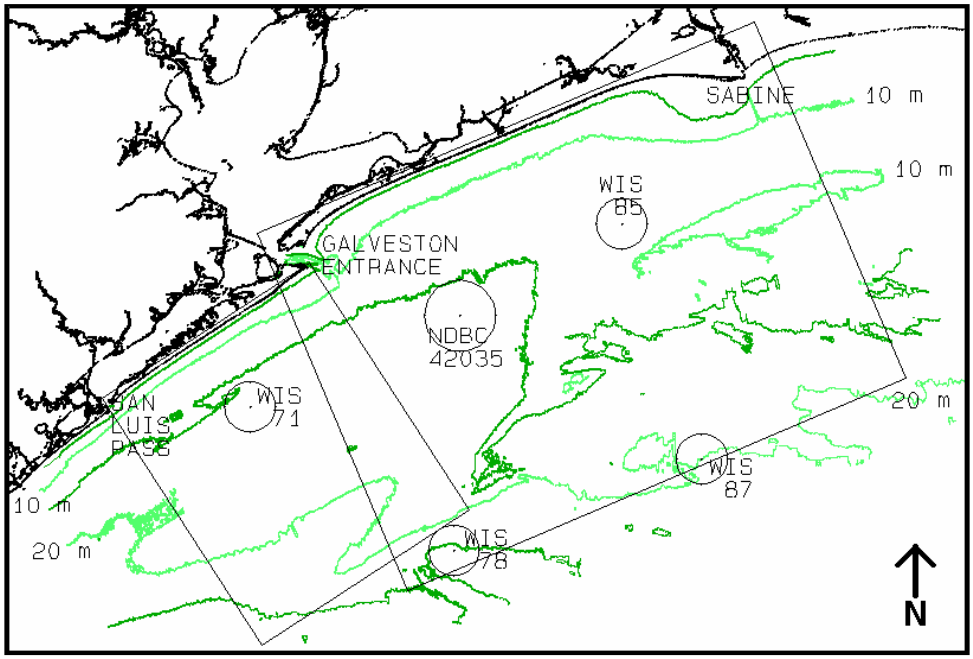

Figure 13. Offshore bathymetry, data stations, and layout of STWAVE grids.

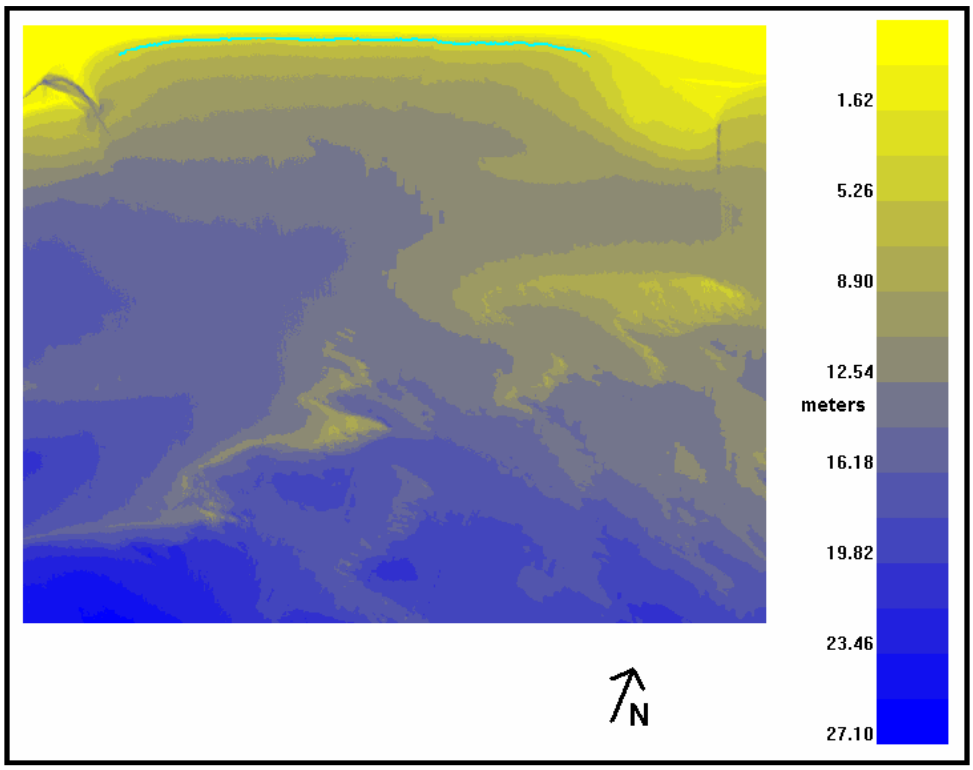

Figure 14. High Island STWAVE grid bathymetry.

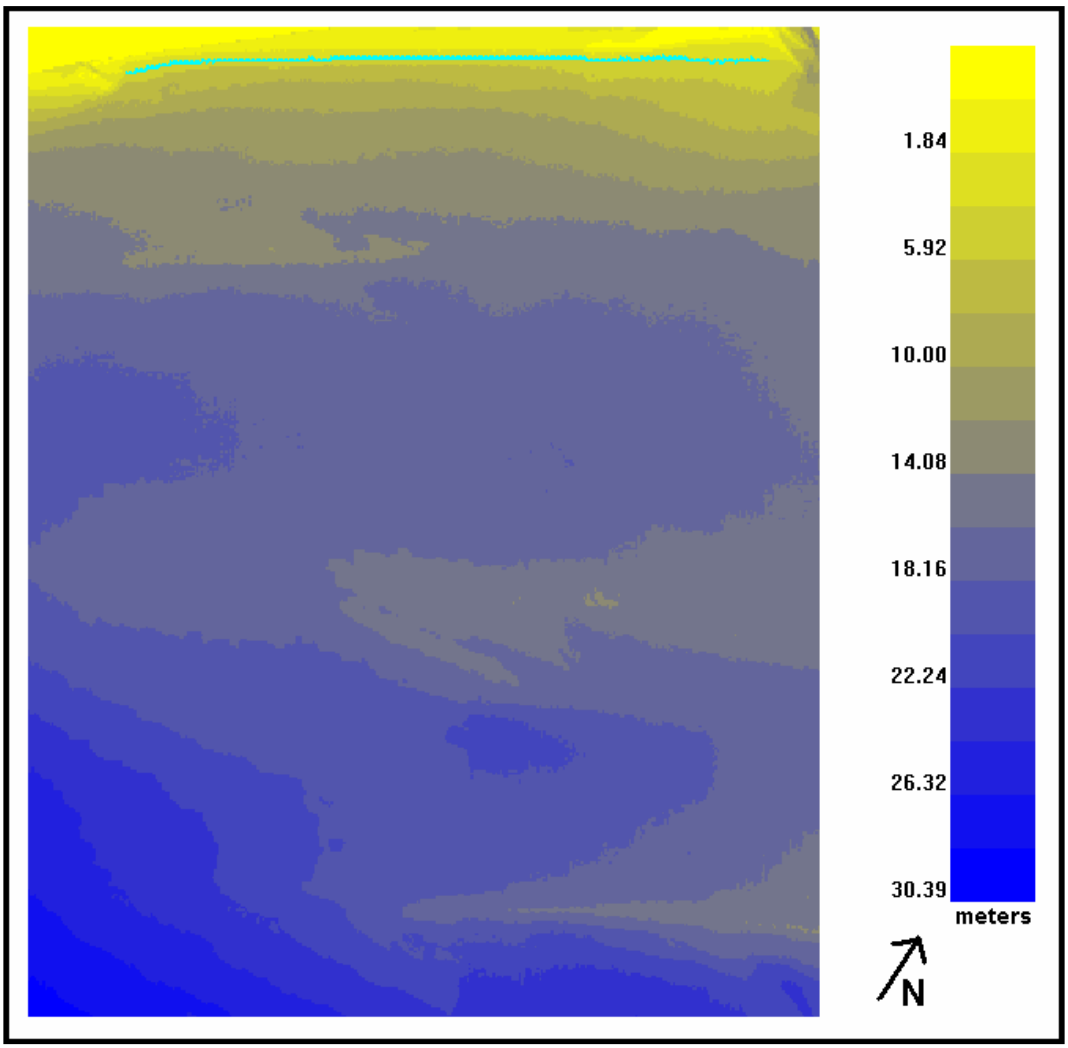

Figure 15. Galveston Island STWAVE grid bathymetry.

In Figures 14 and 15, shallow bathymetry is shown in yellow, and deep in blue. The depth scale to the right is in meters. The light blue line (actually, a series of grid cells) near the top of both figures shows the save stations (in approximately 6 m water depth) where the wave transformation data from STWAVE are saved for input into GENESIS.

The shallow bathymetry, which is the most important for wave refraction, is more complex for the High Island grid than it is for Galveston Island. Sabine Bank is the large shoal feature offshore of Sabine Pass (middle right of Figure 14). Smaller Heald Bank is further offshore to the left of center in the High Island grid. Both shoals rise to depths of less than 10 m. In the nearshore there is a large shallow shelf or ebb shoal feature at Sabine Pass and a smaller one at the Galveston Ship Channel Entrance (upper right and left of Figure 14, respectively). The shallow bathymetry

off Galveston Island is confined to a narrow band near shore and is composed of mostly straight and parallel contours, though there is a small seaward protrusion in the vicinity of San Luis Pass (upper left of Figure 15). Further offshore the grid contains two ridge features sloping up to the right (northeast); however, both are in fairly deep water.

High Island and Galveston Island GENESIS grids

A GENESIS grid is one-dimensional (1-D; a series of cells running along the axis of the beach). The layouts for the two GENESIS grids used in this study are shown in Figures 16 and 17. One model requirement is that near breaking-depth wave data be available at each cell boundary. Both GENESIS grids have cell widths of 500 ft (152.4 m), half that of the STWAVE cell dimensions. By aligning the STWAVE and GENESIS grids, nearshore wave data from the STWAVE output save stations were available at every other GENESIS cell wall. Wave data for the intervening GENESIS cell boundaries were obtained by linear interpolation.

The High Island grid is 400 cells long and extends from the western part of Sea Rim State Park (cell H1) to the vicinity of Crystal Beach (cell H400). The consolidated mud beach east of Sea Rim State Park was not included within the grid for the reasons discussed in Chapter 3. West of Crystal Beach, the beach is in the shadow of the Galveston Entrance Channel north jetty. It was not possible to realistically include the jetty in the STWAVE bathymetry, so GENESIS outputs in this region would not be expected to behave realistically.

The Galveston Island GENESIS grid starts near the Galveston Ship Channel south jetty (cell G1) and extends to near San Luis Pass on the right (cell G300). A prominent feature of this grid is the Galveston Seawall, which extends from grid cell G38 to G110.

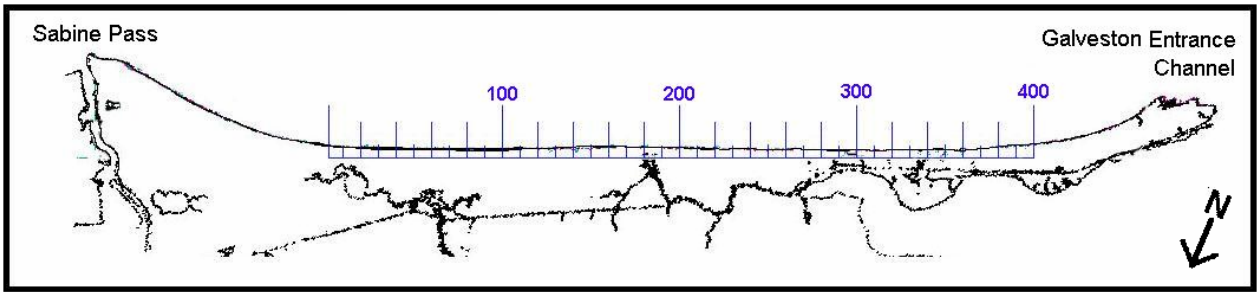

Figure 16. GENESIS grid for High Island.

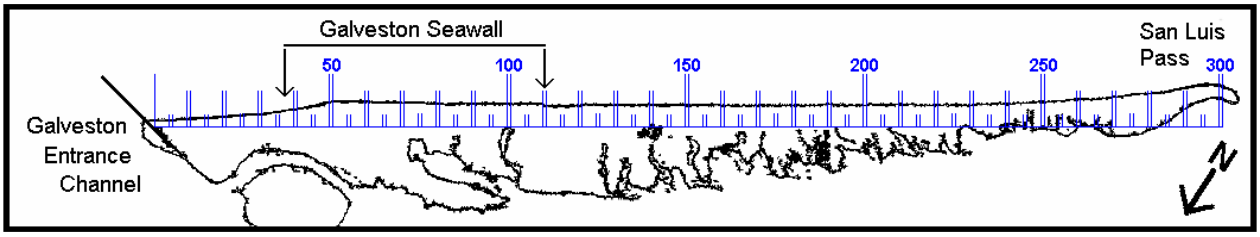

Figure 17. GENESIS grid for Galveston Island.

Important beach features within the GENESIS grids

Jetties and groins

Sabine Pass and the Galveston Entrance Channel have large jettied entrances that serve major commercial ports. The Sabine Pass jetties were first constructed in the 1880s. The east and west jetties have lengths of 25,000 and 22,000 ft (7,600 and 6,700 m), respectively. Jetty construction at the Galveston Entrance Channel first started in 1874, and construction of the present jetties occurred between 1887 and 1898. The north and south jetty lengths are 34,800 and 35,600 ft (10,600 and 10,900 m), respectively. Sargent and Bottin (1989) discuss the jetty history, while Morton (1977) and Mason (1981) discuss adjacent bathymetry changes at these two inlets. Although these jetties are not within either of the GENESIS grids, they have significant effects on the adjacent beaches.

Rollover Pass does not have jetties per se. However, depending upon the state of erosion of the beach, the sheet-pile walls that line the channel and associated terminal structures may extend into the gulf a few meters and act as short groins or jetties. San Luis Pass is an unjettied inlet.

The groin field in front of the Galveston Seawall is the only federal groin project within the study site. Originally constructed in 1939 and rehabilitated in 1970 (USACE 1971), the project consists of 15 groins between 10th Street and 61st Street in Galveston (Figure 18). Minimum crown elevations are 6.5 ft (1.9 m) above mean low tide, and most are 500 ft (150 m) in length. The GENESIS cell walls closest to these structures are listed in Table 6.

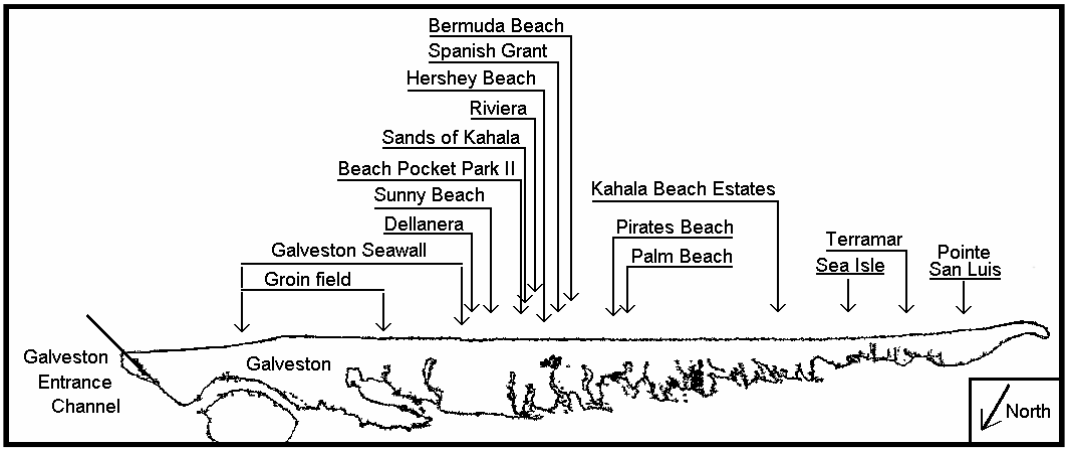

Figure 18. Locations of subdivisions on west Galveston Island.

Table 6. Locations of jetties and groins in GENESIS grids.

Name	Location	UTM at Beach		Seaward Length (m)	GENESIS Cell Wall
		Easting	Northing		
Sabine West Jetty	Sabine River	418939	3283435	4040	20,700 m east of H1
Rollover Pass East	Bolivar Peninsula	354708	3265099	5	H300
Rollover Pass West	Bolivar Peninsula	354708	3265099	5	H301
Galveston North Jetty	Port Bolivar	330109	3250349	7490	13,000 m west of H400
Galveston South Jetty	East Beach	332293	3245989	3500	250 m east of G1
Groin 1	10th St	327501	3242569	91	G38
Groin 2	16th St	326928	3241974	152	G43
Groin 3	20th St	326546	3241642	152	G46
Groin 4	24th St	326200	3241346	152	G50
Groin 5	27th St	325836	3241060	152	G52
Groin 6	29th St.	325628	3240913	152	G54
Groin 7	33rd St.	325281	3240675	152	G57
Groin 8	37th St.	324902	3240401	152	G60
Groin 9	39th St.	324619	3240201	152	G62
Groin 10	44th St	324318	3240011	152	G65
Groin 11	45th St.	323919	3239763	152	G68
Groin 12	52nd St	323555	3239510	152	G71
Groin 13	53rd St	323176	3239301	152	G73
Groin 14	57th St	322805	3239046	152	G76
Groin 15	61st St	322571	3238893	152	G78

Seawalls, geotextile tubes, and revetments

Construction of the Galveston Seawall was initiated after the devastating 1900 hurricane and, was completed to its present length of 9.7 miles (15.6 km) in 1963 (Figure 18). Of this length, 6.9 miles (11.1 km) directly face the gulf (from 10th St. westward). A little over half was built by Galveston County, the rest by USACE. For a history of the construction, see USACE (1981).

Prior to the 1915 storm, the beach was as much as 300 ft (90 m) wide in front of the seawall in places. However, that storm moved almost the entire beach into an offshore bar. Though some sand returned to the beach, it was never again as wide as before 1915 (USACE 1981). By 1934, most of the beach had largely disappeared, and the Beach Erosion Board of USACE began designing the groin field discussed above. This groin field has retained enough sand to prevent the seawall from being undermined, but the above-water portion of the beach has generally not been wide or attractive to bathers. Through the mid 1960s, there was some sand beach in front of much of the seawall, but this had largely disappeared by the early 1980s (Benton and Bolleter 1987).

Geotextile tubes are sediment-filled fabric sleeves, typically having a 12-ft (4-m) oval cross section, that are placed along the back of the beach or along the foredunes. They rest on a fabric scour apron that has sediment-filled anchor tubes along each edge and are typically placed in a shallow trench and covered with sand and natural beach vegetation. In recent years, geotextile tubes have been installed between Gilchrist and Caplen (one on each side of Rollover Pass), at Dellanera and at Pocket Park II, both near the west end of the Galveston Seawall, and at Pirates Beach (Gibeaut et al. 2002). For locations, see Figures 1 and 18. For GENESIS grid reference locations, see Table 7.

Other revetments have included a series of modest barriers in Jefferson County installed by the Texas Highway Department to protect State Highway 87 between High Island and Sea Rim State Beach. Installation and maintenance of these structures ended when the road was abandoned following Tropical Storm Chantal and Hurricane Jerry in 1989. Since then these structures have all almost entirely disappeared, along with much of the roadbed. (For a chronology, see USACE (1995).) In addition to these, numerous individual property owners have erected revetment-type structures of various designs and effectiveness to protect individual

beachfront lots. In erosion prone areas, many of these have failed. Some of the existing structure locations are noted in Table 7.

Table 7. Locations of seawalls, revetments, and geotubes in GENESIS grids.

Location	Name and Type	Date	Length (m)	UTM Coordinates of Ends			GENESIS Cells	
				E/W	Easting	Northing	End No.	No. of
Bolivar Peninsula	Gilchrist Geotube	7/2001	3,446	E	358346.05	3266663.81	H274	26
				W	354708.02	3265098.75	H299	
Bolivar Peninsula	Caplen Geotube	6/2001	4,339	E	354639.87	3265077.46	H301	29
				W	350595.51	3263362.25	H329	
City of Galveston	Galveston Seawall	1906-1963	11100	E	327580.69	3242595.05	G38	73
				W	318408.61	3236238.91	G110	
West Beach	Dellanera Geotube	6/2000	459	E	318211.89	3236233.92	G112	3
				W	317824.03	3235993.33	G114	
West Beach	Concrete rubble		145	E	317725.54	3235880.30	G116	1
				W	317596.44	3235812.16	G116	
West Beach	Pocket Park II Geotube	12/1999	152	E	315833.94	3234689.18	G130	1
				W	315733.31	3234624.75	G130	
West Beach	Riviera Geotube	1/2001	146	E	315196.04	3234249.80	G135	1
				W	315068.99	3234167.75	G135	
West Beach	Pirates Beach Geotube	10/1999	2,499	E	312741.20	3232631.01	G155	16
				W	310643.67	3231268.95	G170	
West Beach	Houses/bulkheads on beach		175	E	299569.17	3223989.87	G258	1
				W	299535.31	3223816.78	G258	

Beachfills

In recent years, numerous beachfill projects have been conducted within the study area. The information summarized in Table 8 was compiled by Neil McLellan of Shiner-Moseley, Inc. Some of these projects are ongoing, and additional projects are planned.

Table 8. Locations of beach fills in GENESIS grids. (TBD = to be determined)

Location	Volume	Date	Length (m)	UTM Coordinates of Ends			GENESIS Cells	
				E/W	E	N	End No.	No. of
Gilchrist and Caplen Beach	33,700	2000	5,377	E	357096.00	3266127	H417	35
				W	352197.00	3264037	H452	
East side of Rollover Pass	229,500	2000	1,609	E	356269.00	3265779	H423	11
				W	354734	3265093	H434	
Gilchrist East Subdivision	13,600	2001	2,170	E	358218.00	3266595	H409	14
				W	356269.00	3265779	H423	
East side of Rollover Pass	229,500	2002	914	E	355561.00	3265474	H428	6
				W	354734	3265093	H434	
West Side of Rollover Pass	143,800	1997	point		354592.00	3265049	H435	1
West Side of Rollover Pass	133,900	1999	point		354592.00	3265049	H435	1
West Side of Rollover Pass	105,900	2000	914	E	354592.00	3265049	H435	6
				W	353721.00	3264723	H441	
West Side of Rollover Pass	96,400	2001	914	E	354592.00	3265049	H435	6
				W	353721.00	3264723	H441	
Caplen Beach Subdivision	10,900	2001	1,747	E	353721.00	3264723	H441	11
				W	352197.00	3264015	H452	
Galveston Seawall	11,500	1985	457	E			G	3
				W			G	
Galveston Seawall	382,500	1992	1,829	E			G	12
				W			G	
Galveston Seawall	543,200	1995	5,791	E			G	38
				W			G	
Seascape and Dellanera	3,100	2000	483	E	318212	3236234	G112	3
				W	317824	3235993	G115	
Sunny Beach Subdivision	TBD	2003	201	E	317196.00	3235507	G120	1
				W	317058	3235422	G121	
Beach Pocket Park No. 2	900	1999	148	E	315834	3234689	G130	1
				W	315733	3234625	G131	
Sands of Kahala Subdivision	TBD	2003	419	E	315682.00	3234486	G132	3
				W	315238	3234239.00	G135	
West Beach Grand and Riviera	800	2001	142	E	315196	3234250	G135	1
				W	315069	3234168	G136	
West Beach Grand and Riviera	TBD	2003	140	E	315196	3234250	G135	1
				W	315069	3234168	G136	
Hershey Beach Subdivision	TBD	2003	280	E	315036.00	3234064	G137	2
				W	314791	3233910	G139	
Spanish Grant Subdivision	4,500	2001	526	E	314499.00	3233742	G140	3
				W	314253.00	3233573	G143	

Location	Volume	Date	Length (m)	UTM Coordinates of Ends			GENESIS Cells	
				E/W	E	N	End No.	No. of
Spanish Grant Subdivision	TBD	2003	532	E	314499.00	3233742	G140	3
				W	314253.00	3233573	G143	
Bermuda Beach Subdivision	15,900	2001	948	E	314253.00	3233573	G143	6
				W	313500	3233065	G149	
Bermuda Beach Subdivision	TBD	2003	945	E	314253.00	3233573	G143	6
				W	313500	3233065	G149	
Pirates' Beach Subdivision	14,900	1999	2,373	E	312741	3232631	G155	16
				W	310644	3231269	G170	
Pirates' Beach Subdivision	TBD	2003	1640	E	312741	3232631	G156	11
				W	310644	3231269	G167	
Palm Beach Subdivision	TBD	2003	349	E	311190.00	3231575.00	G166	2
				W	310929.00	3231414.00	G168	
Pirates' Beach West Subdivision	TBD	2003	393	E	310929.00	3231414.00	G168	2
				W	310644	3231269	G170	
Kahala Beach Estates	TBD	2003	351	E	305190.00	3227644	G214	2
				W	304944	3227490	G216	
Kahala Beach Estates	TBD	2003	1,344	E	305574	3227889	G211	9
				W	304438	3227152	G220	
Sea Isle Subdivision	7,700	2001	1,286	E	302543.00	3225880	G235	8
				W	301529.00	3225204	G243	
Sea Isle Subdivision	TBD	2003	2,612	E	303050.00	3226234	G231	17
				W	300915.00	3224759	G248	
Terramar Subdivision	15,200	2001	869	E	300178.00	3224237	G254	6
				W	299425	3223699	G260	
Terramar Subdivision	TBD	2003	841	E	300178.00	3224237	G254	6
				W	299425	3223699	G260	
Pointe San Luis Subdivision	10,200	2001	399	E	297351.00	3222133	G277	3
				W	296982	3221856	G280	

GENESIS locations of public beachfront

Most of the beachfront property between Sabine Pass and High Island is in public ownership, including Texas Point National Wildlife Refuge (NWR) Sea Rim State Beach, and McFaddin NWR (Figure 1a). Some private beachfront ownership occurs between Texas Point NWR and Sea Rim State Beach and also near High Island. Most of the beachfront in the rest of the study area is in private ownership. Exceptions include East Beach between the Galveston Entrance Channel south jetty and the Galveston

Seawall, Galveston Island State Park between Pirates Beach and Jamaica Beach on Galveston Island, and the semi-private Audubon Shorebird Sanctuary adjacent to the north jetty of the Galveston Entrance Channel. The GENESIS boundaries of these public lands are listed in Table 9.

Table 9. Locations of public property in GENESIS grids.

Name	UTM Coordinates of Ends			GENESIS
	East/West	Easting	Northing	Cell Wall Number
Texas Point NWR	E	418638	3283437	20,400 m east of H1
	W	409264	3283764	11,900 m east of H1
Sea Rim State Park	E	405095	3283975	8,300 m east of H1
	W	396477	3282423	H3
McFaddin NWR	E	396477	3282423	H3
	W	371783	3272128	H179
Bolivar Flats Audubon Shorebird Sanctuary	E	332748	3251502	10,100 m west of H400
East Beach	E	332292.8	3245989	G1
	W	327500.77	3242569.4	G38
Galveston Island State Park	E	310582.5	3231110	G171
	W	308517.8	3229803.5	G187

Sand transport through Rollover Pass

Sediment that is lost to the interior of Rollover Pass is a sink that should be accounted for in the High Island grid. Several researchers have published estimates of these yearly amounts (Table 10). Unfortunately, due primarily to different methodologies and assumptions, the estimates vary widely, by well over an order of magnitude.

Table 10. Yearly beach sand loss to the interior of Rollover Pass.

Researcher	m^3/yr	m^3/hr
USACE (1959)	14,000	1.60
Mason (1981)	20,000	2.28
Bales and Holley (1989)	6,700-20,000	0.76-2.28
Bales and Holley (1989)	185,000	21.10
Bales and Holley (1989)	221,000	25.20
Parchure et al. (2000)	100,000	11.40
PIE (2001)	190,000	21.66

5 STWAVE/GENESIS Wave and Wind Climatology

Characterization of waves

Waves are the dominant driving mechanism in longshore sediment transport and are a primary input to STWAVE and GENESIS. A 10-year hindcast (1990-1999) of wave heights, periods, and directions (at hourly intervals) and 2-D spectra (at 3-hr intervals) was obtained from two WIS stations located in 20 m of water depth; WIS station 87 off High Island and WIS station 78 off Galveston Island (Table 11 and Figure 19). Wave direction data from these WIS stations were referenced to the local shore normal as shown in Figure 20. The zero deg wave direction is 157 deg azimuth for WIS station 87 (High Island) and 147 deg azimuth for WIS station 78 (Galveston). Positive wave angles are those approaching the coast from the east or northeast (from the left of shore normal for a person standing on the beach looking offshore).

The wave climatology from these stations has been characterized by binning the significant wave heights, peak spectral wave periods, and vector mean wave directions at the peak spectral frequencies, as shown in Figures 21-24. Appendix A lists definitions of the wave period and direction parameters.

Table 11. Locations of wave, wind, storm, and water level input data stations.

Gage	Latitude deg N	Longitude deg W	Northing UTM (m)	Easting UTM (m)	Depth (m)
WIS 71	29.083	94.833	3218606.271	321560.691	15.00
WIS 72	28.833	94.750	3190778.326	329263.110	20.00
WIS 78	28.833	94.417	3190344.744	361788.412	20.00
WIS 81	28.916	94.250	3199395.840	378147.376	22.00
WIS 85	29.416	94.083	3254638.171	394906.088	13.00
WIS 87	29.000	93.917	3208331.902	410714.695	20.00
WIS 1078	29.000	94.750	3209247.954	329535.970	18.00
NDBC 42035	29.250	94.410	3236507.834	362990.578	16.00
WLS 09	29.165	94.989	3227954.888	306579.632	0.27
WLS 17	29.495	94.523	3263843.734	352346.203	3.00
WLS 21	29.617	94.202	3276938.194	383576.051	0.22

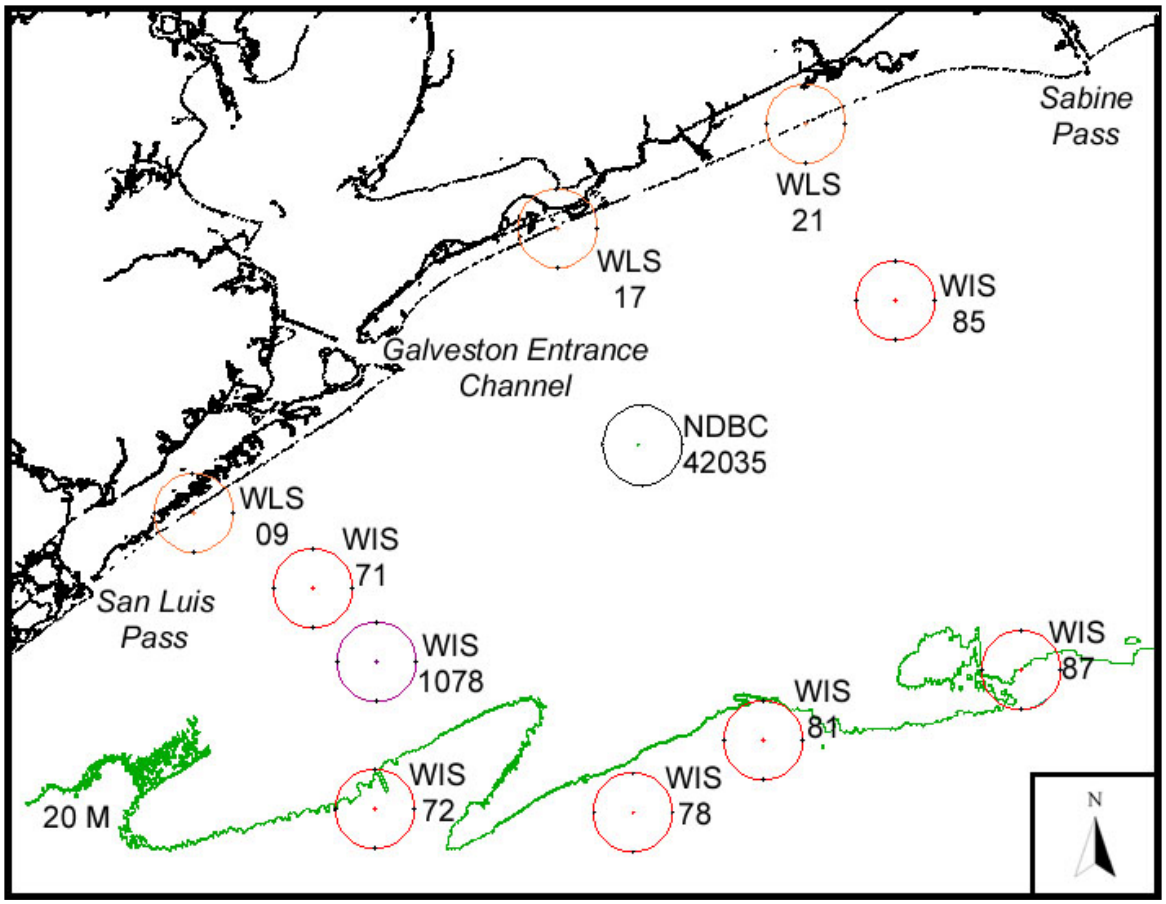

Figure 19. Locations of wave, wind, and water level data sources.

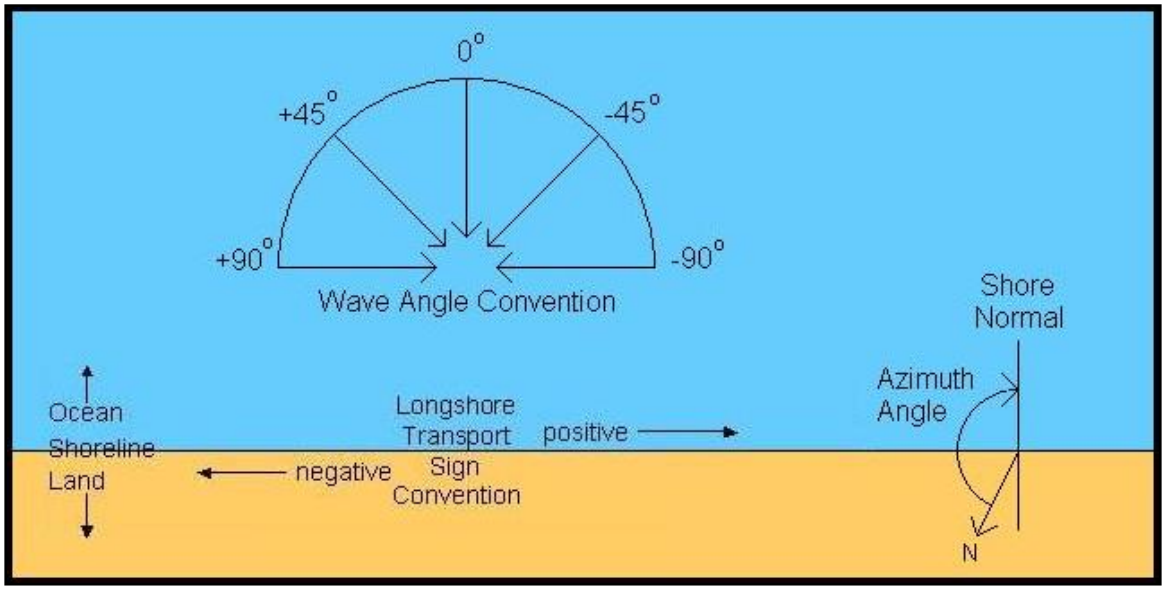

Figure 20. Angle and sign convention definition sketch.

Figure 21 is a histogram of WIS station 87 (High Island) wave heights, periods, and directions shown as percentage occurrence. Bright yellow bins indicate those occurring most frequently and bright blue, least frequently. Figure 22 is the corresponding block diagram of wave height versus wave direction. These figures show that average wave heights are around a meter, average wave periods are 4 to 5 seconds, and the predominant direction of wave approach is from the left of shore normal (from an easterly direction). The waves for WIS station 78 (Galveston Island), Figures 23 and 24, are similar; however, the wave direction is less predominantly from the east and the 10-degree angle bin with the most waves is the one just to the right (south) of shore normal. This difference is partially due to the 10-deg difference in reference shoreline orientation between the two stations.

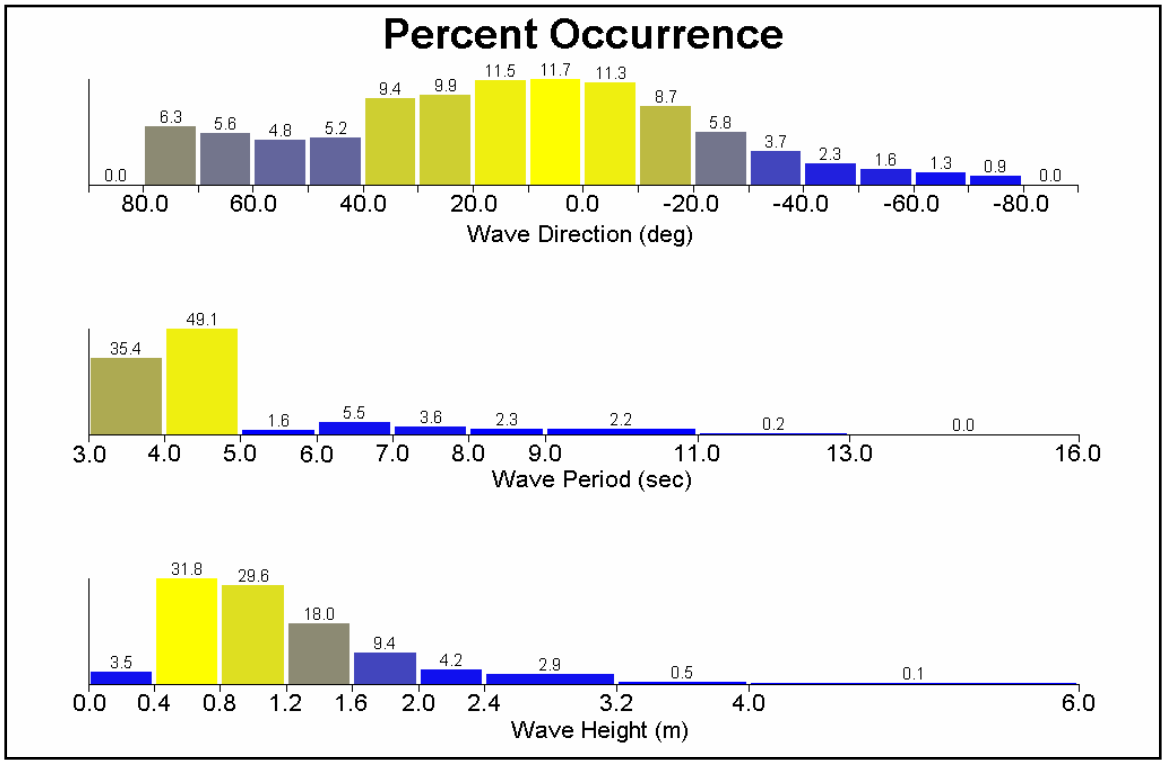

Figure 21. Histogram of wave heights, periods, and directions for 1990-1999 WIS station 87 data, shore-normal: 157 deg.

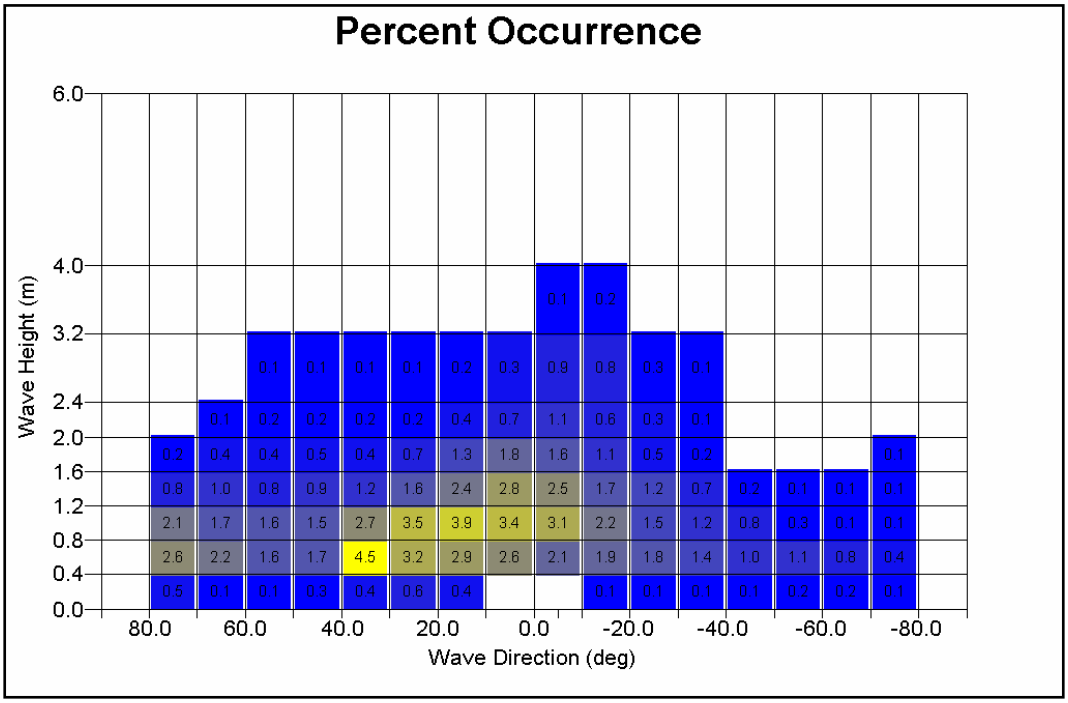

Figure 22. Block diagram of wave height versus direction for 1990-1999 WIS station 87 data, shore-normal: 157 deg.

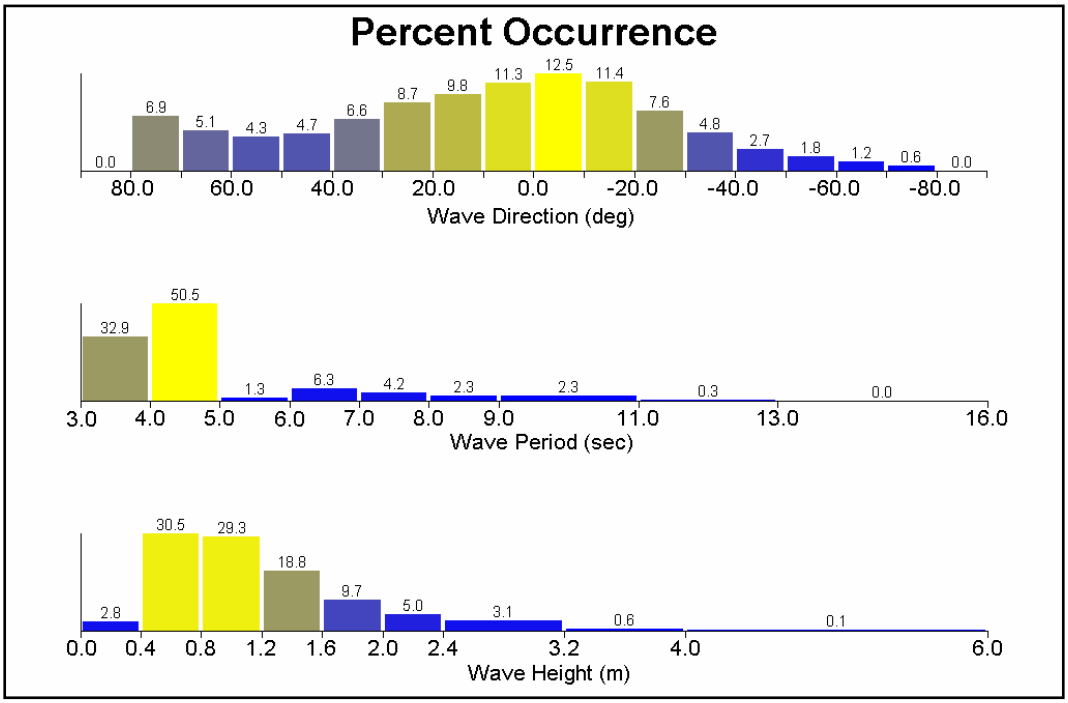

Figure 23. Histogram of wave heights, periods, and directions for 1990-1999 WIS station 78 data, shore-normal: 147 deg.

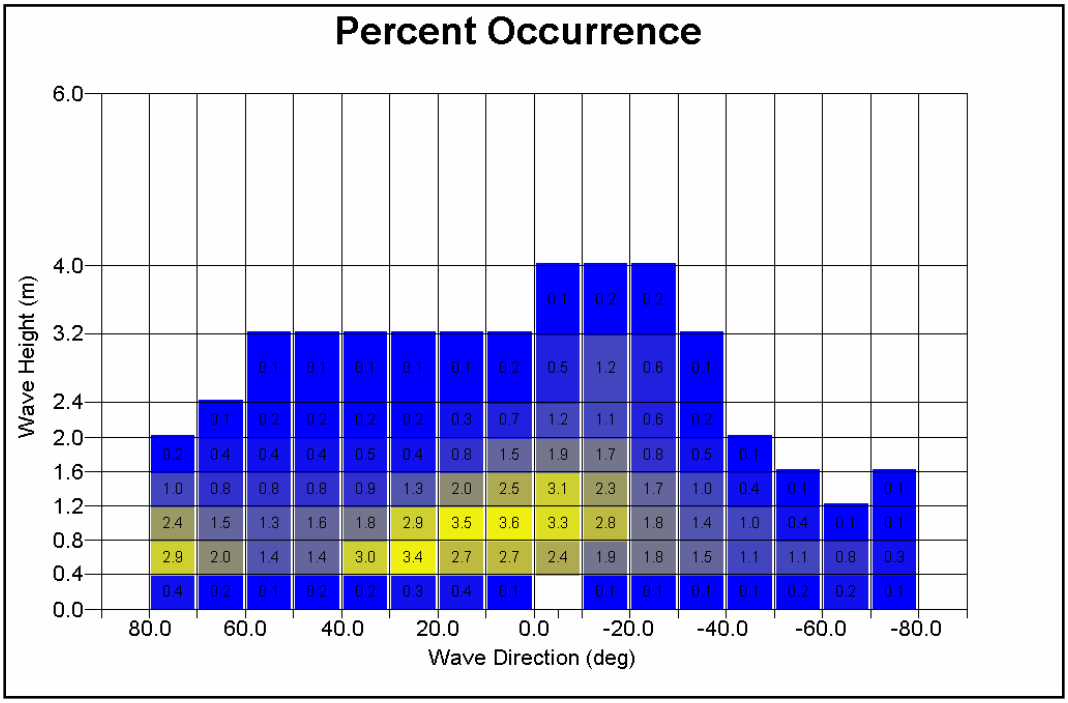

Figure 24. Block diagram of wave height versus direction for 1990-1999 WIS station 78 data, shore-normal: 147 deg.

Measured directional wave data are also available from the National Data Buoy Center (NDBC) Buoy 42035 located in 16 m water depth (Figure 19) for the time interval between mid 1998 through 2001 (with gaps). Waves from this source (Figures 25 and 26) were used for comparison with the data from WIS station 78. This analysis used the shore normal direction of Galveston Island, 147 deg azimuth. Typical wave heights and periods measured at the buoy are similar to those obtained from the WIS stations, though the buoy measured wave directions are shifted more from the right of shore normal.

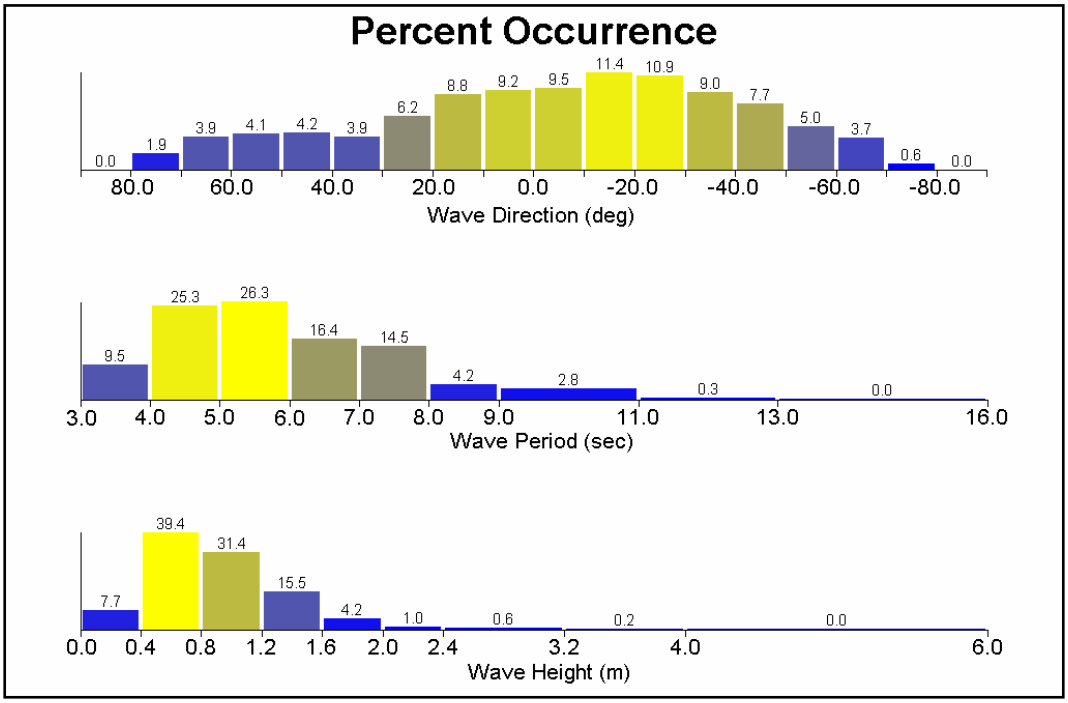

Figure 25. Histogram of wave heights, periods, and directions for 1998-2001 NDBC Buoy 42035 data, shore-normal: 147 deg.

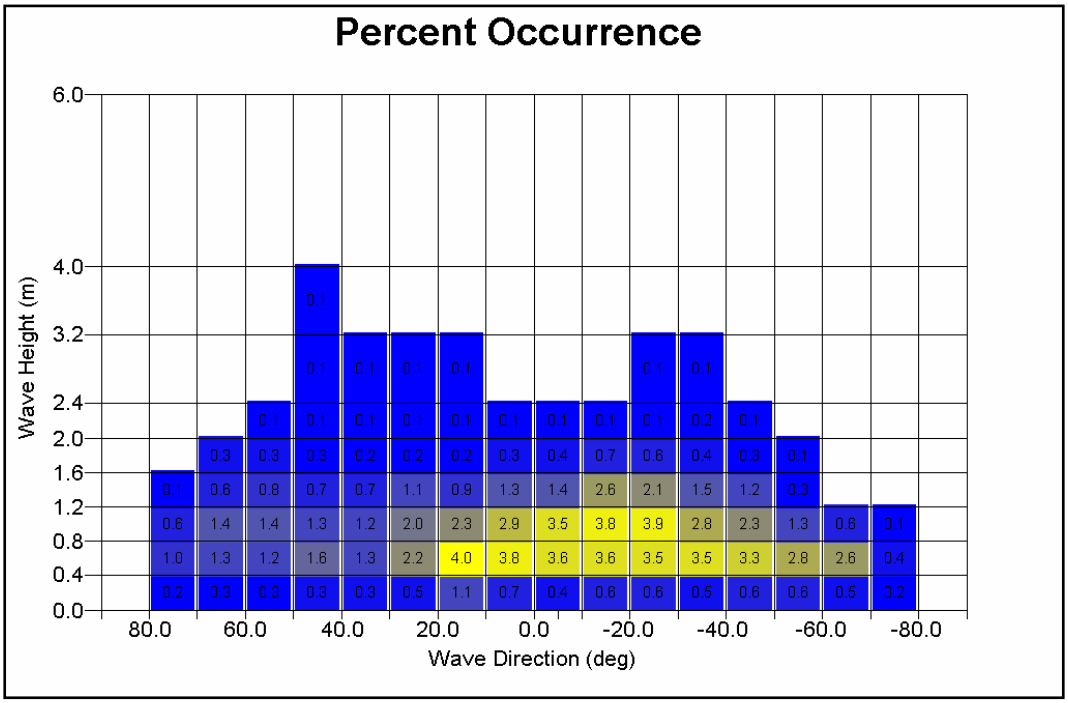

Figure 26. Block diagram of wave height versus direction for 1998-2001 NDBC Buoy 42035 data, shore-normal: 147 deg.

Characterization of winds

Nearshore winds can have two effects on longshore sediment transport rates. First, they can be an important wave generating mechanism within the STWAVE grid where the offshore waves are transformed to near-breaking depths. With the mild wave conditions that characterize the Gulf of Mexico, this mechanism is likely to be more important than at typical Atlantic or Pacific coast study sites. Also, the cross-shore STWAVE grid distances in this study, 45 miles (73 km) and 36 miles (58 km) for High Island and Galveston Island, respectively, are larger than for typical studies and allow significant opportunity for the local windfield to affect the waves. STWAVE is capable of including locally wind-generated waves in its transformation procedure, but due to the added complexity and additional computation time, this step is usually omitted. Secondly, the local winds can directly modify longshore currents within the surf zone. Several researchers, including Price (1947, 1951, 1954), Hall (1976), USACE (1983), and Bales and Holley (1989), have all commented on the important influence of local winds to the understanding of sediment transport rates and directions along the northeastern Texas coastline.

Local wind data offshore of High Island and Galveston Island for the years 1990-1999 were obtained from WIS station 85 and WIS station 71, respectively (Table 11, Figure 19). The winds at WIS station 71 are characterized in the block diagram of speed versus direction shown in Figure 27. In this figure, the wind speed is given in meters per second. A meter per second is approximately 2 miles per hour or 2 knots. For reference, a wind speed of approximately 10 knots (5 m/s) over a water body will start to cause noticeable whitecapping. Figure 27 shows that average wind speeds are approximately 7 m/s.

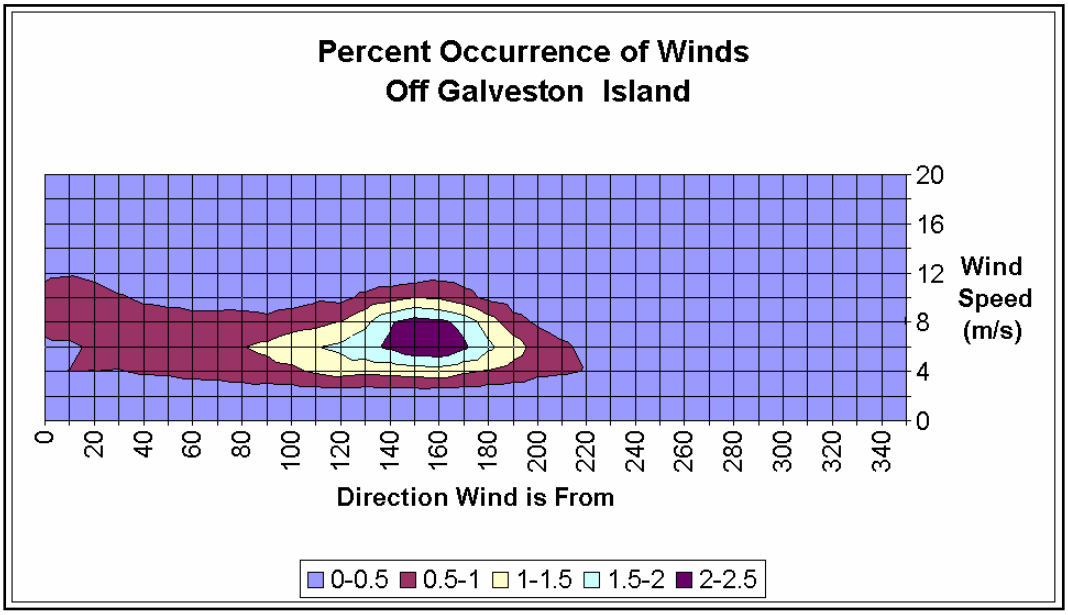

Figure 27. Block diagram of wind speed versus direction for 1990-1999 WIS station 71 data.

This figure indicates that the winds most commonly blow on-shore (Galveston Island azimuth is 147 deg). The most frequently occurring winds blow from an angle that is slightly south of shore-normal. These winds will produce waves that drive transport toward the northeast. However, because of the skewed distribution of winds from the northeast, the mean onshore wind direction (the average of all winds between ±80 degrees of shore-normal) is 7 degrees to the east of shore-normal. The wind stress weighted mean wind direction is also 7 degrees east of shore-normal. This wind climatology will, therefore, locally generate waves that tend to drive the longshore transport toward the southwest. The winds from WIS station 85 off High Island are similar.

Figures 28 and 29, which are subsets of Figure 27 shown at an expanded scale, indicate the distribution of those winds that blow within approximately ±30 degrees of the axis of the Galveston shoreline (57 deg and 237 deg, respectively). These winds are the most effective in generating wind-driven longshore currents in the surf zone. These figures indicate that winds from the northeast are more frequent than those from the southwest (20 percent versus 5 percent of the time) and that the average wind speed from the northeast is stronger (average of 6.5 versus 5 m/s). As a result, these local winds will produce longshore currents in the surf zone that are expected to help drive the yearly net longshore transport direction more to the southwest.

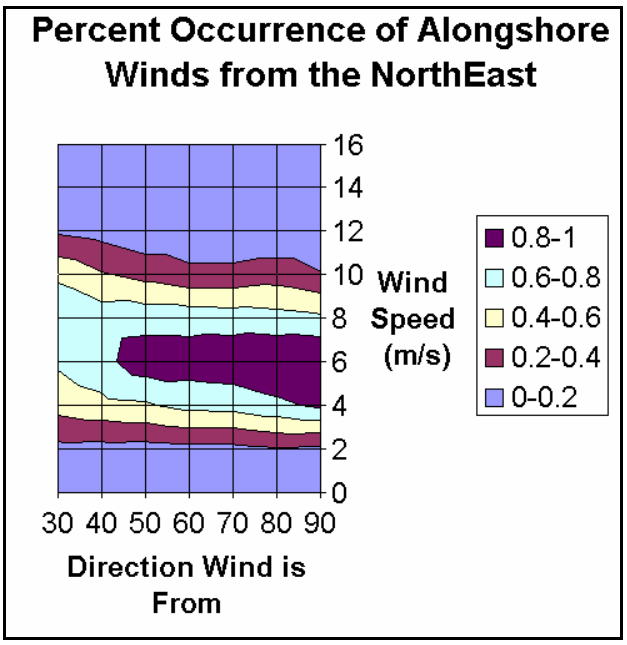

Figure 28. Winds from the northeast (1990-1999 WIS station 71 data).

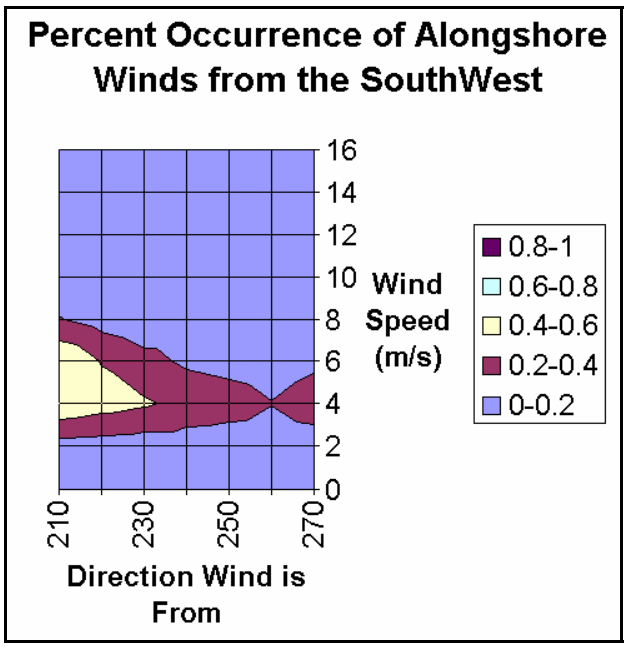

Figure 29. Winds from the southwest (1990-1999 WIS station 71 data).

6 STWAVE/GENESIS Methodology and Calibration

Estimates of longshore sediment transport rates

Simplified sediment transport rate calculations using WIS data

Early in this study, prior to performing the computationally intensive STWAVE transformations, it was useful to obtain general estimates of the average annual transport rate magnitudes and directions. This preliminary analysis helped guide the direction and focus of the study. The specific details of the simplified approach and equations used to obtain these estimates are outlined in Gravens (1989). The calculation procedure used the assumptions of a single shoreline orientation, straight and parallel contours, linear wave theory, a breaking depth criterion, Snell's Law, and conservation of wave energy prior to breaking. Under these conditions, there is no variation in wave height and angle along the beach for a given offshore wave condition and thus no spatial variation in the transport rate. The procedure involved computing breaking wave conditions for each event in the 10-yr WIS offshore time series under the assumptions stated and estimating the resulting longshore sand transport rate using the CERC formula. Data were combined by years to obtain average annual transport rates to the east and west, along with net and gross rates. The temporal distribution of transport between percentages of time of eastward, westward, and no-transport were also recorded.

Potential transport estimates for High Island and Galveston Island are shown in Tables 12 and 13. These results were compiled using peak spectral wave periods, vector mean wave directions at the peak spectral frequency, and a CERC formula K value of 0.4. (The K parameter in the CERC formula is the same as the K_1 parameter in GENESIS. K values of 0.4 and 0.7 are two commonly used default values. K values are directly proportional to the gross transport rate but do not alter the sign of the net transport rate. The final value used in this study would be based upon the GENESIS calibration.) The sign convention used in this report is that longshore transport to the west or southwest (toward Mexico) is positive (Figure 20). For High Island (Table 12), about 65 percent of the time that transport occurs, it is to the west. The estimated average net transport rate is 75,000 m^3/yr to the west, in general agreement with previous studies.

For Galveston Island (Table 13), the transport is to the west about 58 percent of the time that transport occurs. However, the estimated average net transport rate is 135,000 m^3/yr to the east. This direction is opposite of that reported from previous studies, as discussed in Chapter 2 (Table 1). Tables 12 and 13 show estimated average gross transport rates of 603,000 and 860,000 m^3/yr for High Island and Galveston Island, respectively.

Table 12. Preliminary yearly transport rate estimates, High Island, 1990-1999 WIS station 87 wave data.

Year	Average Transport Rate m^3/yr				Percent to East	Percent to West	Percent Calm
	To East	To West	Net West	Gross			
1990	-207,000	338,000	131,000	545,000	26.8	53.9	19.4
1991	-271,000	413,000	142,000	684,000	26.7	54.5	18.8
1992	-168,000	273,000	105,000	441,000	28.4	49.4	22.2
1993	-197,000	345,000	148,000	542,000	29.3	48.6	22.1
1994	-278,000	281,000	3,000	559,000	24.6	56.3	19
1995	-279,000	355,000	76,000	634,000	23.2	53.6	23.2
1996	-351,000	293,000	-58,000	644,000	33.1	48.3	18.6
1997	-246,000	347,000	101,000	593,000	30.3	45.2	24.5
1998	-281,000	504,000	223,000	785,000	30.8	51.5	17.7
1999	-361,000	245,000	-116,000	606,000	27.2	50.5	22.3
AVE	-263,000	339,000	75,000	603,000	28.1	51.2	20.8
ST D	62,000	75,000	103,000	92,000	3.0	3.4	2.3

While for both study areas the majority of time transport is to the west, the estimated annual net transports are in opposite directions. This direction difference is primarily due to the 10-degree difference in shoreline orientation between the two grids. Figures 30 and 31 plot the directional distribution of the most energetic 20 percent of the waves, those with wave heights of 1.6 m or greater. (The corresponding histograms for the total wave fields are shown in Figures 21 and 23, respectively.) These largest waves tend to dominate the longshore transport. For the High Island grid (Figure 30) the directional distribution of the largest waves is very nearly balanced with about 3 percent more waves arriving from northeast of shore-normal than from southwest. However, on Galveston Island (Figure 31), due to the different shoreline orientation, about 20 percent more of the largest waves arrive from the southwest than from the east. It

is these occasional large southerly wave events that shift the direction of net transport on Galveston Island to the northeast.

Table 13. Preliminary yearly transport rate estimates, Galveston Island, 1990-1999 WIS station 78 wave data.

Year	Average Transport Rate m³/yr				Percent to East	Percent to West	Percent Calm
	To East	To West	Net West	Gross			
1990	-457,000	340,000	-117,000	797,000	34.2	49.3	16.5
1991	-507,000	453,000	-54,000	960,000	34.5	49.6	15.9
1992	-315,000	307,000	-8,000	622,000	34.2	47.0	18.8
1993	-380,000	347,000	-33,000	727,000	35.8	45.6	18.6
1994	-475,000	326,000	-149,000	801,000	30.2	55.6	14.2
1995	-496,000	372,000	-124,000	868,000	30.7	50.5	18.8
1996	-645,000	315,000	-330,000	960,000	42.6	40.7	16.7
1997	-426,000	382,000	-44,000	808,000	36.4	42.8	20.9
1998	-598,000	533,000	-65,000	1,131,000	38.5	46.3	15.3
1999	-681,000	252,000	-429,000	933,000	33.4	47.9	18.7
AVE	-498,000	362,000	-135,000	860,000	35.0	47.5	17.4
ST D	115,000	79,000	137,000	142,000	3.6	4.2	2.0

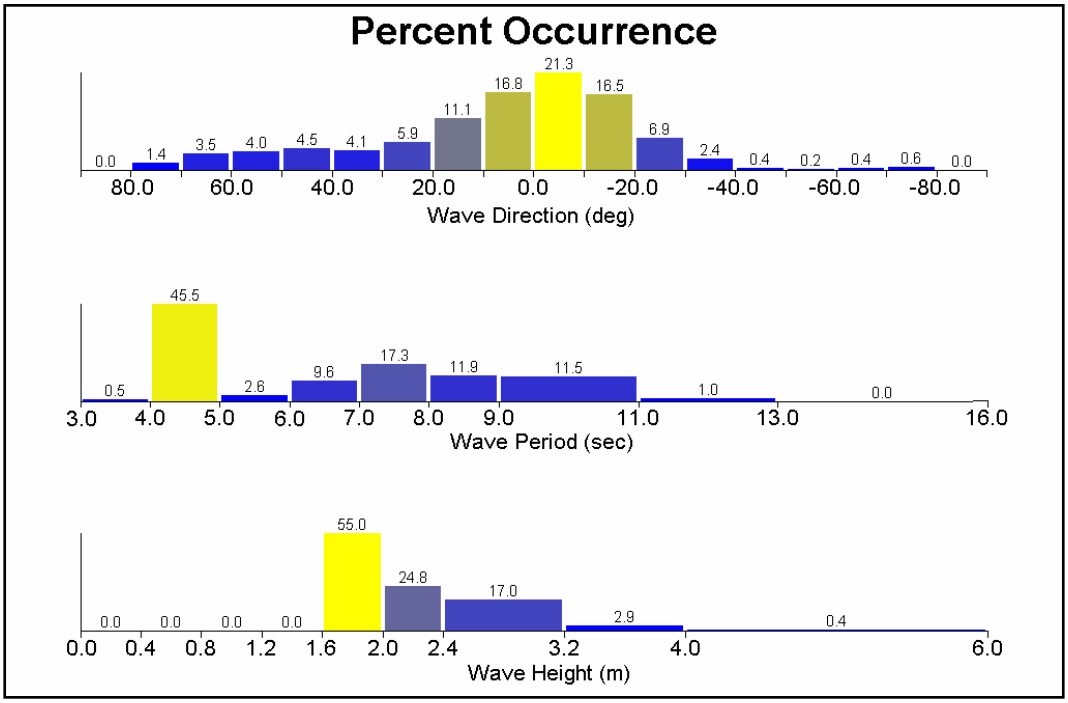

Figure 30. Highest 20 percent histogram of wave heights, periods, and directions for 1990-1999 WIS station 87 data, shore-normal: 157 deg.

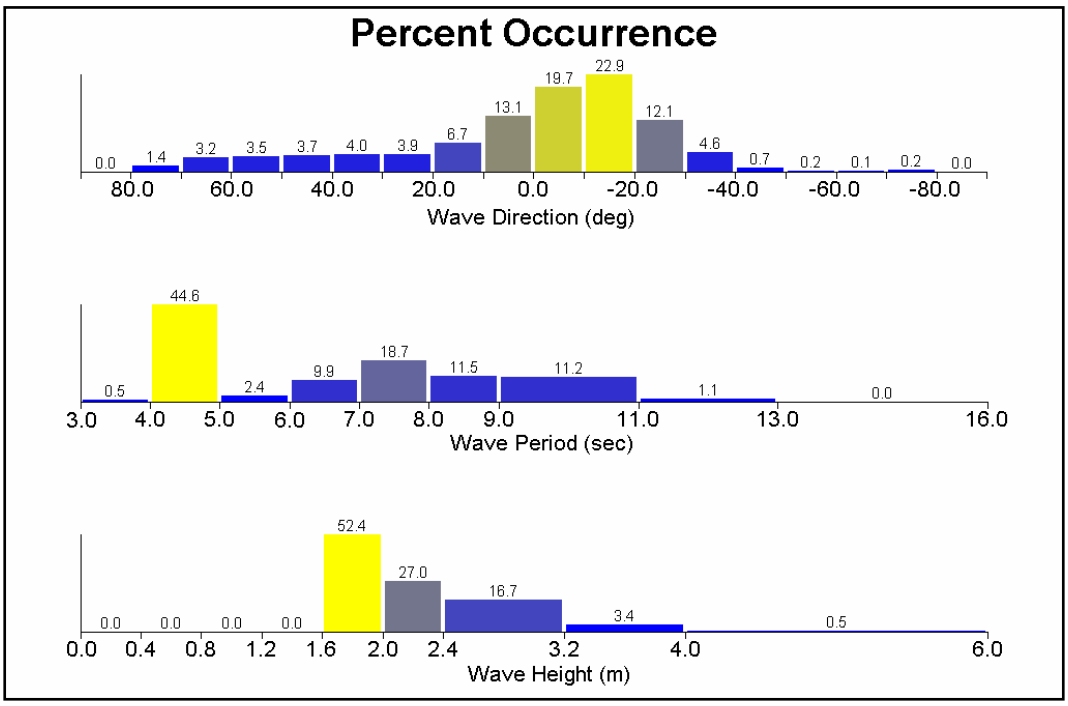

Figure 31. Highest 20 percent histogram of wave heights, periods, and directions for 1990-1999 WIS station 78 data, shore-normal: 147 deg.

The rest of the analysis presented in this section of the report was performed to help interpret the apparent disparity between the calculated direction and the commonly assumed direction of net sediment transport on Galveston Island and to develop a methodology for the final analysis.

Comparison of WIS station 78 and NDBC Buoy 42035 data

Wave data were obtained from other sources to determine if they also predicted net northeastward transport rates along Galveston Island. Measured directional wave data were available from NDBC Buoy 42035 from mid 1998 through 2001. Because of significant gaps in the data, yearly transport rate estimates are not directly comparable with those from the WIS stations. However, the average rates for the whole time period are given in Table 14. Calculations for this table used a shoreline orientation of 147 deg (Galveston Island orientation), the peak spectral wave period, the vector mean wave direction at the peak spectral frequency, and a CERC formula K value of 0.4. Values are similar to those given in Table 13 for Galveston Island derived from WIS station 78 data, except that a majority of time the transport direction is to the northeast.

Table 14. Preliminary transport rate estimates, Galveston Island, 1998-2001 NDBC Buoy 42035 wave data.

1998-2001	Average Transport Rate m³/yr				Percent to East	Percent to West	Percent Calm
	To East	To West	Net West	Gross			
Ave	-314,000	279,000	-112,000	670,000	52	37.9	10.2

A more detailed comparison of the NDBC buoy and WIS data was made during the time period from mid 1998 through 1999 when simultaneous information was available. Figure 32 shows the cumulative transport rate for both buoy and hindcast, along with their running difference. The transport rates shown in this figure and in Figure 36 below were calculated using the procedure presented at the beginning of this chapter, a shoreline orientation of 147 deg, the peak spectral wave period, the vector mean wave direction at the spectral peak frequency, and a CERC formula K value of 0.7. This figure shows numerous times when both data sets predict similar significant transport events. However, each data set also includes times of significant transport that are not reflected in the other set.

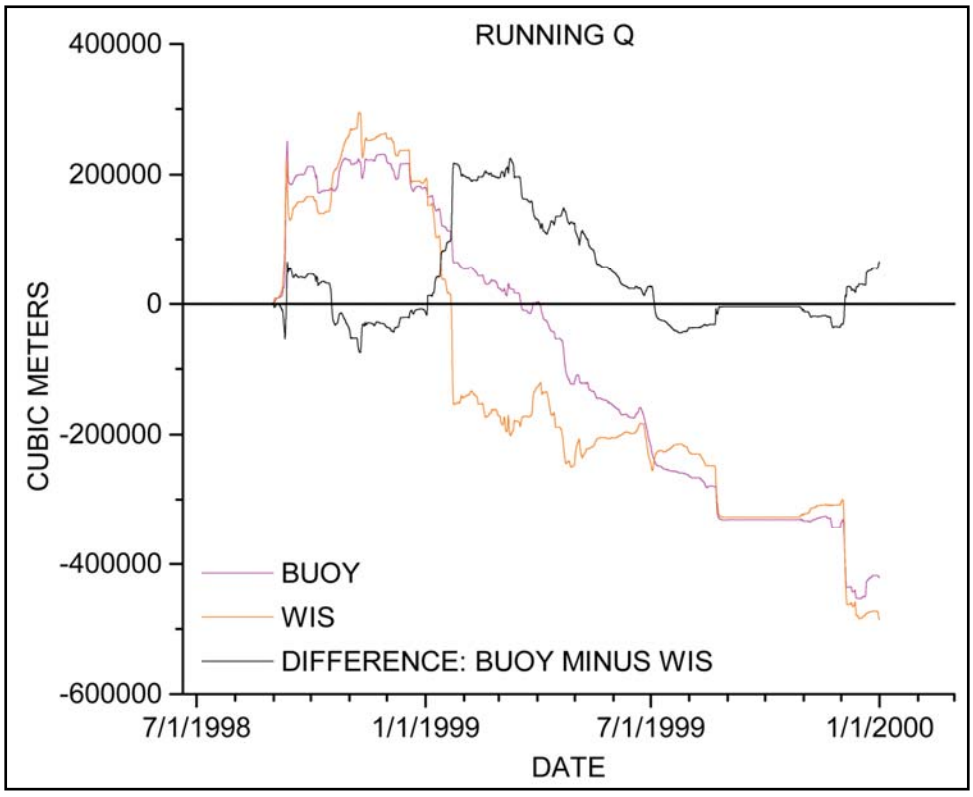

Figure 32. Cumulative transport estimates from NDBC Buoy 42035 and WIS station 78 1998-1999 data.

Figures 33-35 show the differences in the buoy and WIS wave heights, periods, and directions during the 1998-1999 time period. On average the measured buoy wave height data (Figure 33) are about a quarter meter lower than the WIS data. The spectral peak period differences (Figure 34) show little bias, but the vector mean wave direction at the peak spectral frequency values (Figure 35) show the buoy data to be an average of about 20 degrees more clockwise than the WIS data. Given the effect that a change of a few degrees can make in the net transport rate (discussed below), this is a much more important disagreement than are the differences in wave height and period. If this difference were used to adjust the WIS wave angles, it would make the waves come more from the south, generating a larger northeastward net transport rate.

Figure 36 shows the difference in transport rate predicted by the buoy and WIS data. Rather than there being a constant offset (bias) between the estimates, the dominant difference is the frequent spikes in this plot that indicate that large transport events are being predicted by one data set but not the other. These spikes correspond to the locations where the cumulative rate differences shift in Figure 32.

Additional comparisons of WIS and NDBC buoy data are given in Appendix C. These comparisons are made between NDBC Buoy 430025 and a co-located WIS station, rather than between the buoy and WIS station 78 (which are 29 miles (46 km) apart), and use both directional data (directional buoy data available after July 1998) and non-directional data (non-directional buoy data available from May 1993). The Appendix C results generally show close agreement between the measured and hindcast data.

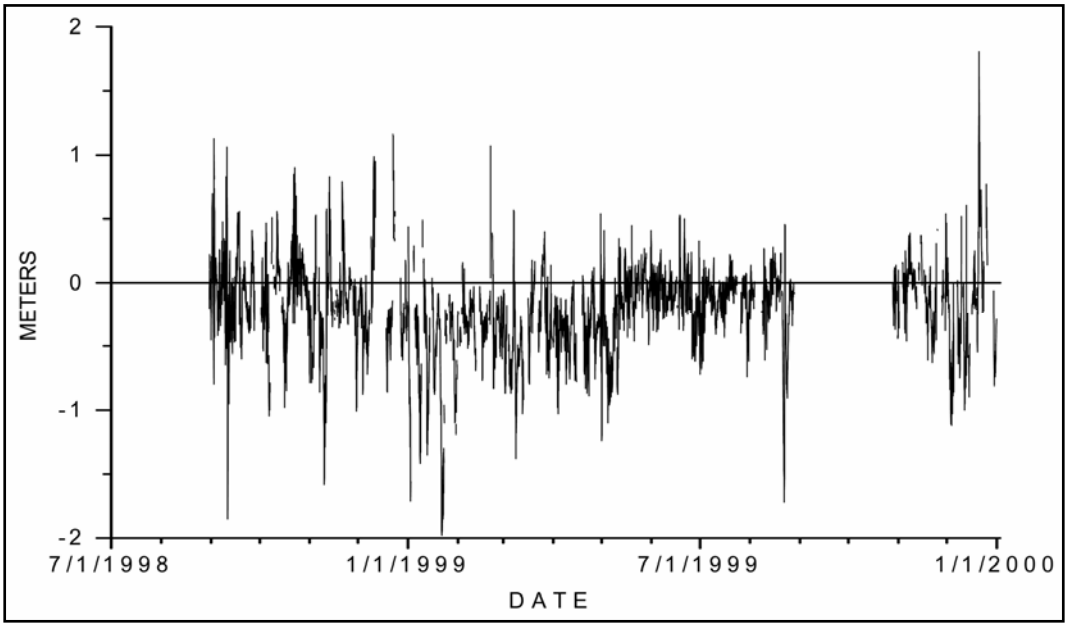

Figure 33. Wave height difference plot, NDBC Buoy 42035 minus WIS station 78 data.

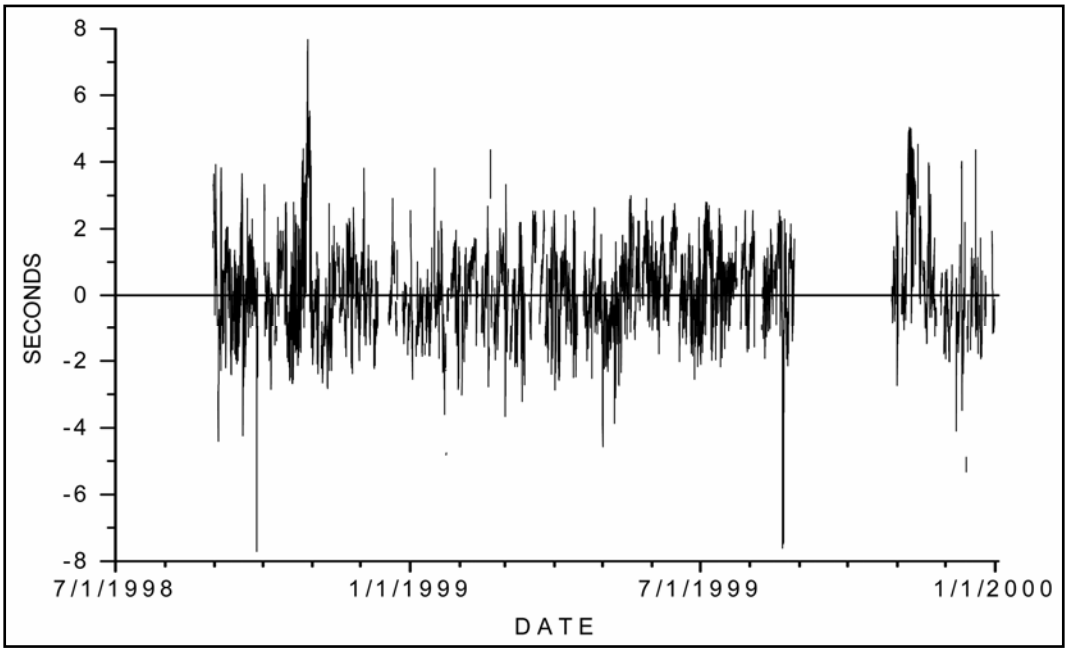

Figure 34. Peak period difference plot, NDBC Buoy 42035 minus WIS station 78 data.

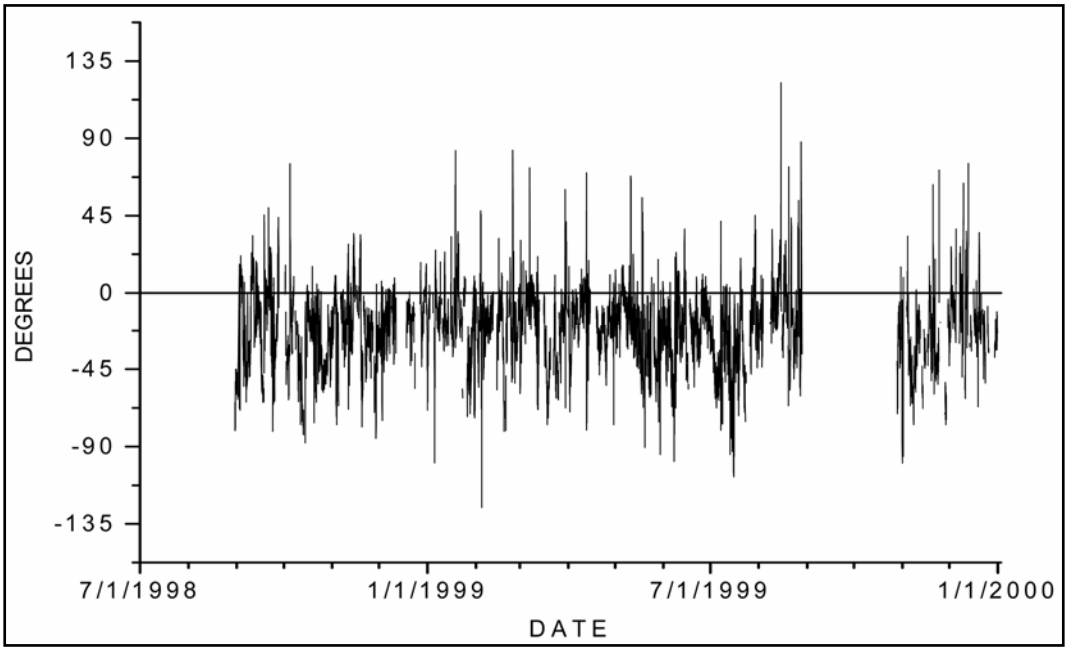

Figure 35. Wave angle difference plot, NDBC Buoy 42035 minus WIS station 78 data.

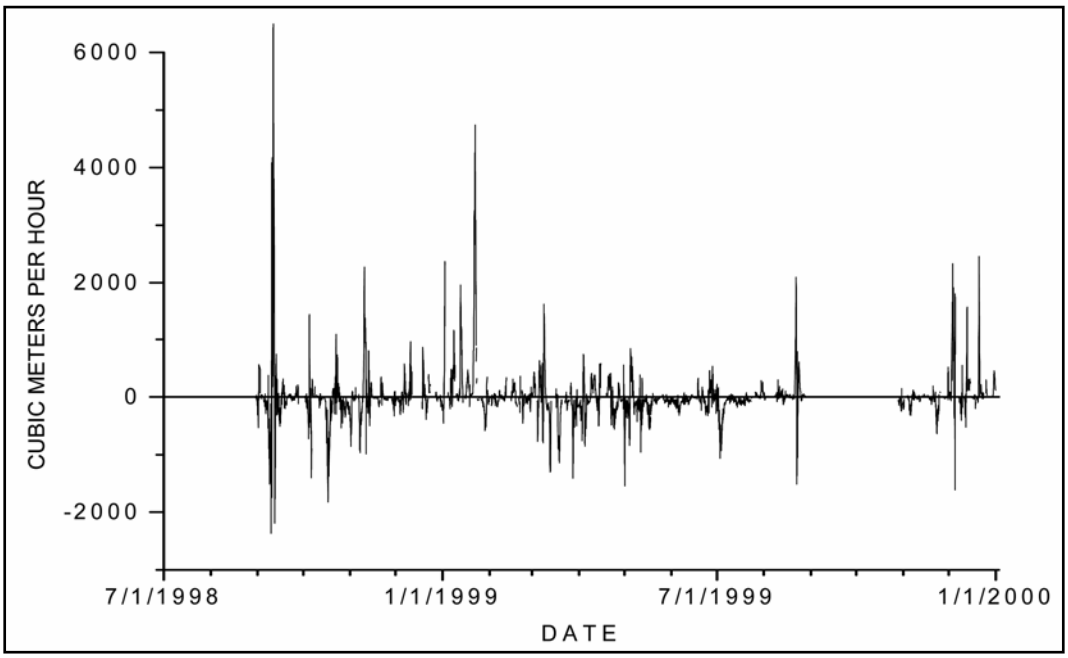

Figure 36. Transport rate estimate difference plot, NDBC Buoy 42035 minus WIS station 78 data.

Estimated transport rates from other wave sources

Wave data were available from other sources. A previous WIS hindcast for the Gulf of Mexico covered the period 1976-1995. Data from this earlier hindcast from WIS station 1078, located in 18 m of water depth near the

center of the Galveston Island STWAVE grid (Figure 19), were used to obtain the transport rate estimates shown in Table 15. Calculations for this table used a shoreline orientation of 147 deg, a two-component set of wave heights periods, and directions, and a CERC formula K value of 0.4. (Two-component wave data sets are described later in this chapter.) Values are similar to those given in Table 13 for Galveston Island for the 1990-1999 WIS data set, and they also predict a net transport direction to the northeast. This result suggests that the northeastward net transport preliminarily predicted from the 1990-1999 data set cannot be explained as the 1990s being an anomalous decade within a longer trend of net transport to the southwest.

Table 15. Preliminary transport rate estimates, Galveston Island, 1976-1995 WIS station 1078 two-component wave data.

1976-1995	Average Transport Rate m³/yr				Percent to East	Percent to West	Percent Calm
	To East	To West	Net West	Gross			
Ave	-541,000	411,000	-130,000	952,000	34.5	47.6	17.9

Wave data were also available from a wave gage deployed 2 miles (3.2 km) off the mouth of the Colorado River in 10 m depth between mid 1990 and fall 1992 (King and Prickett 1998). This location is about 59 miles (96 km) south of the study site. Transport rate estimates obtained using these data are shown in Table 16. Calculations for this table used a shoreline orientation of 147 deg, the peak spectral wave period, the vector mean wave direction at the peak spectral frequency, and a CERC formula K value of 0.4. These transport rate estimates yield a substantial net transport rate to the southwest, but this site was considered too remote and the data set too short to be used as a data source or as a calibration for the WIS data used in this study.

Table 16. Preliminary transport rate estimates, Galveston Island, 1990-1992 Colorado River field site wave data.

1990-1992	Average Transport Rate m³/yr				Percent to East	Percent to West	Percent Calm
	To East	To West	Net West	Gross			
Ave	-69,000	240,000	171,000	310,000	24.5	65.8	9.7

Effect of changes in wave angle on longshore transport rates

The effect of making bulk adjustments to the offshore wave angle was also investigated. Table 17 shows the transport rate estimates obtained by rotating each wave angle counterclockwise in the WIS station 78 data set prior to calculating the transport. Calculations for this table used a shoreline orientation of 147 deg, the peak spectral wave period, the vector mean wave direction at the peak spectral frequency, and a CERC formula K value of 0.4. This table shows that a few degrees change in the bulk wave angles (or, equivalently, a rotation of the shoreline orientation in the opposite direction) would change the estimated direction of net transport and is typical of the sensitivity to shoreline orientation shown by the CERC formula. An increase in the wave angle rotation also decreases the gross transport. This is in agreement with Figure 31. As the bulk of the large-event wave angles are shifted toward zero degrees (to the left in the upper panel, Figure 31), their impact on the overall transport (as well as the northeastward-directed net transport) is decreased. A procedure of this type could have been used to force the net direction of sediment transport on Galveston Island to the southwest, but this was not found to be necessary.

Table 17. Preliminary transport rate estimates (m^3/yr) as a function of adjustments in wave angle, Galveston Island, 1990-1999 WIS station 78 wave data.

	Counterclockwise Wave Angle Change					
	0 deg	2 deg	4 deg	6 deg	8 deg	10 deg
Net	-135,000	-64,000	8,000	80,000	151,000	221,000
Gross	860,000	827,000	796,000	769,000	746,000	729,000

Analysis of wave angles and wave periods

Unlike earlier versions of WIS standard products, the 1990-1999 WIS Gulf of Mexico hindcasts included 2-D energy density spectra for each station at 3-hr intervals. Figure 37 plots the 2-D spectrum for WIS station 78 (referenced to a shore-normal direction of 147 deg) for 19 April 1998 at 0600 hours. The angle convention is as before, positive angles indicate waves that approach the beach from the left of shore-normal (Figure 20). The figure shows a narrow peaked spectrum (swell) having a period of approximately 8 seconds, and approaching the coast at an angle of approximately 10 degrees to the left of shore-normal. The significant wave height for this spectrum is 1.3 m.

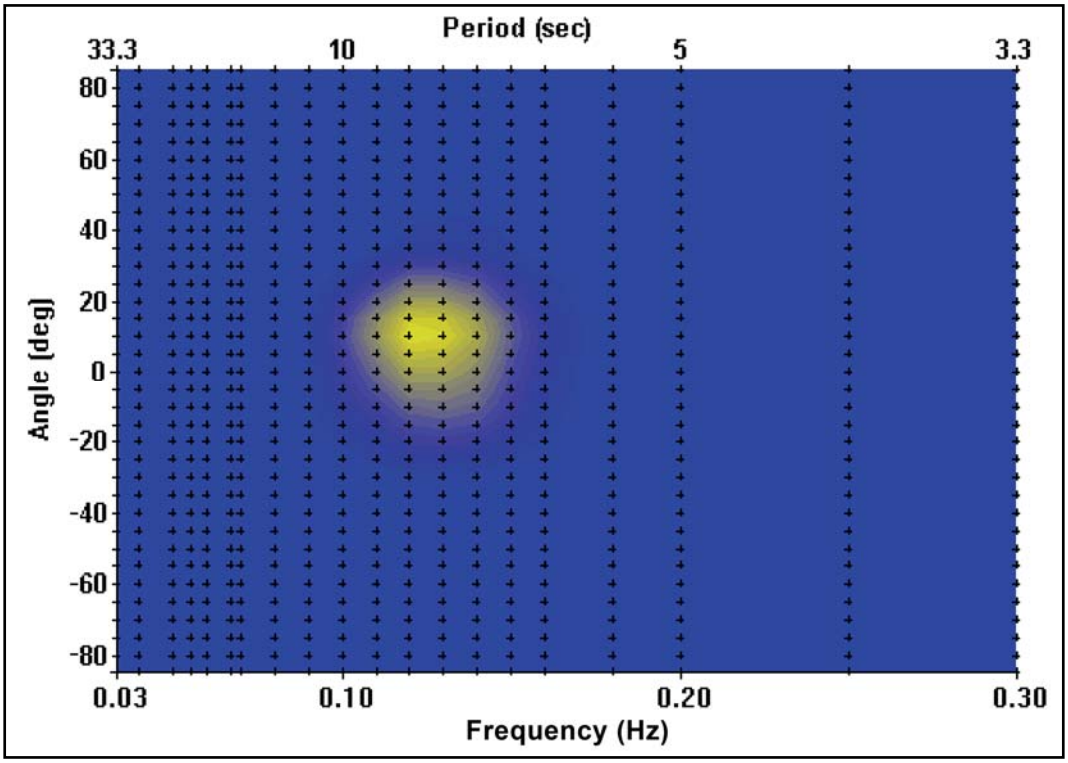

Figure 37. WIS station 78 2-D spectrum for 19 April 1998 at 0600 hours.

Figure 38 shows the conditions at the same location a day and a half later, at 1500 hours on 20 April 1998. Here the narrow-peaked energy has decreased and spread a little in direction. Also, the swell waves have been joined by a second, distinctly different wave train composed of broadbanded sea waves having a peak period of approximately 5 seconds and approaching the coast from a direction of more than 60 deg to shore-normal. The significant wave height for this spectrum has decreased to about 0.8 m.

The data inputs required for the calculation of a sediment transport rate using the CERC formula (which is incorporated within GENESIS) are a breaker wave height and breaker wave angle at each time-step. In the analyses used in this report, the wave period is also needed to shoal the waves either from an offshore or from a near-breaking condition to breaking. While there is a single standard methodology for calculating the significant wave height from a 2-D spectrum, there are several definitions of wave period and angle in common use. For the narrow-peaked spectrum shown in Figure 37, all standard definitions yield similar values. However, when the energy is broadly spread, and in multiple peaks, as in Figure 38, different definitions can give significantly different values.

While narrow-peaked spectra, similar to the one shown in Figure 37, are common in the WIS data sets; broadband spectra, similar to Figure 38, are also common.

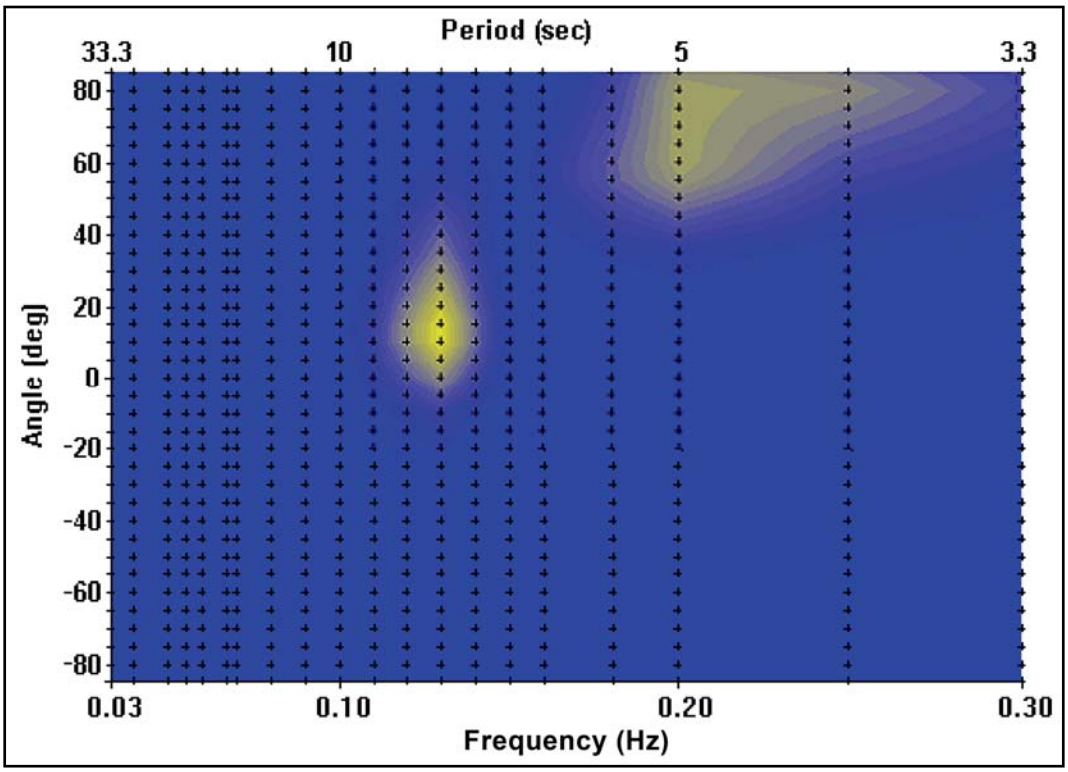

Figure 38. WIS station 78 2-D spectrum for 20 April 1998 at 1500 hours.

The question of which of these period and angle parameters are the most appropriate for use in sediment transport calculations has not been addressed through much research. For instance, the Coastal Engineering Manual (USACE 2002) does not give guidance on this topic. The question can be thought of in this way. A typical directional wave measurement might consist of three simultaneous time series of 2,048 data points each obtained from adjacent wave sensors. These time series can be converted into a 2-D spectrum, which might typically have 20 frequencies and 36 directions. That is, using our understanding of the physics of surface gravity waves, the 6,000 plus data values can be characterized by just 720 (20 x 36) data values. Then, further using our understanding of waves, these values could be characterized by just three parameters, a wave height, a wave period, and a wave direction. The question becomes, what three parameters will best characterize the wavefield, for the purposes of predicting longshore sediment transport rates. (WIS wave data are

hindcasted from calculated windfields rather than being measured, but the point is the same.)

Earlier versions of WIS products partially addressed this issue by providing a two-component set of wave statistics. For multi-peaked spectra, such as shown in Figure 38, two heights, periods, and directions were provided. (The transport rates shown in Table 15 were calculated using this double set of values.) In this report, this issue has been addressed by investigating the sediment transport rates estimated by a variety of wave periods and angles calculated from the WIS 2-D spectra. Some of these are standard definitions, while others were developed specifically for this investigation as potentially useful transport rate predictors. These wave periods and angles are briefly defined in Tables 18 and 19. Their full definitions and methods of calculation are given in Appendix A.

Table 18. Definitions of wave period parameters.

Parameter	Definition
Mean Period	The zeroth frequency moment divided by the 1st frequency moment of the energy density spectrum
Peak Spectral Period, Discrete	Inverse of the frequency band containing the greatest energy density
Peak Spectral Period, Parabolic Fit	The period containing the greatest energy obtained by parabolic smoothing of adjacent near-peak period bands

Table 19. Definitions of wave angle parameters.

Parameter	Definition
Vector Mean Angle	Overall mean direction from vector analysis
Moment Mean Angle	The 1st angle moment divided by the zeroth angle moment of the energy density spectrum
Energy Flux Mean Angle	Mean wave direction based upon longshore energy flux
Energy Vector Mean Angle	Overall mean direction from vector analysis of (energy density spectrum)$^{1.25}$
Vector Mean Angle at the Peak Spectral Frequency	Mean direction of the energy in the peak frequency band obtained from vector analysis
Moment Mean Angle at the Peak Spectral Frequency	Mean direction of the energy in the peak frequency band obtained from moment analysis
Peak Band Angle, Discrete	Direction band containing the greatest energy density
Peak Peak Angle, Discrete	Direction bin containing the greatest energy density within the peak frequency band

Using these definitions, Tables 20 and 21 list the wave periods and angles, respectively, calculated for the spectra shown in Figures 37 and 38. For the first spectrum, all the periods are in close agreement, as are all the angles. However, for the second spectrum, the wave periods disagree by almost 3 seconds and the wave angles disagree by over 60 deg.

Table 20. Wave period values in seconds for spectra in Figures 37 and 38.

Period Parameter	Figure 37	Figure 38
Mean Period	7.71	4.93
Peak Spectral Period, Discrete	7.69	7.69
Peak Spectral Period, Parabolic Fit	7.95	7.72

Table 21. Wave angle values in degrees for spectra in Figures 37 and 38.

Angle Parameter	Figure 27	Figure 38
Vector Mean Angle	8.0	53.1
Moment Mean Angle	8.2	52.4
Energy Flux Mean Angle	5.8	18.1
Energy Vector Mean Angle	7.5	54.4
Vector Mean Wave Angle at the Peak Spectral Frequency	7.6	19.1
Moment Mean Wave Angle at the Peak Spectral Frequency	7.7	19.2
Peak Band Angle, Discrete	10.0	80.0
Peak Peak Angle, Discrete	10.0	15.0

Initial results, such as those presented in Tables 20 and 21, suggested that average yearly transport rate estimates would likewise vary substantially. However, this was not the case. While transport rates for individual time-steps could vary substantially, the average yearly rates did not show striking variations, leading to the conclusion that the variations tended to cancel out. These preliminary transport rate comparisons are shown in Table 22 (for mean period values) and Table 23 (for peak spectral period values). Calculations for these tables used WIS data from station 78, a shoreline orientation of 147 deg, and a CERC formula K value of 0.4. Because of these results, further investigations of this type were not warranted. (Most of the spectra in the WIS data set have at least some onshore-directed energy, and that portion was used to determine the wave parameters in the transport rate calculations, resulting in only the small percentage of calm conditions shown in Tables 22 and 23.)

Table 22. Comparison of preliminary transport rate estimates using mean wave period and various angle parameters, Galveston Island, 1990-1999 WIS station 78 wave data.

Angle Parameter	Average Transport Rate m³/yr				Percent to East	Percent to West	Percent Calm
	To East	To West	Net West	Gross			
Vector Mean Angle	-440,000	343,000	-97,000	783,000	40.3	59.2	0.6
Moment Mean Angle	-439,000	344,000	-95,000	783,000	40.4	59.1	0.6
Energy Flux Mean Angle	-311,000	242,000	-69,000	554,000	39.3	60.2	0.6
Energy Vector Mean Angle	-438,000	337,000	-100,000	775,000	40.1	59.4	0.6
Vector Mean Wave Angle at the Peak Spectral Frequency	-414,000	328,000	-86,000	743,000	39.7	59.7	0.6
Moment Mean Wave Angle at the Peak Spectral Frequency	-413,000	328,000	-85,000	741,000	39.8	59.7	0.6
Peak Band Angle, Discrete	-430,000	315,000	-114,000	745,000	39.0	60.5	0.6
Peak Peak Angle, Discrete	-409,000	319,000	-90,000	729,000	38.8	60.6	0.6

Table 23. Comparison of preliminary transport rate estimates using peak spectral period, discrete and various angle parameters, Galveston Island, 1990-1999 WIS station 78 wave data.

Angle Parameter	Average Transport Rate m³/yr				Percent to East	Percent to West	Percent Calm
	to East	to West	Net West	Gross			
Vector Mean Angle	-516,000	390,000	-125,000	906,000	40.3	59.2	0.6
Moment Mean Angle	-514,000	391,000	-123,000	906,000	40.4	59.1	0.6
Energy Flux Mean Angle	-366,000	275,000	-91,000	641,000	39.3	60.2	0.6
Energy Vector Mean Angle	-513,000	383,000	-129,000	896,000	40.1	59.4	0.6
Vector Mean Wave Angle at the Peak Spectral Frequency	-492,000	365,000	-126,000	857,000	39.7	59.7	0.6
Moment Mean Wave Angle at the Peak Spectral Frequency	-490,000	366,000	-124,000	856,000	39.8	59.7	0.6
Peak Band Angle, Discrete	-503,000	363,000	-140,000	866,000	39.0	60.5	0.6
Peak Peak Angle, Discrete	-480,000	363,000	-116,000	844,000	38.8	60.6	0.6

Effect of local winds on STWAVE transformation and on longshore currents

Local nearshore winds can have two significant impacts on longshore sediment transport rates. First, they can be an important wave generating mechanism within the STWAVE grid where the offshore waves are transformed to near-breaking depths. With the mild wave conditions that characterize the Gulf of Mexico, this mechanism is likely to be more important than at typical Atlantic or Pacific study sites. Secondly, the local winds can directly modify longshore currents within the surf zone. The

mathematics of the longshore current modification are included as Appendix B in this report.

To examine the importance these two effects, STWAVE was run twice using the Galveston Island grid (discussed in Chapter 4) and the 1998 wave set from WIS station 78; the first time with no wind input and the second with wind input from WIS station 71 (Figure 19). The year 1998 was chosen as a year with a fairly average net transport rate (Table 13). Then GENESIS was run four times on the Galveston Island grid (discussed below). For each of the two STWAVE output wave sets, GENESIS was run once with no wind-induced component to the longshore current and once with that component, again using wind data from WIS station 71. (Though varying in time, this windfield was assumed to be spatially constant over the STWAVE grid. It was also assumed to be spatially constant along the beach, so the same wind-driven longshore current was included at each GENESIS cell wall (for a given time-step)).

The results of these tests showed that both effects were about equally important in modifying the net longshore transport rate on Galveston Island. Together they produced a modest net westward transport (of 25,000 to 50,000 m^3/yr) along most of west Galveston Island. These realistic results led to the decision to use this procedure for the entire 10-yr wave data set.

Wave transformation model setup procedures

The standard STWAVE/GENESIS procedure has been to operate within the NEMOS (***N***earshore ***E***volution ***MO***deling ***S***ystem) environment. STWAVE and GENESIS grids are laid out in a GIS database using shoreline and bathymetry data, which are then imported into NEMOS. Offshore height, period, and direction wave data from a WIS station are also imported into NEMOS where they are analyzed, and the time series is binned into typically 20 to 40 wave period/direction bins. A representative unit wave height spectrum is generated for each bin, and these representative spectra are STWAVE transformed across the grid to near-breaking depths where the heights and angles are saved at each station for use by GENESIS.

This procedure was modified to take advantage of the availability of spectra at the offshore WIS stations and to include local wind generation of waves across the transformation grid. The new procedure transformed

the entire 10-yr data set (29216 wave spectra) by running STWAVE on a high-speed computer, rather than transforming 20 to 40 representative spectra on a PC. To do this, STWAVE grids were established and imported into NEMOS. Then the STWAVE grid was exported and modified to run with a stand-alone version of STWAVE. WIS wave spectra were combined with WIS winds (different stations), formatted into month-long files, and then transformed over the STWAVE grid on a high-speed computer. After post-processing, the output spectra at the nearshore save stations were stored for use in GENESIS.

Shoreline change analysis procedures

A modified version of GENESIS within NEMOS was developed to include the effects of a wind-generated longshore current on the sediment transport rate and to include the availability of nearshore wave data at each save station at each time-step. Historical shorelines were input into the GENESIS grid. The STWAVE processed wave spectra were converted into heights, periods, and directions and formatted for entry into NEMOS. Likewise, wind-generated surf zone longshore currents were calculated using the same wind field data used in the STWAVE transformation, formatted, and entered into NEMOS. Then the GENESIS model was run and calibrated.

GENESIS calibration

The GENESIS grids were calibrated by visually and mathematically comparing the GENESIS shoreline change rates with historical change rates, by comparing the calibration parameters with those developed by previous GENESIS efforts within the study area, and by using engineering judgment as a check on the reasonableness of the results. The shorelines listed in Table 24 were paired as shown in Table 25, and changes in shoreline location were calculated for each GENESIS grid cell (accretion is positive). The differences were divided by the time between surveys and adjusted to a rate of shoreline change in meters per ten years. The Gibeaut et al. (2002) shoreline change rate, discussed in Chapter 2, was also adjusted to the same units. The Gibeaut et al. (2002) change rate is not an independent parameter, as it is an RMS best-fit estimate of the changes in shoreline position using these four surveys.

Table 24. Shoreline pairs for change rate analysis.

Shoreline Pair Number	Beginning Shoreline Year	Ending Shoreline Year	Days of Difference	
			High Island	Galveston Island
1	1974	1982	2,933	2,904
2	1974	1995	7,506	7,506
3	1974	2000	9,461	9,461
4	1982	1995	4,573	4,602
5	1982	2000	6,528	6,557
6	1995	2000	1,955	1,955

RMS differences in these seven shoreline change rates (the six pairs in Table 24 plus the Gibeaut rate) were then calculated for both grids (Table 25). G stands for the Gibeaut et al. (2002) change rate. This gave a baseline for interpreting the natural variability in the different change rates. Note that the change rate based upon short time intervals between surveys (the comparison of pair 1 with pair 6) had substantially greater variability than the longer interval rates. Based upon this analysis, the GENESIS grids were calibrated to the Gibeaut et al. (2002) change rate, and change rates 3 and 4 (long time interval, independent rates) were used as a check. The RMS differences between the shoreline change rates of the calibrated GENESIS grids and these three change rates are shown in Table 26. This table shows that the amount of variation between the GENESIS grids and these measured rates is of the same magnitude as the variations between the long time-interval measured rates.

Table 25. RMS differences in the different shoreline change rates.

Shoreline Pairs	High Island	Galveston Island
1,6	23.22	93.05
2,5	7.17	30.00
3,4	6.63	10.81
G,1	8.11	30.20
G,2	5.58	13.34
G,3	3.75	3.20
G,4	7.22	8.19
G,5	5.28	16.83
G,6	19.24	65.18

Table 26. RMS differences in GENESIS shoreline change rates and measured rates.

Lines	High Island	Galveston Island
GEN,3	7.60	14.25
GEN,4	7.92	13.81
GEN,G	7.87	12.93

The final GENESIS grid calibration parameters are listed in Table 27. These parameters all are physically reasonable based upon conditions at the study site, are in reasonable agreement between the two grids, and are in reasonable agreement with previous GENESIS models within the study site (Table 28). The GENESIS grid of Brown and Kraus (1994) modeled the area in front of the Galveston Seawall, and the Howard (1999) GENESIS grid modeled the portion of Jefferson County between Sea Rim State Park and High Island, where Highway 87 has been destroyed by erosion.

Table 27. GENESIS grid parameters.

Parameter	High Island	Galveston Island
Number of Cells	398	300
Cell Widths	500 ft	500 ft
Median Grain Size	0.16 mm	0.16 mm
Berm Height	1.5 m	1.5 m
Depth of Closure	6.0 m	6.0 m
K_1	0.4	0.4
K_2	0.2	0.2
K_3	1.5	1.5
Left Lateral Boundary Condition	moving 0.00550 m/day	moving 0.00650 m/day
Right Lateral Boundary Condition	moving 0.00185 m/day	moving 0.03591 m/day
Number of Groins	0	15
Groin Permeability	--	0.2
Number of Seawalls	0	1

Table 28. Parameters used in previous GENESIS studies.

Parameter	Brown and Kraus (1994)	Howard (1999)
Number of cells	400	40
Cell Widths	100 ft	1,440 m
Berm Height	3 ft	1.5m
Depth of Closure	15 ft	4 m
Sediment Grain Size	0.14	
Seawalls	1	0
Groins	15	0
Groin Permeability	0.2	--
East Lateral Boundary Condition	no transport	various
West Lateral Boundary Condition	pinned	various
K1	0.4	1
K2	0.2	0.5
Shoreline Position	1991 aerial photos	1974 and 1995 aerial photos

7 SBEACH Setup

SBEACH hurricanes

SBEACH is designed to model erosional events and inland flooding caused by storms and hurricanes. The primary model inputs are storm wave heights, wave periods, and water elevations. Twenty-four historical hurricanes and tropical storms that impacted the study area between 1886 and 1998 were selected for analysis. These storms, listed by HURDAT number (NOAA HURricane DATabase storm identifier number) and name (post-1950 storms) are shown in Table 29. Atlantic hurricane storm tracks can be found on the web at *http://weather.unisys.com/hurricane/atlantic/*, and early storm tracks are published in Neumann et al. (1981). In Table 29, the hurricane category at landfall is based upon the Saffir-Simpson Scale (*http://www.nhc.noaa.gov/index.shtml*). TS refers to tropical storm. The ADCIRC and WIS models were used to generate storm surges and waves, respectively, for these storms.

Characterization of storm water levels

The storm-induced water elevations for these hurricanes were calculated using the ADCIRC model as described in Scheffner et al. (2002). Model outputs were obtained at a series of stations within the study area. Figure 39 (modified from Scheffner et al. 2002) is an example of the ADCIRC output, showing the computed storm surge elevations along the coast caused by Hurricane Alicia (HURDAT No. 812). Three of the ADCIRC output stations WLS (***W***ater ***L***evel ***S***tation) 09, WLS 17, and WLS 21 were chosen as being representative of the study area (Figure 19). WLS 09 water levels were used for all Galveston Island SBEACH runs. SBEACH runs for Bolivar Peninsula used WLS 17, and Jefferson County SBEACH runs used WLS 21. Storm surge frequency-of-occurrence relationships for these three stations are shown in Table 30.

The ADCIRC and WIS data were then inspected for quality and time synchronized by producing plots of wave height, wave period, water elevation, and wind speed and direction for each storm, as shown in Figure 40. In this example, the horizontal scale is the 1961 September date.

Table 29. Storms used in SBEACH analysis.

HURDAT Storm Number	Storm Name	Landfall				
		Month	Day	Year	Location	Category
5	unnamed	August	19-20	1886	Indianola	4
117	unnamed	September	7-8	1900	Galveston	4
183	unnamed	July	21	1909	Valesco	3
211	unnamed	August	16	1915	Galveston	4
232	unnamed	September	6	1918	Cameron, LA	2
295	unnamed	June	28	1929	Freeport	1
310	unnamed	August	13-14	1932	Freeport	4
324	unnamed	July	22-23	1933	Central TX coast	2
397	unnamed	August	7-8	1940	Cameron, LA	2
405	unnamed	September	23	1941	Matagorda	TS
445	unnamed	August	28	1945	Port Aransas	4
565	Audrey	June	27	1957	Sabine Pass	4
586	Debra	July	24	1959	Freeport	1
602	Carla	September	14	1961	Port Lavaca	4
690	Celia	August	3	1970	Corpus Christi	3
704	Fern	September	10	1971	Central TX coast	TS
722	Delia	September	5	1973	Freeport	TS
809	Chris	September	11	1982	Sabine Pass	TS
812	Alicia	August	18	1983	Galveston	3
841	Bonnie	June	26	1986	High Island	1
867	Chantal	August	1	1989	High Island	1
874	Jerry	October	15-16	1989	Galveston	1
923	Dean	July	31	1995	Freeport	TS
965	Frances	September	10-11	1998	Matagorda	TS

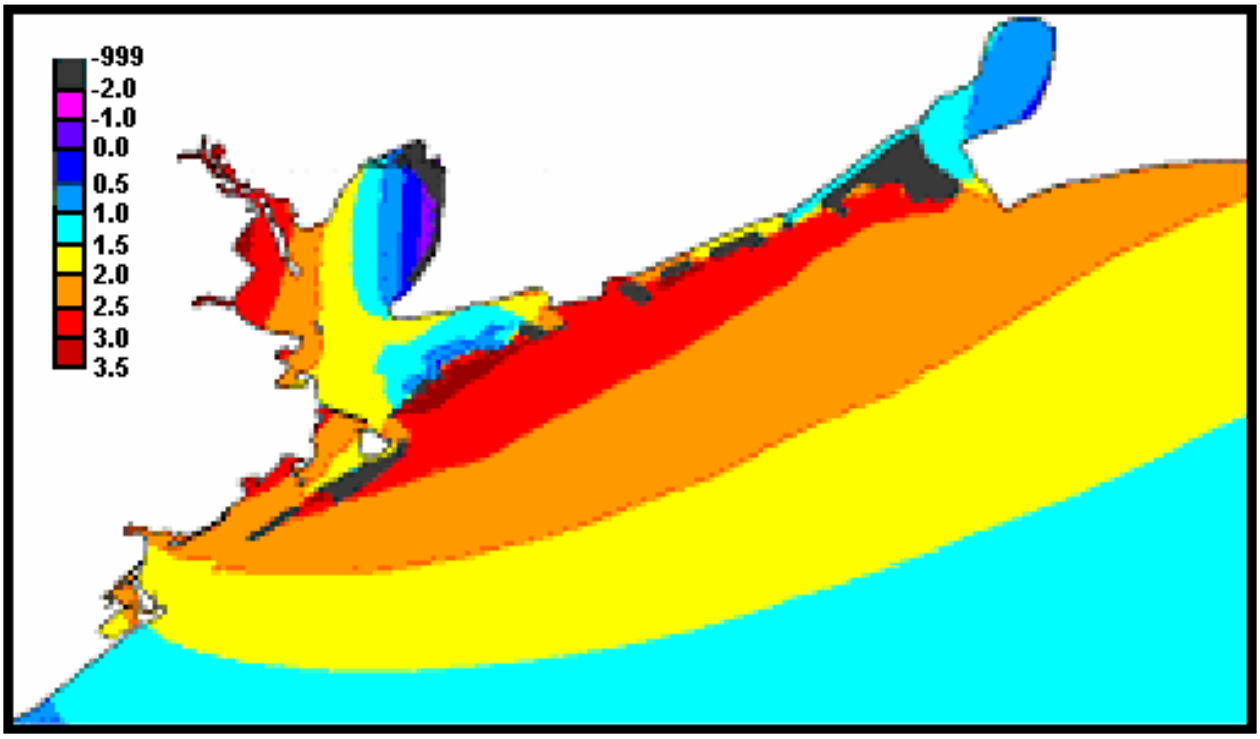

Figure 39. Maximum storm surge elevation plus tide in meters for Hurricane Alicia along the upper Texas coast, 18 August 1983 (after Scheffner et al. 2002).

Table 30. ADCIRC storm surge frequency-of-occurrence relationships (after Scheffner et al. 2002).

Return Period in Years	WLS 09		WLS 17		WLS 21	
	Maximum Surge	Standard Deviation	Maximum Surge	Standard Deviation	Maximum Surge	Standard Deviation
5	0.5417	0	0.6266	0	0.6615	0
10	0.93	0.225	1.06	0.234	1.099	0.256
15	1.305	0.261	1.539	0.349	1.559	0.335
25	1.834	0.387	2.202	0.456	2.147	0.366
50	2.496	0.397	3.004	0.433	2.938	0.503
75	2.791	0.389	3.404	0.431	3.366	0.541
100	2.966	0.425	3.662	0.492	3.623	0.601
150	3.323	0.532	4.054	0.573	4.081	0.697
200	3.503	0.657	4.251	0.678	4.312	0.81

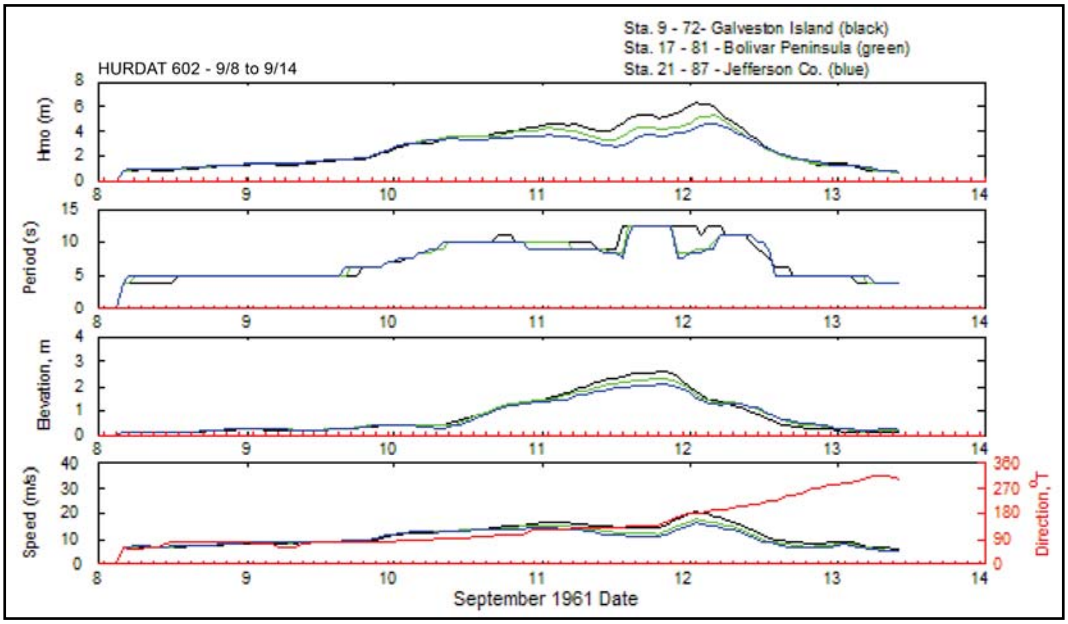

Figure 40. Example plot of wave heights, wave periods, water levels, wind speeds, and wind directions for Storm 602 (Hurricane Carla, 1961) WLS 09 (black lines), WLS 17 (green lines), and WLS 21 (blue lines).

Using this procedure, portions of the time series that were clearly before or after each storm event were removed, and appropriate start and end times were selected for each storm (Table 31). Start and end times were the same for all three water level stations (WLS).

The ADCIRC storm surges were calculated for each hurricane without including tidal fluctuations. The goal of this analysis is to reasonably predict the effect of future hurricanes. A suite of past hurricanes is used to represent the likely range of future hurricanes. However, future storms will strike the coast at random times relative to the tide cycle. Therefore, a variety of tide signals have been added to the ADCIRC storm surges to reasonably cover potential future events and to increase the size of the data set used to predict these events.

The tide along this section of coastline is mixed, partially diurnal and partially semi-diurnal, and is of small amplitude. Tidal data used in this analysis were obtained from NOAA Tide Station 8771510, located on the Galveston Pleasure Pier (Figure 1 and Table 5). For the purposes of this simulation, it was reasonable to characterize the tide as a 12-hour sine wave with a spring amplitude of 0.45 m (1.48 ft), a midrange amplitude of 0.30 m (0.98 ft), and a neap amplitude of 0.15 m (0.49 ft). Tidal phases were randomized by synchronizing the peak of the tide with the peak of

the storm surge and by then shifting the peak phases by 90, 180, and 270 degrees. These four phases combined with the three amplitudes, produced 12 representative tide curves for each storm. These were added to the ADCIRC storm surges at each of the three water level stations.

Table 31. Start and end times for SBEACH storms.

HURDAT No.	Name	Year	Start Date – Time	End Date – Time
5	unnamed	1886	8/18 – 0000	8/21 – 1200
117	unnamed	1900	9/6 – 0000	9/8 – 0000
183	unnamed	1909	7/19 – 0000	7/22 – 0000
211	unnamed	1915	8/16 – 0000	8/19 – 1700
232	unnamed	1918	8/4 – 0000	8/7 – 0000
295	unnamed	1929	6/27 – 0100	6/29 – 1200
310	unnamed	1932	8/12 – 0100	8/14 – 1800
324	unnamed	1933	8/1 – 1900	8/5 – 1600
397	unnamed	1940	8/2 – 1200	8/8 – 0000
405	unnamed	1941	9/22 – 0000	9/24 – 2300
445	unnamed	1945	8/25 – 0000	8/29 – 0400
565	Audrey	1957	6/25 – 0600	6/28 –1600
586	Debra	1959	7/23 – 0100	7/26 – 2300
602	Carla	1961	9/8 – 0300	9/13 – 1000
690	Celia	1970	8/2 – 1600	8/4 – 0800
704	Fern	1971	9/9 – 1200	9/16 – 0000
722	Delia	1973	9/1 – 1900	9/6 – 1100
809	Chris	1982	9/9 – 0100	9/12 – 1100
812	Alicia	1983	8/15 – 1300	8/19 – 0200
841	Bonnie	1986	6/23 – 1900	6/27 – 0200
867	Chantal	1989	7/30 – 1300	8/2 – 0200
874	Jerry	1989	10/13 – 1100	10/16 – 1500
923	Dean	1995	7/28 – 1900	7/31 – 2100
965	Frances	1998	9/8 – 1900	9/13 – 1500

Examples of these tide plus storm surge curves are shown in Figure 41. This figure shows four water elevation curves for HURDAT 812, Hurricane Alicia, for WLS17 between 15 and 20 August 1983. The four curves are for the four tidal phases (from top to bottom, phase 0, 90, 180, and 270 degrees with respect to surge peak) with a spring tidal amplitude of 0.45 m.

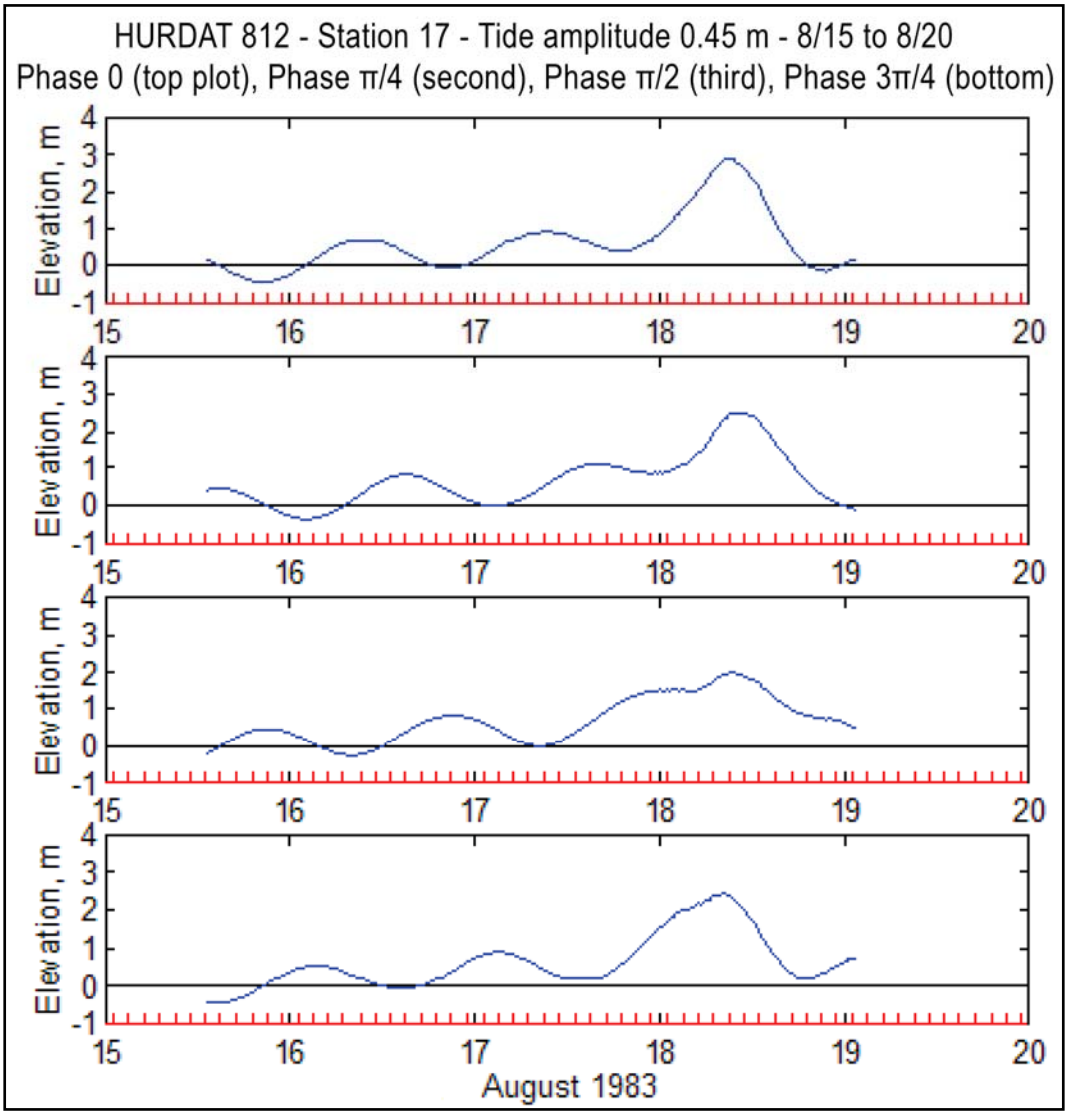

Figure 41. Four representative water elevation curves for Hurricane Alicia (1983).

Characterization of storm waves

WIS hindcasts were made for the storms in Table 29 at all WIS stations in the Gulf of Mexico as described in Tracy (2002). An example of this hindcast, showing the maximum wave heights at the location of NDBC Buoy 42035 (Figure 19) is given in Figure 42.

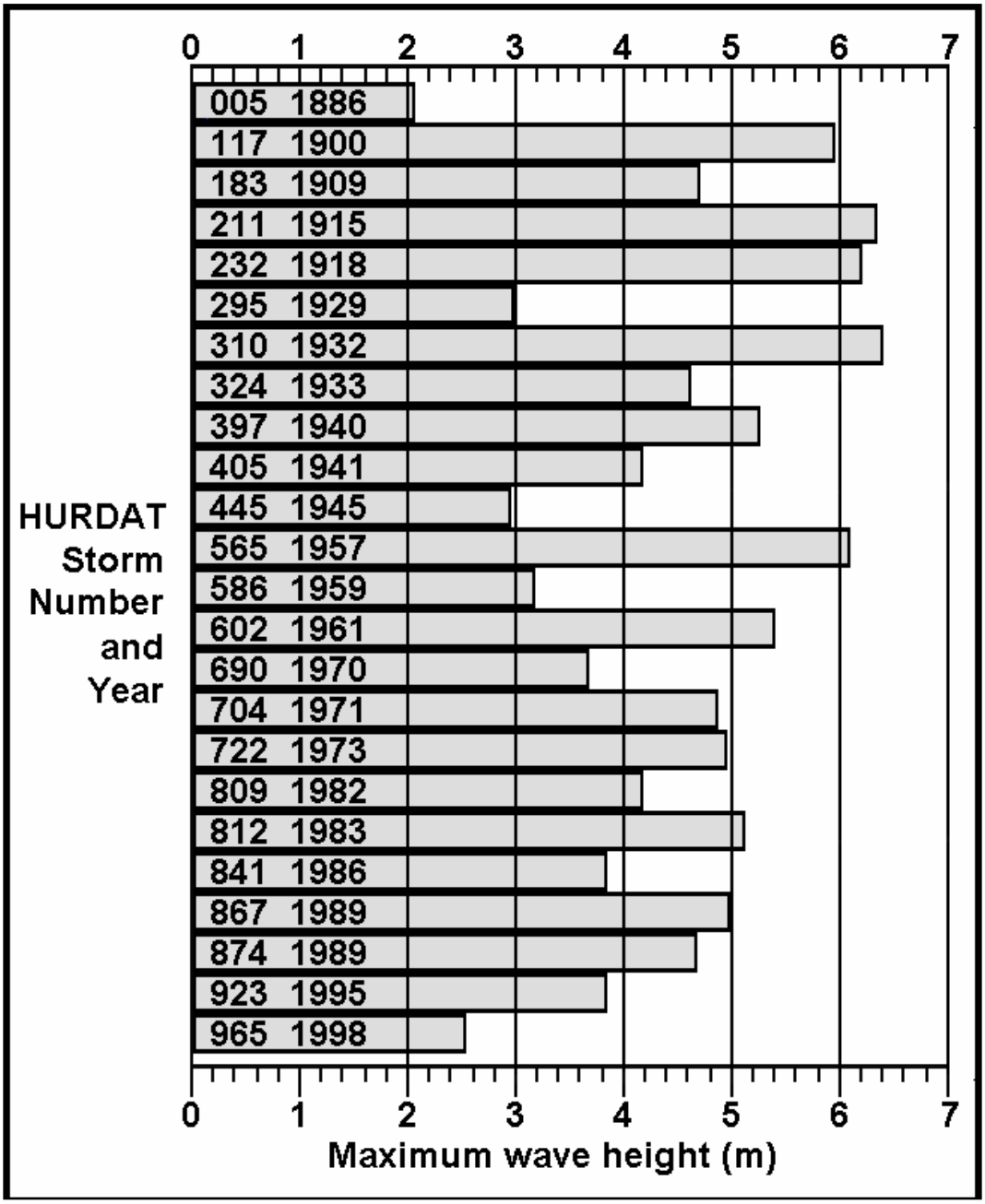

Figure 42. Maximum WIS hindcast wave heights at NDBC Buoy 42035 location for the hurricanes used in this study. See Table 29 for additional information on each hurricane.

Three WIS stations (WIS 72, WIS 81, and WIS 87), shown in Figure 19, that were offshore of the three water level stations (WLS 09, WLS 17, and WLS 21) were chosen as input wave data locations for the SBEACH model. The hurricane waves were then Phase-3 transformed from the offshore WIS locations (at approximately 20-m depth) to 8-m depth. This was approximately the depth of the profiles used in the SBEACH grid (discussed below). For these transformations, an offshore direction of

147 degrees was used for Galveston Island (WIS station 72), and an offshore direction of 157 degrees was used for Bolivar Peninsula (WIS station 81) and Jefferson County (WIS station 87).

The Phase-3 transformation is a less complex (though still sophisticated) procedure than an STWAVE transformation, and it does not require the use of a bathymetry grid. It is the standard procedure used to generate SBEACH wave input data. From basic parametric wave descriptions (H, T, theta) supplied by the deepwater WIS data, the procedure generates theoretical directional spectra, performs shoaling and refraction, and considers shore-induced sheltering (in a simplified fashion) at a user-specified nearshore location (Jensen 1983).

SBEACH grids

Beach profiles

Profile data were collected to develop SBEACH representative profile grids. As part of this study, the Ocean and Hydraulic Engineering Program at Texas A&M University, under the direction of Dr. Billy Edge, collected wading and fathometer profiles during the fall and winter of 2002. The locations of the 58 Galveston Island and 101 Bolivar to Sabine surveys are shown in Figure 43. Profile lines were run nominally every half mile and extended from the dunes to 5,500 to 7,000 ft (1,700-2,100 m) offshore and to depths of 6 to 8 m (20-25 ft). Most of profiles along Galveston Island showed two bar formations. A single bar was present on most of the Bolivar Peninsula profiles, and in Jefferson County, a distinct bar was present in about half the profiles.

Since the profiles only typically extended shoreward to the duneline, 2002 LIDAR survey data of the coastal zone were obtained from the Texas Bureau of Economic Geology. This would be used to extend the profiles landward.

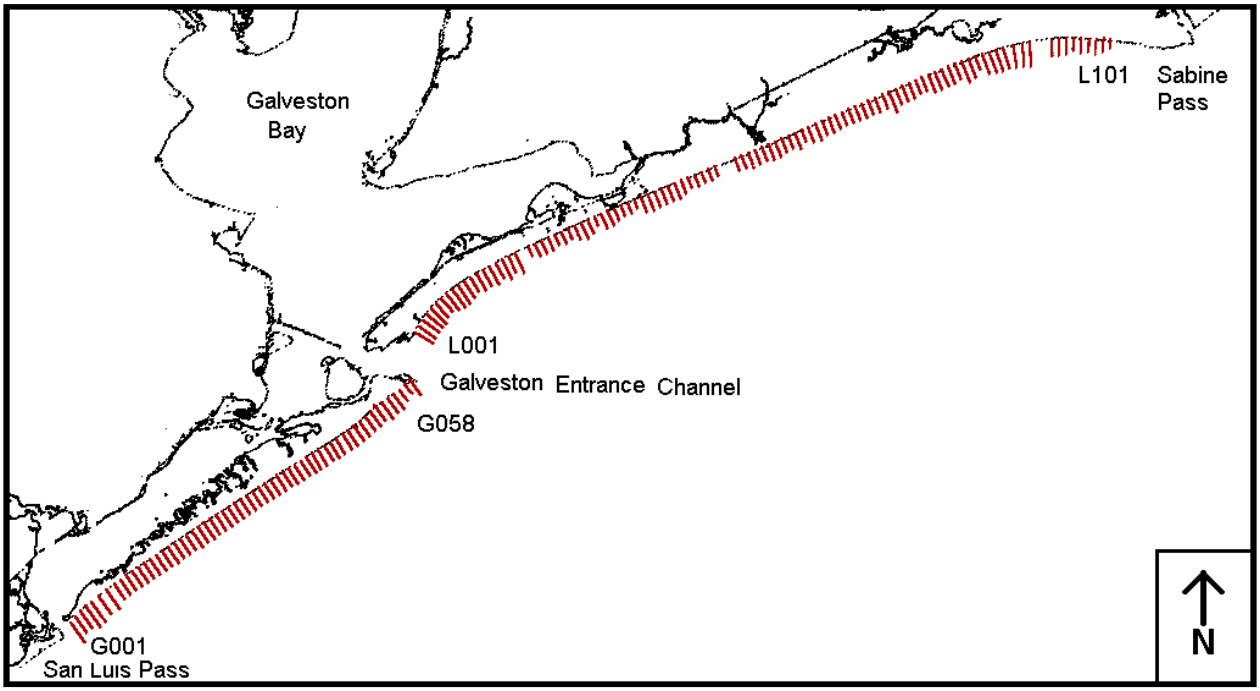

Figure 43. Locations of beach profiles used to generate SBEACH representative profiles.

Representative profiles

Representative profiles were developed to characterize sections of the coastline, termed reaches. Typically, several similar adjacent profiles were combined in a way that captured the important elements of the morphology. These profiles were imported into SBEACH so that the model runs for each reach would be applicable throughout the reach.

To begin this process, the beach profiles and the LIDAR data were combined within a GIS database. The horizontal datum used was NAD83, UTM, Zone 15, meters, and the vertical datum was NAVD88, meters, the same datum used throughout this study. After being quality checked, the profiles, which were originally in (x, y, z) coordinates, were converted to (x, z) coordinates using an azimuth of 147 degrees for the Galveston Island profiles and 157 degrees for (most of) the High Island profiles. The LIDAR data were used to extend the profiles a minimum of 150 m landward of the shoreline or as far inland as the LIDAR data extended.

The 159 profiles were imported into RMAP (Batten and Kraus 2005), a profile manipulation program, and aligned to their shorelines. They were manually compared and broken into groups having similar characteristics. Typically, 5 to 8 adjacent profiles were grouped together, with the

extremes being groups of 3 and 14 profiles. Factors other than profile shape, such as coastal features (e.g., geotextile tubes, Galveston Seawall, Rollover Pass) also influenced the selection of the groups. Then the profiles in each group were broken at the shoreline into bar (subaqueous) and berm (subaerial) profile portions. The most typical bar and berm profiles within the group were selected to be the appropriate portion of the representative profile. Dune position, elevation and width, berm position and width, foreshore slope, and volume were all factors considered in selecting the representative berm profile. Inner surf-zone slope, bar location, elevation, and volume, and offshore slope were all factors considered in selecting the representative bar profile. Additional profile comparisons were made by temporarily aligning the profiles about the dune crests, the berm/foreshore slope break, the bar crest, and various vertical elevations.

The representative bar and berm profiles were then combined. If the berm profile did not extend 150 m landward of the shoreline or the bar profile did not extend 2,000 m seaward, portions of other profiles within the group were used to extend the representative profile to achieve a minimum length. Finally, the representative profiles were interpolated at 2-m intervals and imported into SBEACH. Representative profile metadata and reach locations are given in Tables 32 and 33 and Figure 44.

Within SBEACH, a variable grid spacing was used because the primary interest was in the behavior of the berm and dune portion of the profile. A 2-m grid spacing was used between 150 m landward and 200 m seaward (typically about a 2-m depth) of the shoreline. Between 200 and 400 m (at about 3-m depth) grid cells are spaced 10 m apart, and seaward of 400 m out to 2,000 m, grid cells are spaced 50 m apart.

SBEACH analysis procedures

The SBEACH model was applied to support the economic analysis (Galveston Island and Bolivar Peninsula) and environmental analysis (Jefferson County) of proposed beach fills and other remedial erosion control efforts. Specifically, SBEACH provides information on flooding and erosion damage caused by storms. The model is run on various reaches using the without project representative profile and also run with the representative profile augmented with various proposed beach fills. These project alternatives generally involve increasing the dune height, the dune width, and the berm width. Comparison of the beach storm response

with various alternative beach fills will greatly assist in selecting the optimal protection strategy.

Table 32. Representative profile metadata.

Rep Profile Name	Region	Area Name	From Profiles	Erosion Control Structures	Priority	WLS
G-R01	Galveston Island	San Luis Pass	G001-G003	No		09
G-R02	Galveston Island	Pointe San Luis	G004-G009	No	Economic	09
G-R03	Galveston Island	Sea Isle	G010-G016	No	Economic	09
G-R04	Galveston Island	Jamaica Beach	G017-G024	No	Economic	09
G-R05	Galveston Island	Pirates Beach	G025-G028	GeoTube	Economic	09
G-R06	Galveston Island	Bermuda Beach	G029-G036	Small	Economic	09
G-R07	Galveston Island	West Seawall	G037-G042	Seawall		09
G-R08	Galveston Island	Seawall / Groinfield	G043-G050	Seawall		09
G-R09	Galveston Island	East Beach	G051-G058	No		17
H-R01	Bolivar Peninsula	Bolivar Flats	L001-L004	No		17
H-R02	Bolivar Peninsula	East Port Bolivar	L005-L012	No	Economic	17
H-R03	Bolivar Peninsula	Crystal Beach	L013-L019	No	Economic	17
H-R04	Bolivar Peninsula	Caplen Shores	L020-L027	No	Economic	17
H-R05	Bolivar Peninsula	Caplen	L028-L032	GeoTube	Economic	17
H-R06	Bolivar Peninsula	Gilchrist	L033-L037	GeoTube	Economic	17
H-R07	Bolivar Peninsula	Dirty Pelican Pier	L038-L045	No	Economic	17
H-R08	Jefferson County	High Island	L046-L059	No	Environmental	21
H-R09	Jefferson County	HY 87 West	L060-L067	No	Environmental	21
H-R10	Jefferson County	Vastar	L068-L079	No	Environmental	21
H-R11	Jefferson County	Hy 87 East	L080-L088	No	Environmental	21
H-R12	Jefferson County	Sea Rim SP	L089-L101	No	Environmental	21

Table 33. SBEACH reach boundaries.

Rep Profile and Reach Name	West End			East End		
	UTM meters		Physical Boundary	UTM meters		Physical Boundary
	Easting	Northing		Easting	Northing	
G-R01			San Luis Pass	295886	3220893	
G-R02	295886	3220893		300363	3224390	
G-R03	300363	3224390		305009	3227555	
G-R04	305009	3227555		310293	3231005	No GeoTube
G-R05	310293	3231005	GeoTube end	312991	3232741	GeoTube end
G-R06	312991	3232741	No GeoTube	318373	3236202	No Seawall
G-R07	318373	3236202	Seawall end	322229	3238665	No Groinfield
G-R08	322229	3238665	Groinfield end	327489	3242457	Seawall end
G-R09	327489	3242457	No Seawall			Ship Channel
H-R01			Ship Channel	334175	3253846	
H-R02	334175	3253846		339216	3257730	
H-R03	339216	3257730		344543	3260579	
H-R04	344543	3260579		350724	3263372	No GeoTube
H-R05	350724	3263372	GeoTube end	354533	3265054	Rollover Pass
H-R06	354533	3265054	Rollover Pass	358167	3266562	GeoTube end
H-R07	358167	3266562	No GeoTube	364162	3269059	
H-R08	364162	3269059		375965	3273980	
H-R09	375965	3273980		381916	3276541	
H-R10	381916	3276541		390797	3280347	
H-R11	390797	3280347		397581	3282823	
H-R12	397581	3282823				

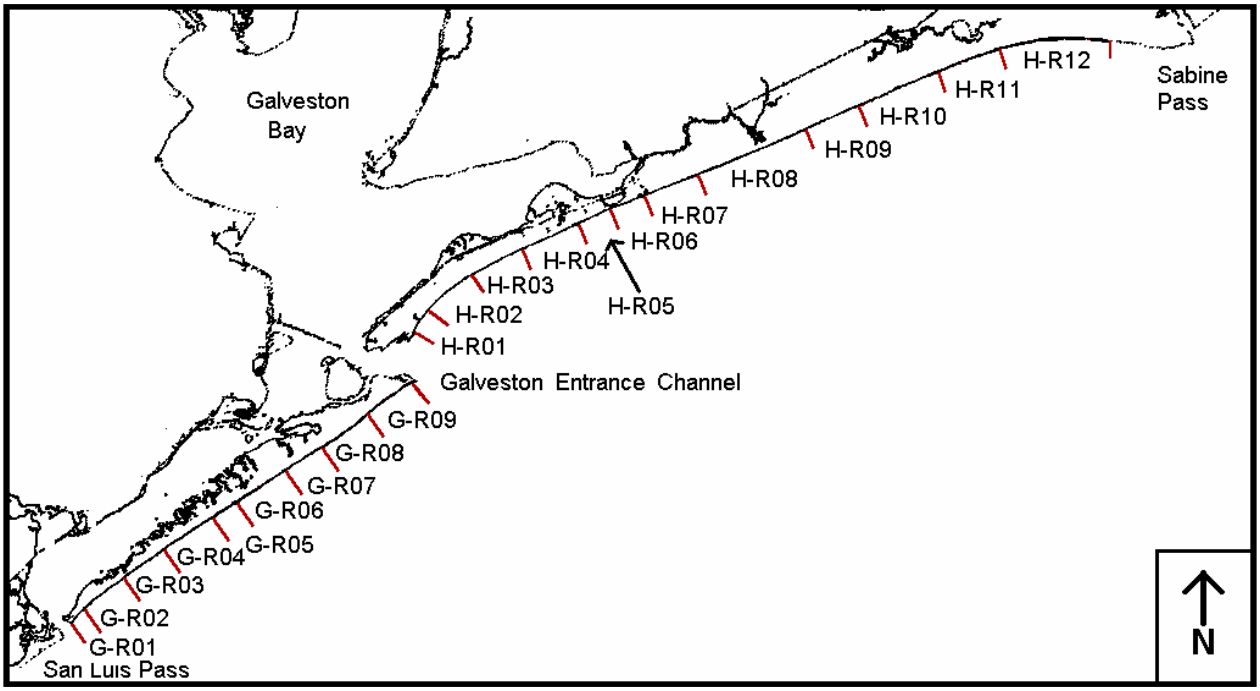

Figure 44. Location of SBEACH reaches.

8 SBEACH Calibration

Hurricane Claudette Data Availability

On 15 July 2003, Hurricane Claudette made landfall on the Texas coast near the entrance to Matagorda Bay about 125 miles (200 km) southwest of Galveston. Storm waves from this hurricane had a significant effect on the beaches in the study area. In April and May 2003, as part of a geotextile tube monitoring program for Galveston County, Shiner Moseley and Associates, Inc. (SMA) of Corpus Christi, TX, (*www.shinermoseley.com*) collected a series of beach profiles along a section of west Galveston Island and another series on Bolivar Peninsula (at different locations than the Texas A&M profiles discussed in Chapter 7). Because of the hurricane-induced changes, Shiner Moseley collected a second set of beach profiles in these same two areas in July and August 2003.

A typical SBEACH calibration requires beach profiles that are collected shortly before and after a significant storm event. The Scope of Work for the research described in the main body of this report did not include a calibration of SBEACH because, at that time, such a data set did not exist. Instead, the initial plans were to set up and run the SBEACH model using the standard, default parameters. However, the availability of the Claudette data provided an opportunity to calibrate the SBEACH model.

Hurricane Storm Track

Claudette formed from a tropical wave that moved off the coast of Africa on 1 July 2003, but the disturbance did not become a tropical storm until 8 July, after it had entered the Caribbean Sea (Figure 45). For a brief time on 10 July, it became a hurricane, but then wind speeds decreased back to tropical storm levels. The storm struck the northeast corner of the Yucatan Peninsula on 11 July and moved north to northwestward into the Gulf of Mexico. Late on 14 July, the storm turned more westerly, and at 0600 (UTM) on 15 July, it again became a minimal hurricane. At this time, it was about 100 miles (160 km) due south of the study area. Throughout 15 July, it moved west northwestward, slightly intensifying until making landfall near Port O'Connor at 1530 UTC as a Category 1 storm (Figure 46).

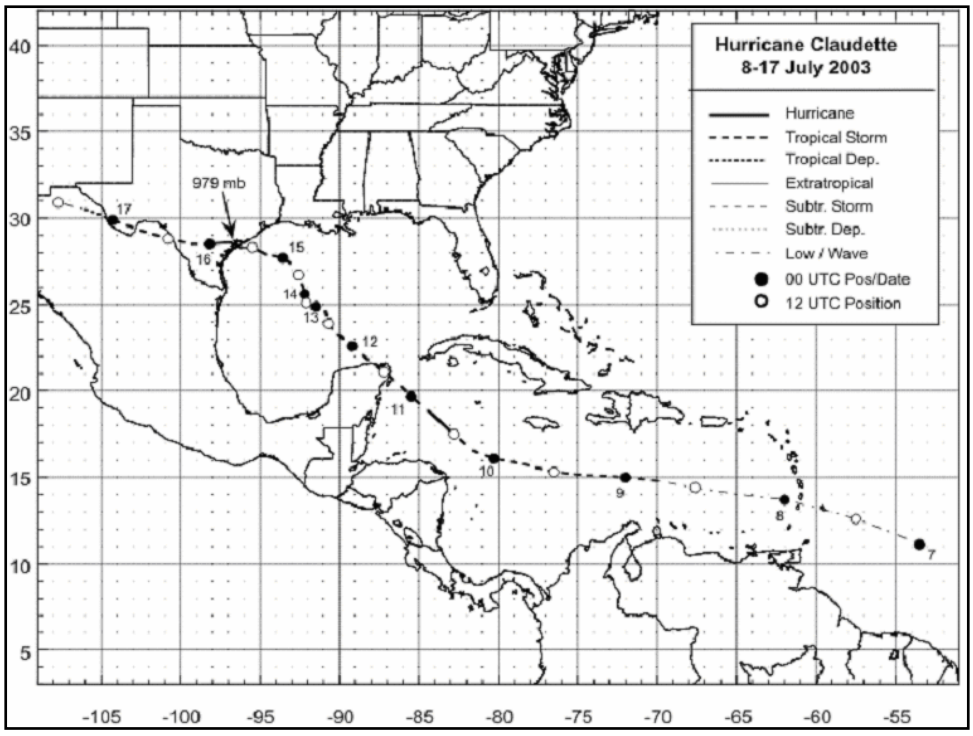

Figure 45. Storm track of Hurricane Claudette (2003). Figure courtesy of NOAA.

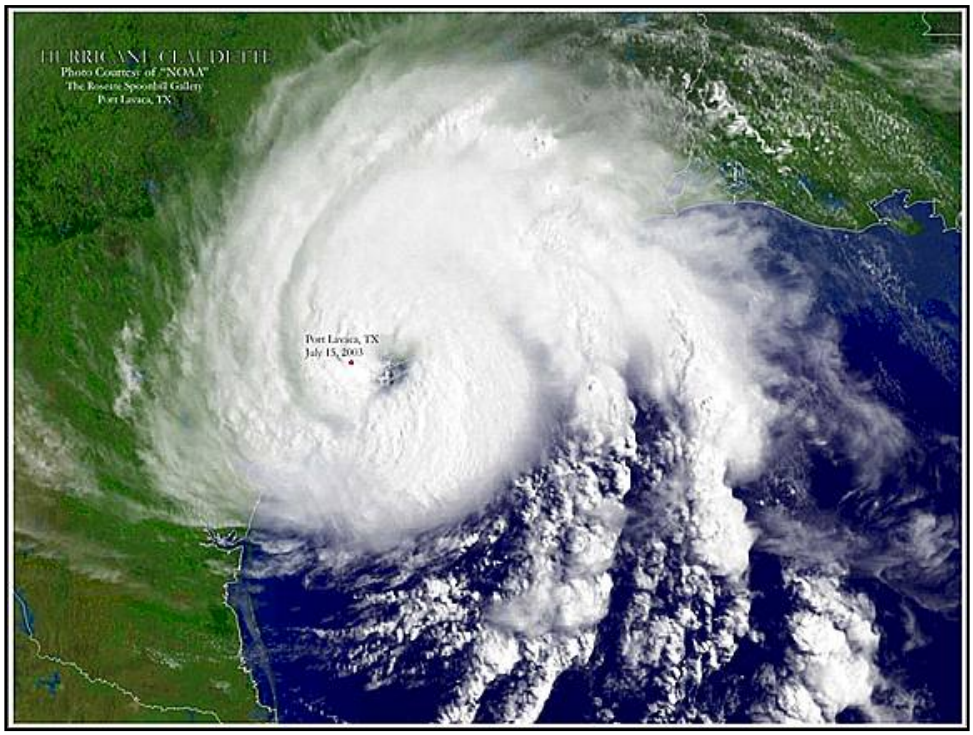

Figure 46. Satellite image of Hurricane Claudette at landfall, 15 July 2003. Photo courtesy of NOAA.

At closest approach on 15 July, the storm was south of the study area and was moving roughly parallel to the coast. At that time it was approximately 90 miles (145 km) from the Galveston Island profile measurement site, approximately 95 miles (150 km) from the Galveston Pleasure Pier and from NDBC Buoy 42035, and approximately 110 miles (178 km) from the Bolivar Peninsula profile measurement site. Satellite imagery revealed a variable eye wall with a radius to maximum winds of the order 10 miles (16 km). Onshore winds of tropical storm intensity occurred throughout the study area. Galveston Pleasure Pier reported maximum sustained winds of 42 knots (22 m/s) with gusts to 54 knots (28 m/s).

Waves and water levels

Wave data were obtained from NOAA NDBC Buoy 42035 and water levels from the Galveston Pleasure Pier for the time period between the pre- and post-storm profile measurements. These data are shown in Figure 47, and the gage locations and profile measurement sites are shown in Figure 48. Water level datums are referenced to NAVD88 (Table 5). With wave heights in excess of 5 m and storm surge water elevations of nearly 2 m, Hurricane Claudette on 15 July (Julian day 196) is clearly the most distinctive event in this data set (Figure 47). The only other tropical storm system in the Gulf of Mexico during this period was Tropical Storm Bob, which made landfall in Louisiana on 30 June (Julian day 181). Within the study area, Bob generated maximum wave heights of 1.8 m and a maximum water elevation of 0.74 m. The other near 2-m wave height events in the data set were from non-tropical storms and were not accompanied by noticeable increases in water elevations. Anecdotal observations support the conclusion that during this time period the only significant changes to the upper portions of the beach (the upper berm and dune area) occurred during the passage of Hurricane Claudette.

Though not optimal, wave and water level data from single locations were acceptable because of the track of this hurricane. When a hurricane makes landfall, variations in both wave height and water level can be substantial between the left and right sides of the eye because of differences in wind direction. However, Claudette was moving roughly parallel to the shoreline of the study area and was far enough away to be well outside the radius of maximum winds, but near enough to cause considerable impacts to the study area. Thus, the Galveston profile site, being west of the Bolivar site and a little closer to the storm track, likely experienced maximum wave heights and water levels that were later in the day and of somewhat greater

intensity. However, it is assumed that the wave heights and water levels at the two profile sites can be adequately represented by data from the measurement stations that were located between them (Figure 48).

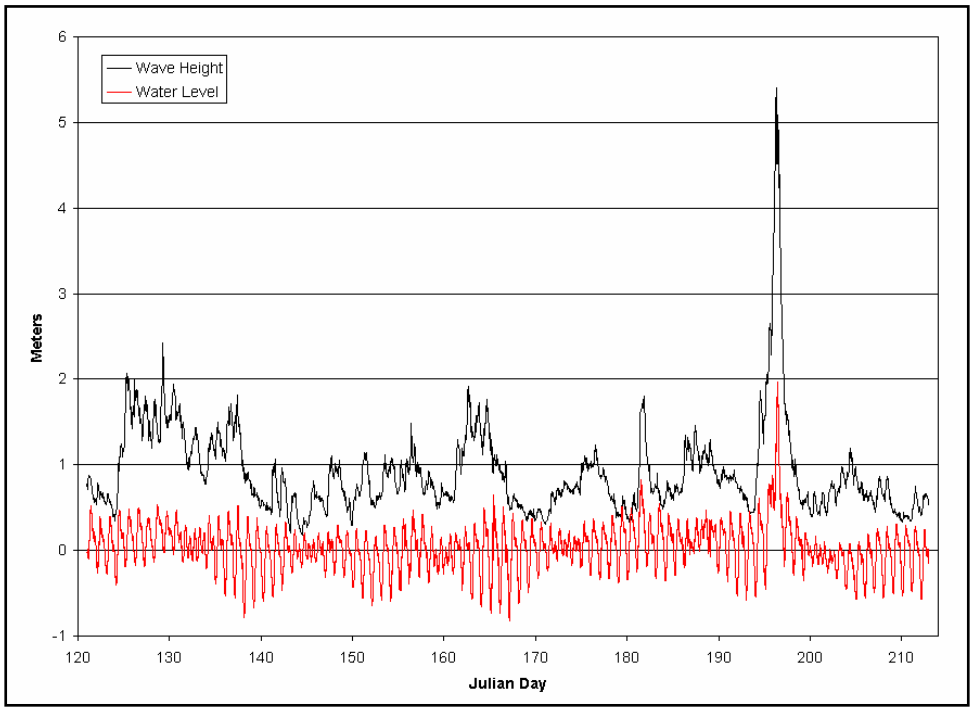

Figure 47. NDBC Buoy 42035 wave heights and Galveston Pleasure Pier water levels for time between surveys (1 May and 31 July 2003).

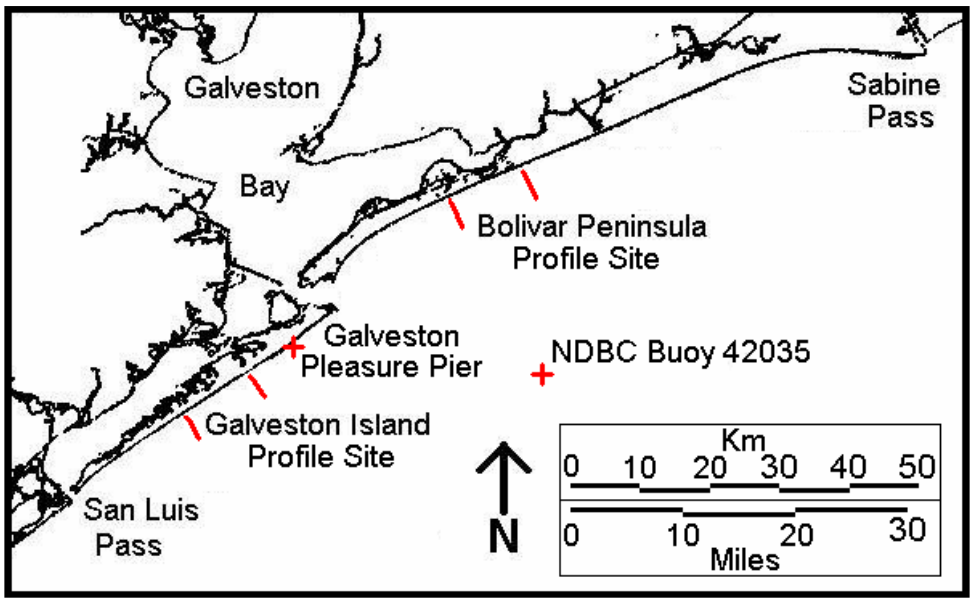

Figure 48. Site map showing locations of profile measurements and wave and water level gages.

The SBEACH calibration was performed using only the wave and water level data from 13 through 17 July (Julian days 194-198), as shown in Figure 49. A limited number of model runs were made using the entire 3-month time series, but these did not noticeably change the model results or improve the agreement between predicted and measured post-storm profiles. Before running the model, the wave data from the 13.7-m deep NDBC buoy were Phase-3 transformed to 8.5-m depth, corresponding to the seaward edge of the SBEACH grid. Differences in shoreline orientation are the main reason for differences in the transformations at the two sites.

The peak water level in Figure 49 lags the peak wave heights by a few hours. This shift is partially due to the Galveston Pleasure Pier being 23 miles (37 km) west of NDBC Buoy 42035. However, given the uncertainty in the exact storm track and speed and in the time of peak wave intensity, plus the water level record being a combination of storm and astronomical tide, it was not considered appropriate for this study to attempt to exactly align the two peaks.

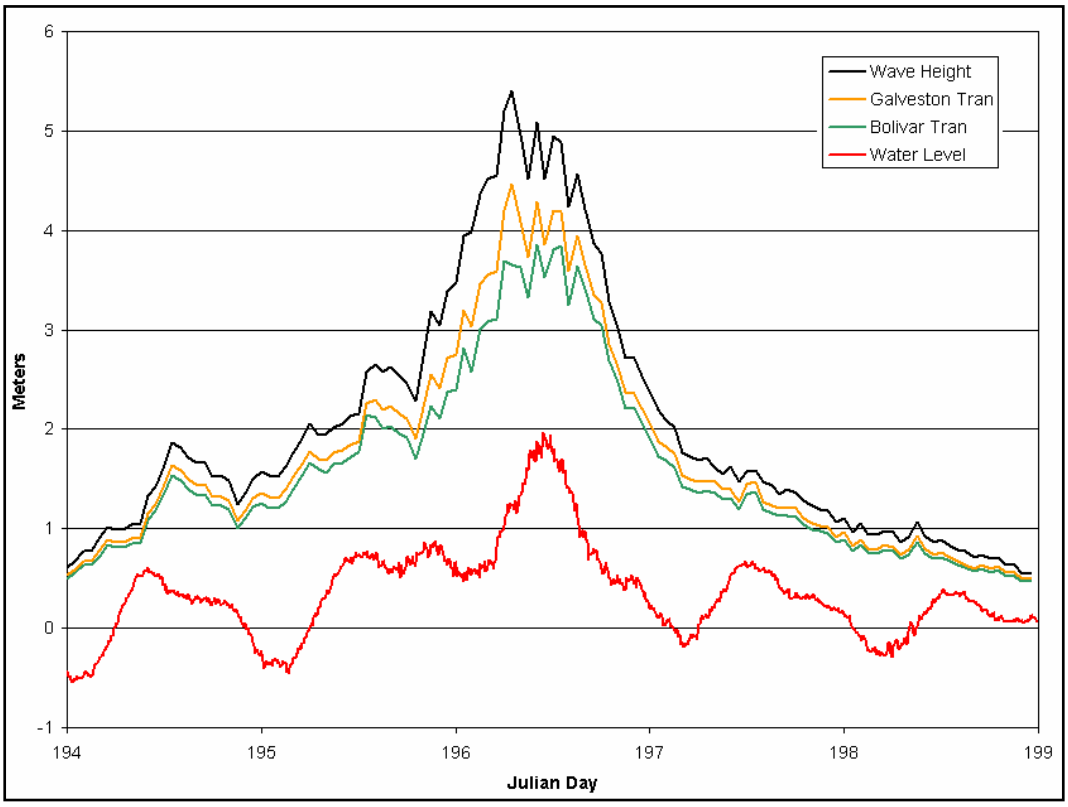

Figure 49. NDBC Buoy 42035 wave heights, Galveston Island transformed wave heights, Bolivar Peninsula transformed wave heights, and Galveston Pleasure Pier water levels for 13 to 17 July 2003.

Storm damage

Within the study area, the impacts of Hurricane Claudette were substantial, but not catastrophic. Examples of damage are shown in Figures 50 and 51. Shiner Moseley (2004) states,

> *Claudette caused… an estimated total damage of $180,000,000 along the Texas coast. Observations and measurements within the monitoring areas indicated that significant erosion to the beaches and dunes as well as damage to some of the geotextile tubes occurred. Fortunately, no houses within the monitoring areas were destroyed. However, many houses that were not protected by geotextile tubes, such as within the Sunny Beach, Spanish Grant, and Bermuda Beach subdivisions, were seaward of the vegetation line following the storm.*

In locations protected by geotextile tubes, practically all the sand and vegetation covering the tubes was removed, and nominal amounts of erosion occurred on the landward side (Figure 52). However, damage to infrastructure was mostly limited to dune walkover and driveover structures and to the geotextile tubes themselves.

The storm's short duration undoubtedly kept the damage from being worse. As seen in Figure 49, mean water levels in excess of 1 m occurred for less than half a day and wave heights in excess of 3 m occurred for less than a day. By comparison, Tropical Storm Francis in September 1998 was the next most significant storm to impact the study area within the last 10 years. Though that storm had lower maximum water levels (1.6 m) and wave heights (4 m), as measured at the same two gages, water elevations above 1 m and wave heights above 3 m both occurred for over two days.

Figure 50. Berm and dune damage on Galveston Island due to Hurricane Claudette (2003). Photo courtesy of Galveston County.

Figure 51. Hurricane Claudette induced localized geotextile tube damage on Bolivar Peninsula (2003). Photo courtesy of Shiner Moseley and Associates, Inc.

Figure 52. Bolivar Peninsula - Geotextile tube is fully exposed with minor erosion damage on landward side (2003). Photo courtesy of Shiner Moseley and Associates, Inc.

Shiner Moseley profiles

On west Galveston Island, SMA collected profiles on 77 range lines covering 7.4 miles (11.9 km) between Galveston Island State Park and the west end of the Galveston Seawall. They collected pre-storm profiles between 7 April and 13 May and post-storm profiles between 21 and 30 July. On Bolivar Peninsula, SMA collected profiles on 72 range lines covering 3.5 miles (5.6 km) on both sides of Rollover Pass (Figure 48). Pre-storm profile collection dates were 15-22 May, and post-storm dates were 22 July to 7 August.

Typical profiles extended from the top of the dune or geotextile tube at about +6 to +9 feet (+2 to +3 m) out to a wading depth of –2 ft (-0.6 m). All elevations are referenced to NAVD88 (Table 5) Typical horizontal distances surveyed were between 300 and 400 ft (90 - 120 m). Profiles were spaced along the beach every 500 ft (152.4 m). The locations of the range lines are given in Tables 34 and 35.

Table 34. Galveston Island Pre- and Post-Hurricane Claudette profile locations.

Rangeline	Distance West of West End of Galveston Seawall		Nearest Closure Depth Profile	Profiles Used in Analysis	Dune / Geotextile Tube	Reference Beach Name
	feet	meters				
385+00	38,500	11,735	G022	yes	low dune	Galveston Island St. Park
380+00	38,000	11,582	G022	yes	low dune no	Galveston Island St. Park
375+00	37,500	11,430	G022	yes	low dune no	Galveston Island St. Park
370+00	37,000	11,278	G022	yes	low dune no	Galveston Island St. Park
365+00	36,500	11,125	G023	yes	low dune	Galveston Island St. Park
360+00	36,000	10,973	G023	yes	low dune no	Galveston Island St. Park
355+00	35,500	10,820	G023	yes	low dune no	Galveston Island St. Park
350+00	35,000	10,668	G023	yes	low dune no	Galveston Island St. Park
345+00	34,500	10,516	G023	yes	low dune	Galveston Island St. Park
340+00	34,000	10,363	G024	yes	low dune no	Galveston Island St. Park
335+00	33,500	10,211	G024	yes	low dune no	Galveston Island St. Park
330+00	33,000	10,058	G024	yes	low dune no	Galveston Island St. Park
325+00	32,500	9,906	G024	yes	low dune	Galveston Island St. Park
320+00	32,000	9,754	G024	yes	low dune no	Galveston Island St. Park
315+00	31,500	9,601	G025	yes	low dune no	Galveston Island St. Park
310+00	31,000	9,449	G025	not used 1		Galveston Island St. Park
305+00	30,500	9,296	G025	not used 1		
300+00	30,000	9,144	G025	yes	Geo tube	Pirates Beach West
295+00	29,500	8,992	G025	yes	Geo tube	Pirates Beach West
290+00	29,000	8,839	G026	yes	Geo tube	Pirates Beach West
285+00	28,500	8,687	G026	yes	Geo tube	Palm Beach

Rangeline	Distance West of West End of Galveston Seawall		Nearest Closure Depth Profile	Profiles Used in Analysis	Dune / Geotextile Tube	Reference Beach Name
	feet	meters				
280+00	28,000	8,534	G026	yes	Geo tube	Palm Beach
275+00	27,500	8,382	G026	yes	Geo tube	Pirates Beach
270+00	27,000	8,230	G026	not used 1	Geo tube	Pirates Beach
265+00	26,500	8,077	G026	yes	Geo tube	Pirates Beach
260+00	26,000	7,925	G027	yes	Geo tube	Pirates Beach
255+00	25,500	7,772	G027	yes	Geo tube	Pirates Beach
250+00	25,000	7,620	G027	yes	Geo tube	Pirates Beach
245+00	24,500	7,468	G027	yes	Geo tube	Pirates Beach
240+00	24,000	7,315	G027	yes	Geo tube	Pirates Beach
235+00	23,500	7,163	G028	yes	Geo tube	Pirates Beach
230+00	23,000	7,010	G028	yes	Geo tube	Pirates Beach
225+00	22,500	6,858	G028	yes	Geo tube	Pirates Beach
220+00	22,000	6,706	G028	yes	high dune	
215+00	21,500	6,553	G028	not used 1		
210+00	21,000	6,401	G029	yes	high dune	
205+00	20,500	6,248	G029	yes	low dune	
200+00	20,000	6,096	G029	yes	low dune	
195+00	19,500	5,944	G029	yes	low dune	Bermuda Beach
190+00	19,000	5,791	G029	yes	low dune	Bermuda Beach
185+00	18,500	5,639	G030	not used 1		Bermuda Beach
180+00	18,000	5,486	G030	yes	low dune	Bermuda Beach
175+00	17,500	5,334	G030	yes	low dune	Bermuda Beach
170+00	17,000	5,182	G030	not used 1		Bermuda Beach
165+00	16,500	5,029	G030	yes	low dune	Bermuda Beach
160+00	16,000	4,877	G030	yes	low dune	Spanish Grant
155+00	15,500	4,724	G031	yes	low dune	Spanish Grant
150+00	15,000	4,572	G031	yes	high dune	Spanish Grant
145+00	14,500	4,420	G031	yes	high dune	Hershey Beach
140+00	14,000	4,267	G031	yes	high dune	Hershey Beach
135+00	13,500	4,115	G031	yes	high dune	
130+00	13,000	3,962	G032	not used 1		

Rangeline	Distance West of West End of Galveston Seawall		Nearest Closure Depth Profile	Profiles Used in Analysis	Dune / Geotextile Tube	Reference Beach Name
	feet	meters				
125+00	12,500	3,810	G032	yes	Geo tube	W Beach Grand & Riviera
120+00	12,000	3,658	G032	not used 1		
115+00	11,500	3,505	G032	yes	high dune	Sands of Kahala
110+00	11,000	3,353	G032	yes	high dune	
105+00	10,500	3,200	G033	yes	low dune	
100+00	10,000	3,048	G033	yes	Geo tube	Beach Pocket Park No. 2
95+00	9,500	2,896	G033	yes	high dune	
90+00	9,000	2,743	G033	yes	high dune	
85+00	8,500	2,591	G033	not used 1		
80+00	8,000	2,438	G034	yes	low dune	
75+00	7,500	2,286	G034	yes	high dune	
70+00	7,000	2,134	G034	yes	high dune	
65+00	6,500	1,981	G034	yes	high dune	
60+00	6,000	1,829	G034	yes	low dune	
55+00	5,500	1,676	G034	yes	high dune	
50+00	5,000	1,524	G035	yes	high dune	Sunny Beach
45+00	4,500	1,372	G035	yes	low dune	
40+00	4,000	1,219	G035	not used 1		
35+00	3,500	1,067	G035	not used 1		
30+00	3,000	914	G035	not used 1		
25+00	2,500	762	G036	not used 1		
20+00	2,000	610	G036	not used 3		Dellanera RV Park
15+00	1,500	457	G036	not used 3		Dellanera RV Park
10+00	1,000	305	G036	not used 3		Seascape condos
5+00	500	152	G036	not used 3		
	0	0				West end of Gal Seawall

Table 35. High Island Pre- and Post-Hurricane Claudette profile locations.

Rangeline	Distance West of Rollover Pass		Nearest Closure Depth Profile	Profiles Used in Analysis	Dune / Geotextile Tube	Reference Beach Name
	feet	meters				
180+00	18,000	5,486	L026	yes	high dune	
175+00	17,500	5,334	L026	yes	high dune	
170+00	17,000	5,182	L026	yes	high dune	Caplen Shores
165+00	16,500	5,029	L027	yes	high dune	Caplen
160+00	16,000	4,877	L027	yes	high dune	Caplen
155+00	15,500	4,724	L027	yes	high dune	Caplen
150+00	15,000	4,572	L027	yes	high dune	Caplen
145+00	14,500	4,420	L027	yes	high dune	Caplen
140+00	14,000	4,267	L027	yes	Geo tube	Caplen
135+00	13,500	4,115	L028	yes	Geo tube	Caplen
130+00	13,000	3,962	L028	yes	Geo tube	Caplen
125+00	12,500	3,810	L028	yes	Geo tube	Caplen
120+00	12,000	3,658	L028	yes	Geo tube	Caplen
115+00	11,500	3,505	L028	not used 1	Geo tube	Caplen
110+00	11,000	3,353	L029	yes	Geo tube	Caplen
105+00	10,500	3,200	L029	yes	Geo tube	Caplen
100+00	10,000	3,048	L029	not used 1	Geo tube	Caplen
95+00	9,500	2,896	L029	yes	Geo tube	Caplen
90+00	9,000	2,743	L029	yes	Geo tube	Caplen
85+00	8,500	2,591	L030	yes	Geo tube	Caplen
80+00	8,000	2,438	L030	not used 1	Geo tube	Caplen
75+00	7,500	2,286	L030	not used 1	Geo tube	Caplen
70+00	7,000	2,134	L030	not used 1	Geo tube	Caplen
65+00	6,500	1,981	L030	not used 1	Geo tube	Caplen
60+00	6,000	1,829	L031	yes	Geo tube	Caplen / Gilchrist
55+00	5,500	1,676	L031	not used 1	Geo tube	Caplen / Gilchrist
50+00	5,000	1,524	L031	yes	Geo tube	Caplen / Gilchrist
45+00	4,500	1,372	L031	yes	Geo tube	Gilchrist
40+00	4,000	1,219	L031	not used 1	Geo tube	Gilchrist
35+00	3,500	1,067	L031	yes	Geo tube	Gilchrist
30+00	3,000	914	L032	yes	Geo tube	Gilchrist
25+00	2,500	762	L032	yes	Geo tube	Gilchrist
20+00	2,000	610	L032	yes	Geo tube	Gilchrist
15+00	1,500	457	L032	yes	Geo tube	Gilchrist

Rangeline	Distance West of Rollover Pass		Nearest Closure Depth Profile	Profiles Used in Analysis	Dune / Geotextile Tube	Reference Beach Name
	feet	meters				
10+00	1,000	305	L032	yes	Geo tube	Gilchrist
5+00	500	152	L033	not used 2	Geo tube	Gilchrist
	0	0				Rollover Pass
-5+00	-500	-152	L033	not used 2	Geo tube	Gilchrist
-10+00	-1,000	-305	L033	not used 2	Geo tube	Gilchrist
-15+00	-1,500	-457	L033	not used 2	Geo tube	Gilchrist
-20+00	-2,000	-610	L034	yes	Geo tube	Gilchrist
-25+00	-2,500	-762	L034	yes	Geo tube	Gilchrist
-30+00	-3,000	-914	L034	yes	Geo tube	Gilchrist
-35+00	-3,500	-1,067	L034	yes	Geo tube	Gilchrist
-40+00	-4,000	-1,219	L034	yes	Geo tube	Gilchrist
-45+00	-4,500	-1,372	L035	yes	Geo tube	Gilchrist
-50+00	-5,000	-1,524	L035	yes	Geo tube	Gilchrist
-55+00	-5,500	-1,676	L035	yes	Geo tube	Gilchrist
-60+00	-6,000	-1,829	L035	yes	Geo tube	Gilchrist
-65+00	-6,500	-1,981	L035	yes	Geo tube	Gilchrist
-70+00	-7,000	-2,134	L035	yes	Geo tube	Gilchrist
-75+00	-7,500	-2,286	L036	yes	Geo tube	Gilchrist
-80+00	-8,000	-2,438	L036	yes	Geo tube	Gilchrist
-85+00	-8,500	-2,591	L036	yes	Geo tube	Gilchrist
-90+00	-9,000	-2,743	L036	yes	Geo tube	Gilchrist
-95+00	-9,500	-2,896	L036	yes	Geo tube	Gilchrist
-100+00	-10,000	-3,048	L037	yes	Geo tube	Gilchrist
-105+00	-10,500	-3,200	L037	yes	Geo tube	Gilchrist
-110+00	-11,000	-3,353	L037	yes	Geo tube	Gilchrist
-115+00	-11,500	-3,505	L037	yes	Geo tube	Gilchrist
-120+00	-12,000	-3,658	L037	yes	Geo tube	Gilchrist
-125+00	-12,500	-3,810	L038	yes	Geo tube	Gilchrist
-130+00	-13,000	-3,962	L038	yes	Geo tube	Gilchrist
-135+00	-13,500	-4,115	L038	yes	high dune	Gilchrist
-140+00	-14,000	-4,267	L038	yes	high dune	near Dirty Pelican Pier
-145+00	-14,500	-4,420	L038	yes	low dune	Gilchrist
-150+00	-15,000	-4,572	L038	yes	low dune	Gilchrist
-155+00	-15,500	-4,724	L039	yes	low dune	Gilchrist
-160+00	-16,000	-4,877	L039	yes	high dune	Gilchrist
-165+00	-16,500	-5,029	L039	yes	low dune	Gilchrist

Rangeline	Distance West of Rollover Pass		Nearest Closure Depth Profile	Profiles Used in Analysis	Dune / Geotextile Tube	Reference Beach Name
	feet	meters				
-170+00	-17,000	-5,182	L039	yes	low dune	Gilchrist
-175+00	-17,500	-5,334	L039	yes	low dune	Gilchrist
-180+00	-18,000	-5,486	L040	yes	low dune	Gilchrist

At each site, the profiles were divided into three groups, high dune, low dune, and geotextile tube. Non-tube profiles that had a maximum pre-storm elevation in excess of 2.7 m were classified as high dune; those with lower maximum elevations, as low dune. The value 2.7 m was picked because it approximately divided the non-tube profiles in half and because it was approximately the elevation at which the SBEACH model predicted overwash for this storm.

Typical gross changes between the pre-and post-storm profiles were similar at both sites and for all three profile types. These included a cutback of the berm and dune areas with accretion at lower elevations causing a flattening of the profile. Since the post-storm profiles were collected one to three weeks after the storm, they include an unknown amount of beach recovery. The accretion seen at the lower elevations may be partially the result of this post-storm recovery. However, it is very unlikely that the erosion seen at the higher elevations is due to anything other than the direct impact of the storm. Therefore, in the calibration analysis, greater emphasis was placed on trying to accurately model the upper portions of the profiles. In addition, lower portions of the profiles tended to show more random scatter in profile elevations.

The major erosion occurred in the vicinity of the berm, at elevations in the 1- to 2-m range. Some profiles showed a horizontal retreat of up to 25 m at these elevations, and a vertical loss of up to 2.5 m. Higher up, in the region of the dunes, the typical retreat was less. Locations protected by geotextile tubes logically showed less retreat at these elevations than unprotected locations; however, this restricted the amount of sand available at the lowest elevations to prograde the beach.

Most profiles switched from erosional to accretional below an elevation of +0.3 to +0.4 m, though there was considerable scatter in the exact

crossover elevation. Below this, most profiles showed substantial accretion.

Profile preparation and model runs

The profile data were first inspected for pairing of pre- and post-storm profiles and for quality control. The data were converted from (x, y, z) format to (x, z) format using an azimuth of 147 degrees for Galveston Island and 157 degrees for Bolivar Peninsula. The most landward point of each pre-storm profile usually occurred near the top of the geotextile tube or crest of the dune and was assigned a horizontal position of zero. The post-storm profiles (which typically started a few meters landward of the pre-storm profiles) were registered to the same pre-storm zero position.

Since the profiles only extended to wading depths, they were extended seaward using the nearest profile from the Texas A&M profile set (see Chapter 7). The Texas A&M profiles extended to approximately –8.5-m depth (the region of the depth of closure). The specific profiles that were combined are listed in Tables 34 and 35. Since the post-storm profiles showed that erosion frequently occurred landward of the most landward points on the pre-storm profiles, both pre- and post-storm profiles were extended to -50 m (landward) using the elevation of the pre-storm zero position. Though the profiles were extended in both landward and seaward directions to help with the stability of the model, for calibration purposes, the model output was compared with the post-storm profiles only between the horizontal distances of zero and +90 to +120 m, the region covered by the pre- and post-storm profiles.

A few profiles from both sites were not used in the analysis. Reasons for rejection included the following: (1) either the pre- or post-storm profile had questionable or missing data, (2) the Texas A&M profile had questionable or missing data, (3) or a beach fill had occurred between the survey dates. These numbers are keyed to individual rejected profiles in Tables 34 and 35.

Finally, the profiles were interpolated at 2-m intervals for use with the SBEACH grid. Preparation of the profiles was primarily accomplished using the computer programs Excel and BMAP. Then the profile data, along with wave height and period data, water level data, and model control data, were entered into SBEACH. The model grid used was the same as described as for the model setup in Chapter 7; 2-m cells between

-50 and +200 m, then 10-m cells to +400 m, and then 50-m cells to the seaward end of the grid. Thus, comparisons with post-storm profiles were made in the region of finest grid spacing (0 to +90 (or +120) m).

The first SBEACH model runs were made using the recommended default parameter, K=1.75 x 10^{-6} m^4/N. Then runs were made throughout the entire recommended parameter range (0.5 to 2.5 x 10^{-6} m^4/N). However, it became clear that the optimum value would be somewhat above the default value, so most runs were made using K values between 1.75 and 2.50 x 10^{-6} m^4/N. Profiles with geotextile tubes were considered seawall profiles in SBEACH (no failure allowed). Since the hurricane removed all the sand from the geotextile tubes, the location of the tube (seawall) was determined by the location of the steepest slope (above +2 m) on the post-storm profiles.

Data analysis and results

The model results were compared with the post-storm profiles, both subjectively and objectively. Subjective analysis consisted of examining pre-storm, post-storm, and model output profile plots. Several objective measures of model performance were utilized, including the following: the most landward position of an erosion depth, erosion volume, recession distances of an elevation, and RMS and residual error analysis.

Profile comparisons

Example profile plots are shown in Figure 53. These show the erosion at the higher elevations and how well the model fits the post-storm profiles. The model profiles generally predict the erosion/accretion crossover point in the vicinity of –0.5 m, substantially below the typical measured crossover point.

Erosion depth

The economics model, which will be used in this study to determine the financial impact of storms on the coastline, uses an erosion depth definition of erosion. That is, damages are estimated based upon how far inland erosion depths of 6 in., 2 ft, and 4 ft occur. While it was considered important to calibrate the model based upon this parameter, unfortunately the profile data were not suitable for this type of analysis. The main problem was that the profiles (mainly pre-storm) did not extend far

enough inland. As seen in Table 36, most of the Bolivar profiles show erosion depths in excess of the criteria at their most landward locations. The Galveston Island results were similar. Therefore, this definition of erosion could not be used in this calibration effort.

Erosion volume

Another definition of erosion is the volume of sediment removed above a certain elevation. For this study, the erosion volume was defined as the change in volume above the 0.5-m line (the white line in Figure 53) and seaward of the horizontal zero position. Pre-storm/post-storm vs. pre-storm/model erosion volume differences are shown in Appendix D, Figure D1 (calibration coefficient $K=2.25 \times 10^{-6}$ m^4/N). These show generally good agreement between measured and predicted volume differences, though measured volumes tend to exceed predicted volumes, particularly for geo tube profiles.

Recession distances

A similar definition of erosion is the amount of retreat of a given elevation contour. Scatterplots of predicted vs. measured recession distances at elevations of 3, 2.5, 2.0, 1.5, 1.0, 0.5, 0.0, and -0.5 m are shown in Appendix D, Figures D2 through D9 (for $K=2.25 \times 10^{-6}$ m^4/N). There is quite good agreement at the upper elevations; however, agreement becomes substantially poorer at the lower elevations. This is also shown in the correlation coefficients listed in Table 37. At elevations of 3.0 and 2.5 m, the agreement is excellent, and the non-tube profiles show distinctly greater erosion rates than the tube profiles. At 2.0 m elevation, there starts to be more scatter in the data. The tube profiles, particularly on Bolivar Peninsula, continue to show less erosion. At elevations of 1.5 and 1.0 m, the measured erosion exceeds the predicted, and there are differences in the profile behavior between the Galveston and Bolivar sites. At 0.0 and –0.5 m, the predicted exceeds the measured, and there is considerable scatter in the data.

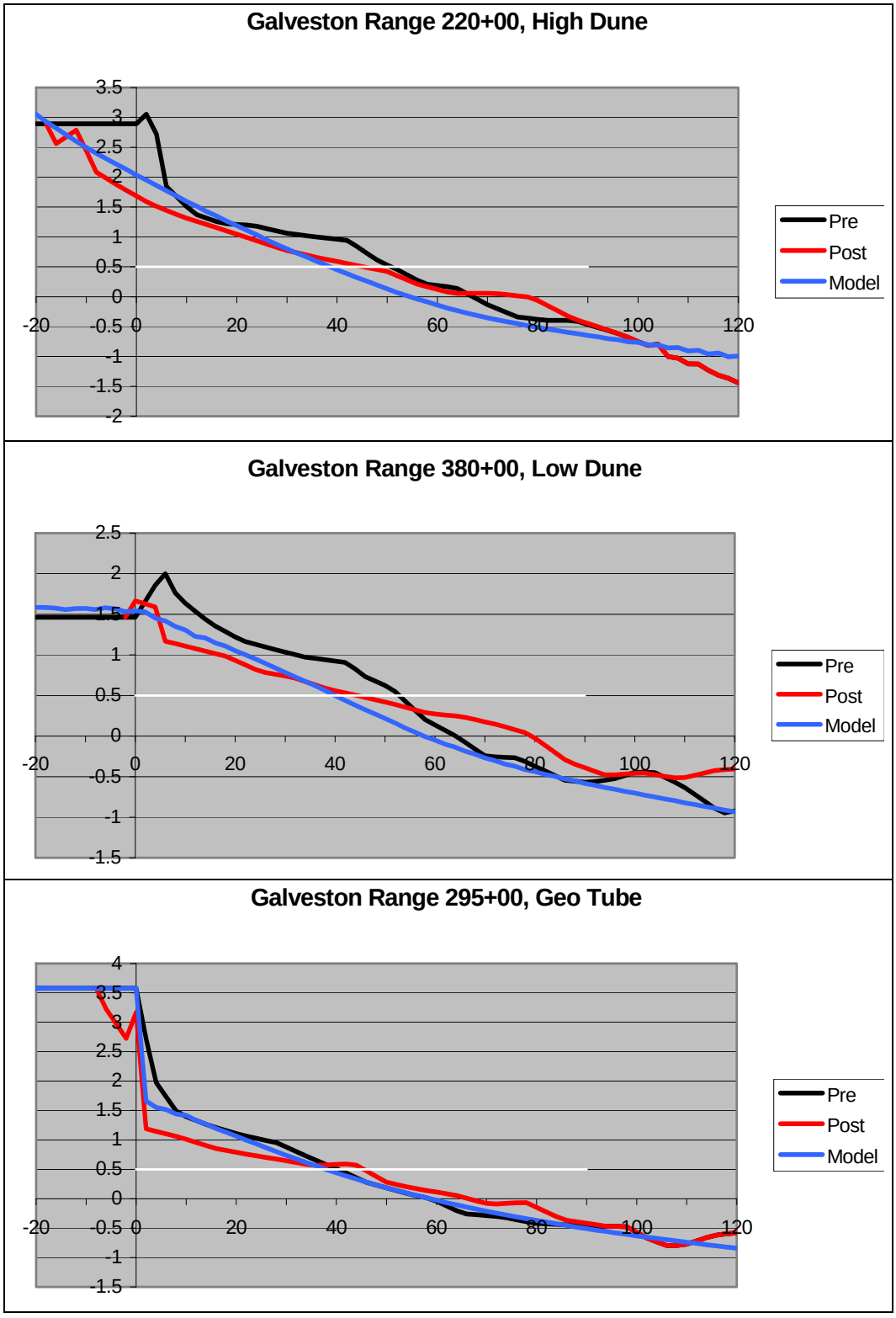

Figure 53. Examples of Galveston Island SBEACH calibration profiles.

Table 36. Distribution of erosion depths - Bolivar Peninsula data, 60 profiles in set.

Profile Type	Post-Storm	Model	Post-Storm	Model	Post-Storm	Model	Post-Storm	Model	Post-Storm	Model
Erosion Depth criterion	6 inches		1 foot		2 feet		3 feet		4 feet	
Profiles where erosion depth did not meet criterion at any location	0	0	0	0	0	6	9	12	15	18
Profiles where erosion depth occurred landward of or at most landward profile position	54	54	52	56	50	49	47	44	43	42
Useful Profiles	6	6	8	4	10	5	4	4	2	0
For all useful profiles, maximum distance from landward end of profile (m)	8.01	4.48	9.42	7.59	13.95	6.87	7.84	10.95	11.92	-

Table 37. Correlation coefficients (r) for measured vs. predicted elevation and volume changes on Galveston and Bolivar profiles.

Elevation	All		High Dune		Low Dune		Geo Tube	
	Gal	Bol	Gal	Bol	Gal	Bol	Gal	Bol
3.0	0.42	0.89	-	0.78	-	-	0.42	0.66
2.5	0.74	0.88	-	0.64	-	-	0.73	0.66
2.0	0.38	0.64	0.30	0.92	0.83	0.43	0.64	0.60
1.5	0.47	0.65	0.56	0.77	0.41	0.88	-0.44	0.62
1.0	0.67	0.25	0.89	0.78	0.74	0.86	0.21	-0.10
0.5	0.08	0.27	0.72	0.37	0.47	0.77	-0.45	0.18
0.0	0.10	0.19	0.10	0.64	-0.34	-0.24	0.58	-0.03
-0.5	0.43	0.07	0.23	0.49	0.16	0.08	0.60	-0.11

RMS and residual model performance

The following is from Wise, Smith, and Larson (1996):

> *Measures of performance . . . are based upon the statistical fit of the calculated profile to the measured profile for a given simulation. These measures of performance include an rms parameter (RMS) and a residual parameter (Res). RMS is a measure of the rms difference between the measured and calculated profiles and is given by:*

$$RMS = \sqrt{\frac{1}{N_p}\sum_{j=1}^{N_p}(y_m - y_c)^2}$$

The residual is given by:

$$\text{Res} = \frac{\sum_{j=1}^{N_p}\sqrt{(y_m - y_c)^2}}{\sum_{j=1}^{N_p}\sqrt{(y_i - y_m)^2}}$$

where:

y_i = *initial profile elevation*

y_m = *measured final profile elevation*

y_c = *calculated final profile elevation, and*

N_p = *number of points across the profile.*

RMS gives a measure of the average absolute difference between the calculated elevations and the measured elevations. The residual, Res, is similar to a parameter used by Zheng and Dean (1995) and provides a relative measure of the difference between the measured and calculated profiles as compared to the amount of actual change that has occurred over a given range of the profile. Smaller values of RMS and Res correspond to a better fit.

Table 38 lists the *RMS* and *Res* calculated values for the optimal calibration coefficient.

Table 38. Model performance.

	RMS		*Res*	
	Gal	Bol	Gal	Bol
All	0.17	0.23	0.60	0.69
High Dune	0.17	0.17	0.76	0.58
Low Dune	0.11	0.15	0.46	0.62
Geo Tube	0.27	0.26	0.70	0.74

Results

SBEACH contains several calibration parameters. The transport rate coefficient *K* is the primary calibration parameter, and SBEACH typically exhibits greater sensitivity to it than to the other parameters. *K* influences the rate at which transport occurs. Larger *K* values produce greater sand transport and more prominent bar features.

The slope-dependent coefficient ε influences the slope of the profile. It is included in the surf zone transport equation to account for local variations in profile slope. Lower values of ε result in steeper nearshore profiles and steeper bars. The transport rate decay coefficient multiplier *decay* affects the transport rate seaward of the breaker line. Larger values of the parameter result in more rapid transport rate decay. The parameter *DFS* defines the landward end of the surf zone on the modeled profile and affects the magnitude of transport in the swash zone. A higher value of *DFS*, corresponding to a greater depth at the boundary between the surf and swash zones, typically increases transport rates in the swash zone, producing more erosion at the foreshore. The *avalanche* angle is the maximum slope that the profile is allowed to achieve prior to avalanching. If the profile reaches an angle greater than this value at the end of any time-step, avalanching occurs and the slope is reduced to 10 degrees less than this value. Further information about these parameters can be found in Larson and Kraus (1989); Larson, Kraus, and Byrnes (1990); Rosati et al. 1993; and Wise, Smith, and Larson (1996).

Model runs were made varying each parameter individually, though the K coefficient was the most intensely studied. The other parameters were found to have little influence on the shape of the upper portion of the post-storm profile, and for these, the default values were kept. The optimal value for the K coefficient was K = 2.25 x 10^{-6} m^4/N. These values are given in Table 39.

Table 39. SBEACH calibration coefficients.

Coefficient		Default Value	Recommended Calibration Range	Final Calibration This Study	Units
Symbol	Name				
K	Transport rate coefficient	1.75 x 10^{-6}	0.5 x 10^{-6} to 2.5 x 10^{-6}	2.25 10^{-6}	m^4/N
ε	Slope dependent coefficient	0.002	0.001 to 0.003	0.002	m^2/sec
decay	Transport rate decay coefficient multiplier	0.5	0.1 to 0.5	0.5	-
DFS	Depth of the foreshore/swash boundary	0.5	0.15 to 0.5	0.5	meters
Avalanche	Avalanche angle	30	15 to 30	30	degrees

9 Results and Recommendations

STWAVE results

The STWAVE output is summarized in Figures 54 and 55. Panel A in both of these figures shows the locations of the output save stations, as the line of dots seaward of (above) the beach. These STWAVE output stations approximately follow the 6-m depth contour. For the High Island grid, only wave data from STWAVE output stations 68 to 267 (of the 300 save stations) were used by GENESIS. For the Galveston Island grid, GENESIS used the wave data from all 151 STWAVE output stations. Panels B and C show output wave heights and angles, respectively.

To produce panel B, wave heights at each save station were normalized by the offshore wave height (the WIS input wave height to STWAVE) and then averaged over the 10-year data set. Larger wave heights will generally lead to greater sediment transport. In Figure 54, the dip in the normalized wave heights at Sea Rim State Park (around save station 75) is due to the effects of wave refraction along the edge of the large shoal offshore of Texas Point and along the western side of Sabine Bank (see Figure 14). In Figure 55, the large changes in normalized wave height between stations 140 and 150 are the result of refraction over the San Luis Pass ebb shoal.

To produce panel C, the output wave angles were binned by the offshore wave angle, and then averaged within each 20-degree bin. The red line labeled “All” is the average of all the wave angles for each output station. The wave refraction effects of the Texas Point shoal, Sabine Bank, and the San Luis Pass ebb shoal are also evident in these angle plots. The greater variation in the High Island wave angles, as compared to the Galveston Island wave angles, is due to the more complicated offshore topography.

Wave angle lines that slope upward to the right are indicative of areas of erosion. Greater wave angles (generally) produce greater transport. For positive angles, sediment transport is to the right (Figure 20). If the wave angle line slopes upward to the right, there is more transport across the right hand wall of a GENESIS cell (out of the cell) than across the left hand wall (into the cell), and the cell experiences erosion. By the same argument, a wave angle line sloping upward to the right still indicates erosion if the angle is negative (meaning transport to the left). Conversely,

a line sloping upward to the left indicates an area of accretion. This effect can be overwhelmed by other transport effects, such as changes in wave height and in shoreline orientation. However, these STWAVE results help explain why much of the study area is experiencing erosion, while such areas as Sea Rim State Park and East Beach are experiencing accretion.

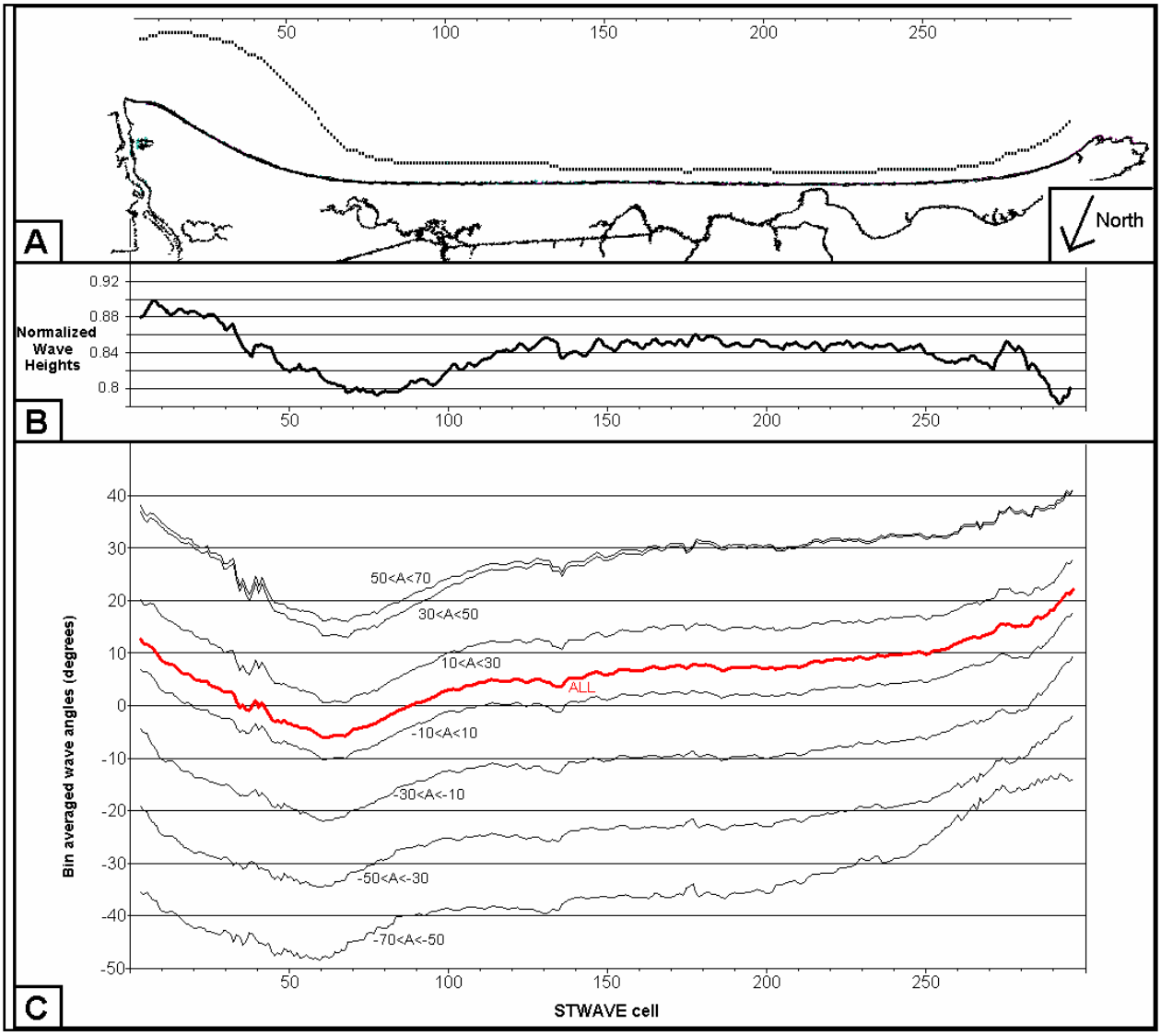

Figure 54. STWAVE results for High Island grid.

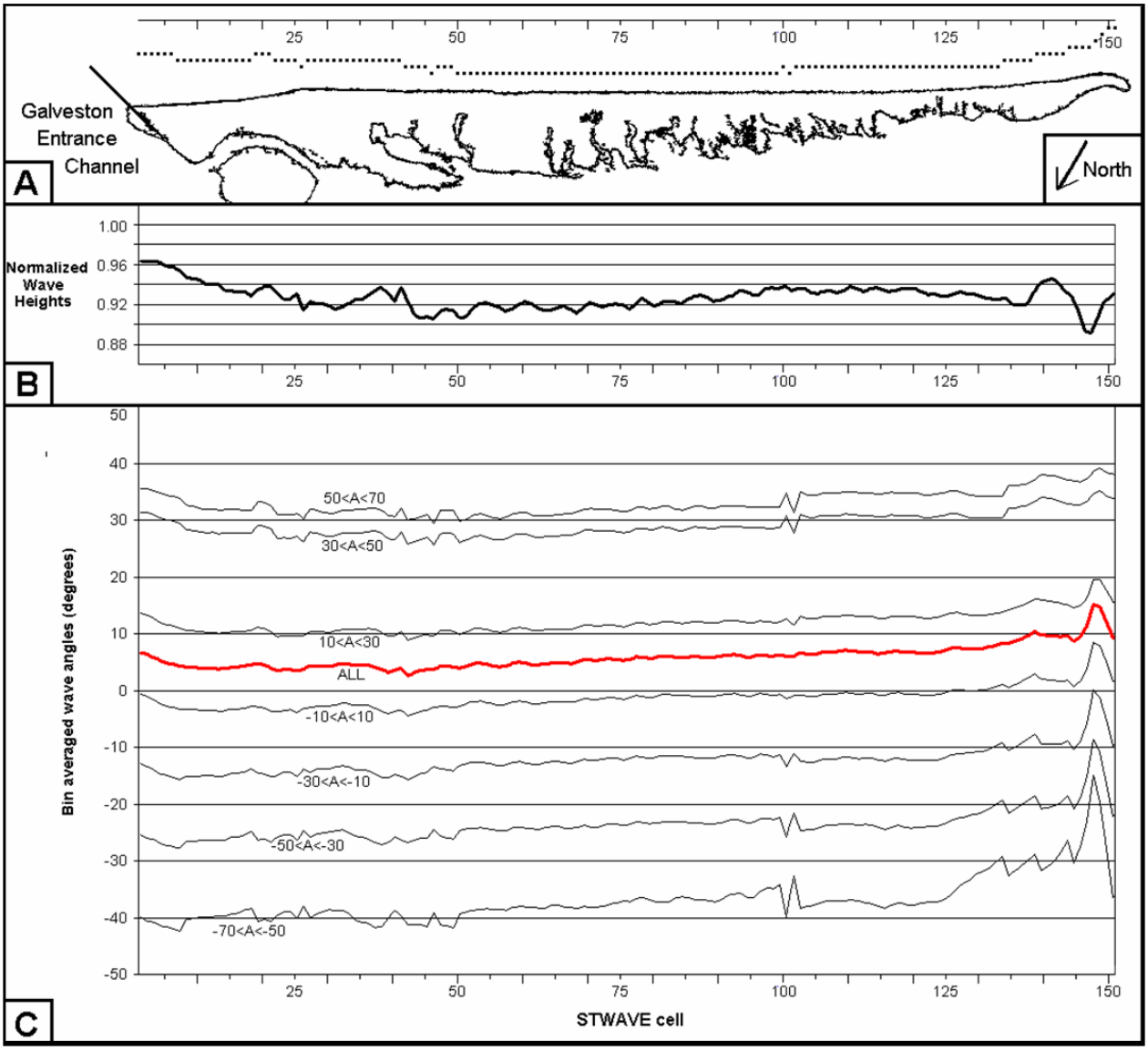

Figure 55. STWAVE results for Galveston Island grid.

Shoreline change results

Figures 56 and 57 show the average annual gross longshore transport rates, net rates, and shoreline change rates predicted by GENESIS. The gross transport rate on the High Island grid is a little smaller (450,000 to 500,000 m^3/yr) than along Galveston Island (600,000 to 750,000 m^3/yr) even though the K_1 and K_2 GENESIS calibration values are a little higher. These results compare favorably with earlier estimates (Tables 12 and 13). Except at the Galveston Seawall, the shapes of the gross transport curves are quite similar to the STWAVE output relative wave height curves shown in Figures 54 and 55.

The majority of both grids show net longshore transport to the southwest (Figure 20); though both show local reversals in the net transport direction, indicating that southwesterly net transport is not as universal along the northeast Texas coastline as has been frequently assumed (Chapter 2). The areas of net northeastward transport (Sea Rim State Park and East Beach) are both areas of accretion (Figures 10 and 11). The eastern end of the Galveston grid near the south jetty has 80,000 to 100,000 m^3 of sediment a year exiting the grid. This is a substantial portion of the 250,000 m^3 of sand on average dredged annually from the adjacent navigation channel (Morang 2006).

The GENESIS shoreline change estimate for the High Island grid shows reasonable agreement with the historical shoreline change indicated by the Gibeaut line (Figure 56). One area of substantial disagreement is along a section of the destroyed Highway 87 in Jefferson County (cells 80-135). One possible reason is the likely presence of highly erodable consolidated mud on the subaqueous profile (Chapter 3). Howard (1999) also had considerable difficulty realistically modeling the shoreline change in this area.

On the Galveston grid, the GENESIS shoreline change results show quite good agreement with the historical Gibeaut et al. (2002) line (Figure 57), generally being within a meter per year. One area of disagreement is at the west end of the Galveston Seawall. Because of the dramatic offset in the shoreline (about 100 m) (Figure 10), GENESIS was not expected to perform well in this area. However, within 2 to 3 miles (3-5 km) down the coast, the GENESIS and Gibeaut lines show good agreement again.

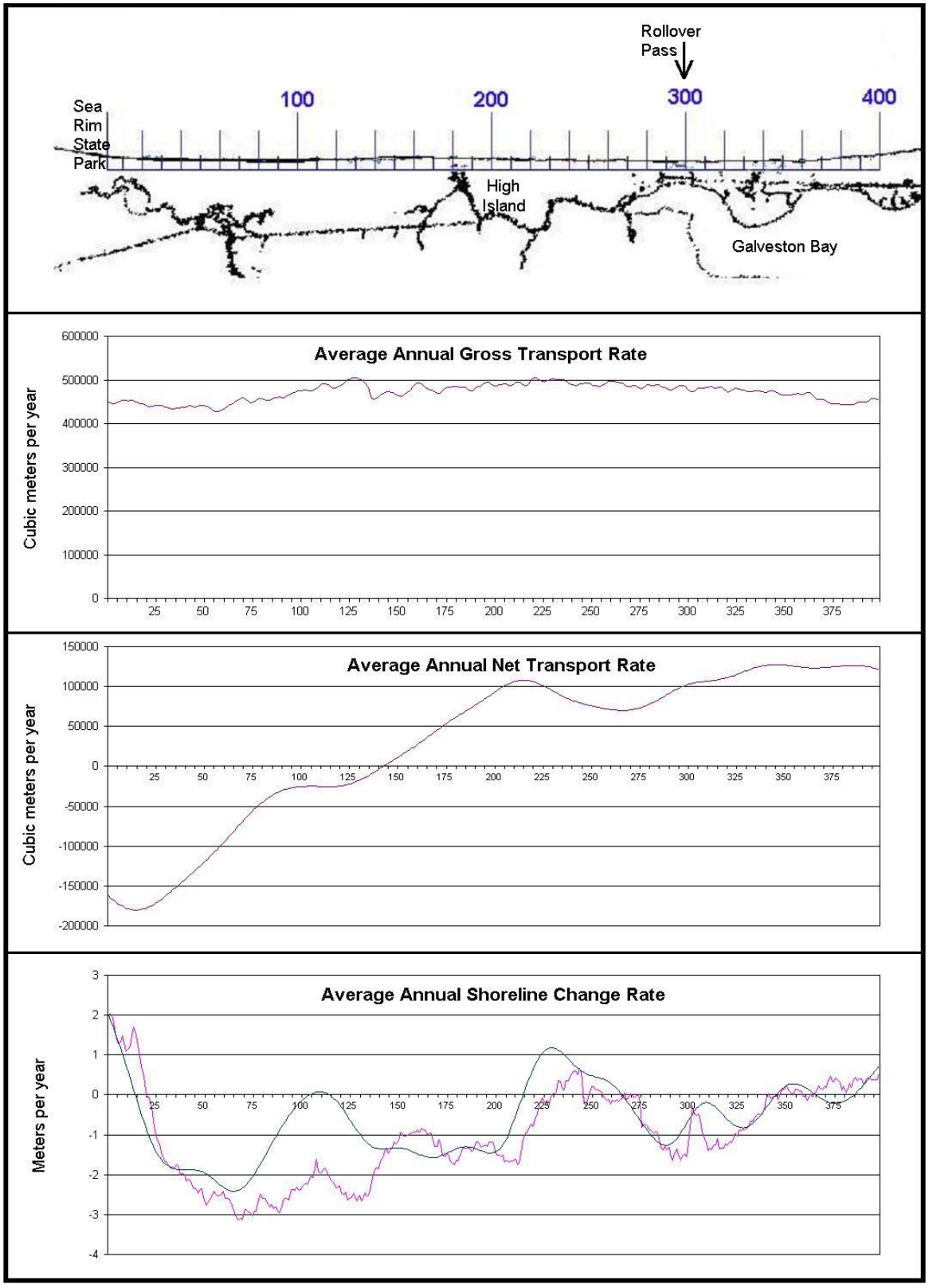

Figure 56. GENESIS results for High Island grid.

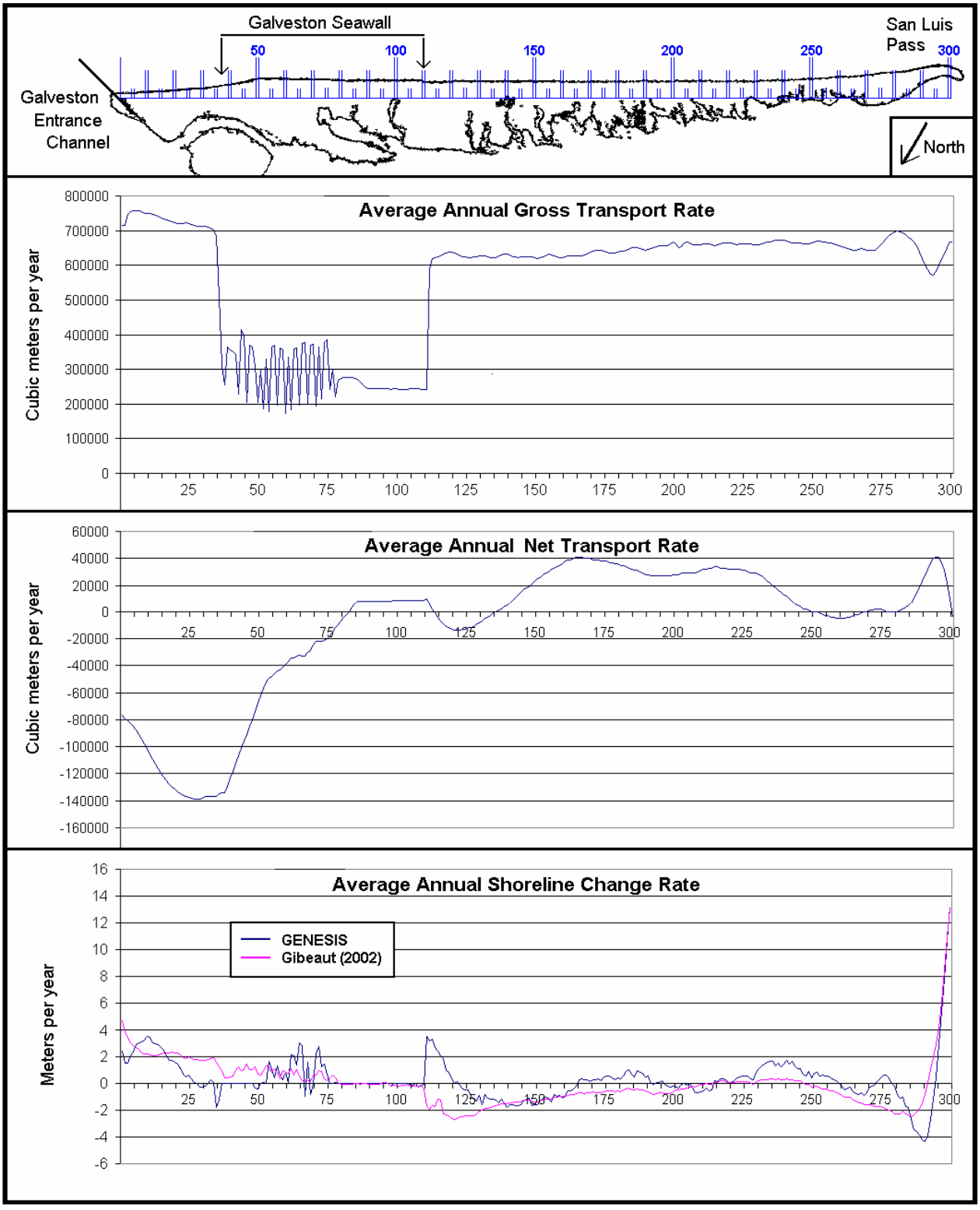

Figure 57. GENESIS results for Galveston Island grid.

SBEACH results

Table 40 shows some typical preliminary SBEACH results. These data are for Reach G-R04, Jamaica Beach on Galveston Island.

Table 40. Typical SBEACH results for Reach G-R04.

HURDAT Number	Name	Dates	Max Wave Height (m)	Max Wave Period (sec)	Max Water Elev (m)	Berm Retreat (m)
005	unnamed	8/18-21/1886	2.61	6.81	1.33	0.00
211	unnamed	8/16-19/1915	6.91	9.39	3.33	17.38
295	unnamed	6/27-29/1929	3.88	7.91	1.78	4.42
310	unnamed	8/12-14/1932	7.27	11.33	3.27	17.71
324	unnamed	8/1-5/1933	5.10	9.72	1.85	9.43
405	unnamed	9/22-24/1941	5.27	9.20	3.20	24.23
445	unnamed	8/25-29/1945	3.18	8.91	1.50	0.19
586	Debra	7/23-25/1959	3.57	7.80	1.91	6.30
602	Carla	9/8-13/1961	6.26	10.30	3.59	29.60
690	Celia	8/2-4/1970	4.61	9.25	1.97	9.74
722	Delia	9/1-6/1973	5.84	9.85	1.94	9.58
809	Chris	9/9-11/1982	5.07	8.72	1.13	0.00
812	Alicia	8/15-19/1983	6.01	9.64	3.17	21.55
841	Bonnie	6/23-26/1986	3.36	7.26	1.11	0.00
867	Chantal	7/30-8/2/1989	5.03	8.93	1.36	0.00
874	Jerry	10/13-16/1989	5.61	9.09	2.23	12.10
923	Dean	7/28-31/1995	4.00	7.82	1.43	0.00
965	Frances	9/8-12/1998	3.40	7.54	1.69	1.60

Recommendation

Much of the study area that was the focus of this report is experiencing serious, long-term erosion. Without remedial action, there is no reason to expect that present trends will not continue. In addition, major storms can be expected to produce significant short-term shoreline retreats and inland flooding. This study has developed tools that will be used to help develop and evaluate alternative designs to mitigate these erosional trends.

One important finding of this research is the discovery (or reaffirmation) of the importance of local winds in determining the angle of wave arrival

at the coastline, and the resultant direction of net longshore transport. Another is that within the study area there are significant reversals of net sediment transport direction. Sea Rim State Park is accreting because it is a convergence zone, with limited amounts of sand arriving from Texas Point to the east and from the destroyed Highway 87 area to the west. East Beach is also an area of net eastward transport and is strongly accreting.

One recommendation from this research is that the benefits and costs of sand-tightening the Galveston Entrance Channel south jetty should be investigated. Significant quantities of sand appear to be moving through or over the jetty from East Beach to the Big Reef bar just inside the jetty and then into the Galveston navigation channel. Preventing sand from being deposited in the entrance channel and making it available for beach renourishment projects will simplify sediment management and lead to significant cost savings.

References

Bagnold, R. A. 1963. Mechanics of marine sedimentation. In *The sea*, M. N. Hill, ed., New York: Wiley Interscience. 3:507-528.

Bard, E., B. Hamelin, R. G. Fairbanks, and A. Zindler. 1990. Calibration of the 14C timescale over the past 30,000 yrs using mass spectrometric U-Th ages from Barbados corals. *Nature* 345: 405-410.

Bales, J. D., and E. R. Holley. 1989. Sand transport in Texas tidal inlet. *Journal of Waterway, Port, Coastal and Ocean Engineering* 115(4): 427-443.

Batten, B. K., and N. C. Kraus. 2005. *Regional Morphology Analysis Package (RMAP), Part 2: Users guide and tutorial*. SWWRP Technical Notes Collection, ERDC TN-SWWRP-05-1. Vicksburg, MS: U.S. Army Engineer Research and Development Center. *https://swwrp.usace.army.mil/*

Benton, A. R., and J. M. Bolleter. 1987. Erosional trends on Galveston Island, Texas. *Bulletin of the Association of Engineering Geologists* XXIV(3): 345-358.

Blum, M. D., T. J. Misner, E. S. Collins, D. B. Scott, R. A. Morton, and A. Aslan. 2001. Middle Holocene sea-level rise and highstand at +2m, Texas Gulf Coast. *Journal of Sedimentary Research* 71: 581-588.

Bridges, W. E. 1959. Beach sediments of Galveston, Chambers, and Jefferson Counties, Texas. MS thesis, University of Texas, Austin.

Brown, C. A., and N. C. Kraus. 1994. Reconnaissance study of wave refraction and shoreline change for the Galveston, Texas, beach nourishment borrow sites. TAMU-CC-CBI-9403. Corpus Christi, TX: Texas A&M University.

Bruun, P., and F. Gerritsen. 1958. Stability of coastal inlets. *Journal of Waterways and Harbors Division* 84 (WW3): 1-49.

Bullard, F. M. 1942. Source of beach and river sands on the gulf coast of Texas. *Geological Society of America Bulletin* 53: 1021-1043.

Bureau of Economic Geology. 2002. *Recent shoreline change along the southeast Texas coast; A proposal to the U.S. Army Corps of Engineers, Galveston District*. Austin, TX: University of Texas.

Carothers, H. P., and H. C. Innis. 1960. Design of inlets for Texas coastal fisheries. *Journal of Waterways and Harbors Division* 86 (WW1): 1-128.

Coastal Tech. 2000. McFaddin National Wildlife Refuge dune restoration project, conceptual design report. Austin, TX: Texas General Land Office.

Crocker, M. C. 1963. A comparison of the textural and mineralogical properties of river and beach sands in southeast Texas. MS thesis, College Station, TX: Texas A&M University.

Curray, J. R. 1960. Sediments and history of Holocene transgression, continental shelf, northwest Gulf of Mexico. In *Recent sediments northwest Gulf of Mexico,* F. P. Shepard, F. B. Phleger, and T. H. Van Andel, ed., AAPG, 221-226.

Dalrymple, R. A., and P. L.-F. Liu. 1978. Wave over soft muds: A two-layer fluid model. *Journal of Physical Oceanography* 8: 1121-1131.

Edge, B. E. 2000. *Jefferson County Highway 87 shoreline assessment summary*. College Station, TX: Texas A&M University.

Fischer, W. L., J. H. McGowan, L. F. Brown, Jr., and C. G. Groat. 1972. *Environmental geologic atlas of the Texas coastal zone – Galveston-Houston area.* Austin, TX: University of Texas, Bureau of Economic Geology.

Frazier, D. E. 1974. *Depositional episodes: Their relationship to the quaternary framework in the northwestern portion of the Gulf Basin*. Geological Circular 74-1. Austin, TX: Bureau of Economic Geology, University of Texas.

Gade, H. G. 1959. Notes on the effect of elasticity of bottom sediments to the energy dissipation of surface waves in shallow water. *Arch. Math. Naturvidenskab* 55: 69-80.

Giardino, J. R., R. S. Bednarz, and J. T. Bryant. 1987. Nourishment of San Luis Beach, Galveston Island, TX – An assessment of the impact. *Coastal Sediments '87, Volume 2*. N. C. Kraus, ed. New York: American Society of Civil Engineers, 1145-1157.

Gibeaut, J. C., T. L. Hepner, R. Waldinger, J. R. Andrews, R. C. Smyth, and R. Gutierrez. 2002. *Geotubes along the gulf shoreline of the upper Texas coast: Observations during 2001*. Austin, TX: University of Texas, Bureau of Economic Geology.

Gravens, M. 1989. *Estimating potential longshore sand transport rates using WIS data*. Coastal Engineering Technical Note CETN-II-19. Vicksburg, MS: U.S. Army Engineer Waterways Experiment Station, Coastal Engineering Research Center.

Gravens, M. B., N. C. Kraus, and H. Hanson. 1991. *GENESIS: Generalized model for simulating shoreline change, Report 2, Workbook and system user's manual.* Technical Report CERC-89-19. Vicksburg, MS: U.S. Army Engineer Waterways Experiment Station, Coastal Engineering Research Center.

Guza, R. T., E. B. Thornton, and N. Christensen, Jr. 1986. Observations of steady longshore currents in the surf zone. *Journal of Physical Oceanography* 16: 1959-1969.

Hall, G. L. 1976. Sediment transport processes in the nearshore waters adjacent to Galveston Island and Bolivar Peninsula. PhD diss. College Station, TX: Texas A&M University.

Hanson, H. 1987. *GENESIS - A generalized shoreline change numerical model for engineering use*. Report No. 1007. Lund, Sweden: University of Lund, Department of Water Resources Engineering.

Hanson, H., and N. C. Kraus. 1989. *GENESIS: Generalized model for simulating shoreline change, Report 1, Technical reference*. Technical Report CERC-89-19. Vicksburg, MS: U.S. Army Engineer Waterways Experiment Station, Coastal Engineering Research Center.

Hayes, M. O. 1967. *Hurricanes and geological agents: Case studies of Hurricanes Carla, 1961 and Cindy, 1963*. Report of Investigations No. 61. Austin, TX: University of Texas, Bureau of Economic Geology.

Howard, S. C. 1999. Impact of shoreline change on proposed Texas highway 87 reconstruction. MS thesis. College Station, TX: Texas A&M University.

Hsiao, S. V., and O. H. Shemdin. 1980. Bottom dissipation in finite-depth water waves. *Proceedings of the 16th Coastal Engineering Conference*. Hamburg, Germany, 434-448.

Hubertz, J. M. 1986. Observations of local wind effects on longshore currents. *Coastal Engineering* 10: 275-288.

Hubertz, J. M. 1987. A wind- and wave-driven nearshore current model, The one-dimensional model. Miscellaneous paper CERC 87-4. Vicksburg, MS: U.S. Army Engineer Waterways Experiment Station, Coastal Engineering Research Center.

Huh, O. K., H. H. Roberts, L. J. Rouse, and D. A. Rickman. 1991. Fine grain sediment transport and deposition in the Atchafalaya and Chenier Plain sedimentary system. *Coastal Sediments '91*. New York: American Society of Civil Engineers. 817-830.

Jarrett, J. T. 1978. *Tidal prism – inlet area relationships*. GITI Report 3. Fort Belvoir, VA: U.S. Army Engineer Coastal Engineering Research Center.

Jensen, R. E. 1983. *Methodology for the calculation of a shallow-water wave climate.* WIS Report 8. Vicksburg, MS: U.S. Army Engineer Waterways Experiment Station, Coastal Engineering Research Center.

Jonsson, I. G. 1990. Wave-current interactions. In *The sea,* B. LeMehaute and D. M. Hanes, ed. New York: John Wiley & Sons, Inc. 9: 65-120.

Kemp, G. P., and J. T. Wells. 1987. Observations of shallow water waves over a fluid mud bottom: Implications for sediment transport. *Coastal Sediments '87*. New York: American Society of Civil Engineers, 363-378.

King, D. B., and T. L. Prickett. 1998. *Mouth of the Colorado River, Texas, monitoring program*. Technical Report CHL-98-2. Vicksburg, MS: U.S. Army Engineer Waterways Experiment Station, Coastal and Hydraulics Laboratory.

Komar, P. D., and D. L. Inman. 1970. Longshore sand transport on beaches. *Journal of Geophysical Research* 75(30): 5914-5927.

Kraus, N. C., and M. Larson. 1991. *NMLONG: Numerical model for simulating the longshore current, Report 1, Model development and tests*. Dredging Research Program Technical Report DRP-91-1. Vicksburg, MS: U.S. Army Engineer Waterways Experiment Station, Coastal Engineering Research Center.

Larson, M., and N. C. Kraus. 1989. *SBEACH: Numerical model for simulating storm-induced beach change; Report 1: Empirical foundation and model development*. Technical Report CERC-89-9. Vicksburg, MS: U.S. Army Engineer Waterways Experiment Station, Coastal Engineering Research Center.

Larson, M., and N. C. Kraus. 1991. Mathematical modeling of the fate of beach fill. In *Artificial beach nourishments,* H. D. Niemayer, J. van Overeem, and J. van de Graaff, ed. (Special issue of) *Coastal Engineering* 16: 83-114.

Larson, M., and N. C. Kraus. 1995. *Representation of non-erodible bottoms in SBEACH*. TAMU-CC-CBI-95-11. Corpus Christi, TX: Texas A&M University.

Larson, M., N. C. Kraus, and M. R. Byrnes. 1990. *SBEACH: Numerical model for simulating storm-induced beach change; Report 2: Numerical formulation and model test*. Technical Report CERC-89-9. Vicksburg, MS: U.S. Army Engineer Waterways Experiment Station, Coastal Engineering Research Center.

Long, C. E., and J. M. Hubertz. 1988. *Nearshore wind-stress measurements: Background, preliminary fieldwork, and experiment design*. Miscellaneous Paper CERC-88-14. Vicksburg, MS: U.S. Army Engineer Waterways Experiment Station, Coastal Engineering Research Center.

Longuet-Higgins, M. S. 1970. Longshore currents generated by obliquely incident sea waves, 1-2. *Journal of Geophysical Research* 75(33): 6778-6801.

Magouirk, D. A. 1981. Shoreline changes along the southeast Texas coast: Galveston, Chambers, and Jefferson Counties. MS thesis, Nacogdoches, TX: Stephen F. Austin University.

Mason, C. 1981. *Hydraulics and stability of five Texas inlets*. Miscellaneous Paper CERC-81-1. Fort Belvoir, VA: U.S. Army Engineer Coastal Engineering Research Center.

Mathewson, C. C. 1987. Factors influencing coastal processes and engineering design along the Texas coast. *Bulletin of the Association of Engineering Geologists* XXIV (3): 333-344.

McGowan, J. H., and R. A. Morton. 1979. *Sediment distribution, bathymetry, faults, and salt diapirs on the submerged lands of Texas*. Special Publication. Austin, TX: University of Texas, Bureau of Economic Geology.

McGowan, J. H., and A. J. Scott. 1975. Hurricanes as geologic agents on the Texas coast. *Estuarine Research.* New York: Academic Press, 23-46.

Morang, A. 2006. *North Texas sediment budget for Sabine Pass to San Luis Pass, Texas*. ERDC/CHL TR-06-17. Vicksburg, MS: U.S. Army Engineer Research and Development Center, Coastal and Hydraulics Laboratory.

Morgan, J. P., L. G. Nichols, and M. Wright. 1958. *Morphological effect of Hurricane Aubrey*. Technical Report 10. Baton Rouge, LA: Coastal Studies Institute, Louisiana State University.

Morgan, J. P., J. R. Van Lopik, and L. G. Nichols. 1953. *Occurrence and development of mudflats along the western Louisiana coast*. Technical Report 2. Baton Rouge, LA: Coastal Studies Institute, Louisiana State University.

Morton, R. A. 1974. *Shoreline changes on Galveston Island*. Geological Circular 74-2. Austin, TX: University of Texas, Bureau of Economic Geology.

Morton, R. A. 1975. *Shoreline changes between Sabine Pass and Bolivar Roads, An analysis of historical changes on the Texas gulf shoreline*. Geological Circular 75-6. Austin, TX: University of Texas, Bureau of Economic Geology.

Morton, R. A. 1977. Nearshore changes at jettied inlets, Texas coast. *Coastal Sediments '77*. New York: American Society of Civil Engineers, 267-286.

Morton, R. A. 1979. Temporal and spatial variations in shoreline changes, Texas coast. *Journal of Sedimentary Petrology* 49: 1101-1111.

Morton, R. A. 1991. Accurate shoreline mapping: Past, present, and future. In *Coastal Sediments '91*. N. C. Kraus, K. J. Gingerich, and D. L. Kriebel, ed. New York: American Society of Civil Engineers. 1: 997-1010.

Morton, R. A. 1994. *Texas barriers*. In *Geology of Holocene Barrier Islands*, R. A. Davis, ed., Berlin: Springer-Verlag, 75-114.

Morton, R. A. 1997. *Gulf shoreline movement between Sabine Pass and the Brazos River, Texas: 1974-1996*. Geological Circular 97-3. Austin, TX: University of Texas, Bureau of Economic Geology.

Morton, R. A., J. C. Gibeaut, and R. Gutierrez. 1995. *Pre-project surveys of beach and nearshore conditions, Galveston beach nourishment project*. Austin, TX: University of Texas, Bureau of Economic Geology.

Nairn, R. B. 1992. Designing for cohesive shores. *Proceedings Coastal Engineering in Canada*. J. W. Kamphuis, ed., Kingston, Canada: Department of Civil Engineering, Queen's University.

Nairn, R. B., B. M. Pinchin, and K. L. Philpott. 1986. A cohesive coast development model. *Proceedings, Symposium on Cohesive Shores*. National Research Council Canada, Associate Committee on Shorelines, 246-261.

Nairn, R. B., and H. N. Southgate. 1993. Deterministic profile modeling of nearshore processes: Part II, Sediment transport processes and beach profile development. *Coastal Engineering* 19: 57-96.

Nairn, R. B., and D. H. Willis. 2002. Erosion, transport, and deposition of cohesive sediments. In *Coastal Engineering Manual, Part III, Coastal Sediment Processes, Chapter 5*, T. Walton, ed., Engineer Manual 1110-2-1100, Washington, DC: U.S. Army Corps of Engineers.

Nelson, H. F., and E. E. Bray. 1970, Stratigraphy and history of the Holocene sediments in the Sabine-High Island area, Gulf of Mexico. Special Publication 15, *Deltaic sedimentation, modern and Ancient, Society of Economic Paleontologists and Mineralogists*, J. P. Morgan and R. H. Shaver, ed., 48-77.

Neumann, C. J., G. W. Cry, E. L. Caso, and B. R. Jarvinen. 1981. *Tropical cyclones of the North Atlantic Ocean, 1871-1980*. Asheville, NC: National Oceanographic and Atmospheric Administration, National Climatic Center.

Otvos, E. G. 2001. Assumed Holocene highstands, Gulf of Mexico: Basic issues of sedimentary and landform criteria-discussion. *Journal of Sedimentary Research* 71: 645-647.

Pacific International Engineering (PIE). 2001. *Physical processes, engineering analysis, and environmental impacts, Shoreline erosion control – Rollover Pass, Texas*. Austin, TX.

Pacific International Engineering (PIE). 2003. *Coastal goemorphology of a non-barrier Gulf of Mexico beach: Analysis for protection of Highway 87 and McFaddin NWR in Jefferson County, Texas*. Austin, TX.

Paine, J. G., and R. A. Morton. 1989. *Shoreline and vegetation-line movement, Texas gulf coast, 1974 to 1982*. Geological Circular 89-1. Austin, TX: University of Texas, Bureau of Economic Geology.

Parchure, T. M., B. Brown, and R. T. McAdory. 2000. *Design of sediment trap at Rollover Pass, Texas*. Technical Report ERDC/CHL TR-00-23. Vicksburg, MS: U.S. Army Engineer Research and Development Center, Coastal and Hydraulics Laboratory.

Penner, L. A. 1993. *Shore erosion and slumping on western Canadian lakes and reservoirs — A methodology for estimating future bank recession rates*. Regina, Saskatchewan: Environment Canada.

Permanent International Association of Navigation Congresses (PIANC). 1986. *List of sea state parameters*. Supplement to Bull. 52, PIANC. Brussels, Belgium: International Association for Hydraulic Research.

Prather, S. H., and R. M. Sorensen. 1972. *An investigation of Rollover Pass, Bolivar Peninsula, Texas*. Sea Grant Publication No. TAMU-SG-72-202. College Station, TX: Texas A&M University.

Price, W. A. 1947. Equilibrium of form and forces in tidal basins of coasts of Texas and Louisiana. *AAPG Bulletin* 31(9): 1619-1663.

Price, W. A. 1951. Reduction of maintenance by proper orientation of ship channels through tidal inlets. *Proc. 2nd Coastal Engineering Conference, Houston, TX*. New York: ASCE, 243-255.

Price, W. A. 1954. *Shorelines and coasts of the Gulf of Mexico*. U.S. Fish and Wildlife Service Fishery Bulletin 89: 39-65.

Ratzlaff, K. W. 1980. *Land-surface subsidence in the Texas coastal region*. Open-File Report 80-969. U.S. Geological Survey.

Resio, D. T. 1987. Shallow-water waves. I: Theory. *Journal of Waterway, Port, Coastal and Ocean Engineering* 113(3): 264-281.

Resio, D. T. 1988a. Shallow-water waves. II: Data comparisons. *Journal of Waterway, Port, Coastal and Ocean Engineering* 114(1): 50-65.

Resio, D. T. 1988b. A steady-state wave model for coastal applications. *Proceedings of the 21st Coastal Engineering Conference.* ASCE, 929-940.

Richardson, R. M. 1948. Sedimentation and shore processes at Bolivar Peninsula, Galveston County, Texas. MS thesis, Austin, TX: University of Texas.

Rosati, J. D., T. Walton, and K. Bodge. 2002. Longshore sediment transport. *Coastal Engineering Manual, Part III, Coastal Sediment Processes Chapter 2,* T. Walton, ed., Engineer Manual 1110-2-1100. Washington, DC: U.S. Army Corps of Engineers.

Rosati, J. D., R. A. Wise, and N. C. Kraus. 1993. *SBEACH: Numerical model for simulating storm-induced beach change; Report 3: User's manual*. Instruction Report CERC-93-2, Vicksburg, MS: U.S. Army Engineer Waterways Experiment Station, Coastal Engineering Research Center.

Sargent, F. E., and R. R. Bottin, Jr. 1989. *Case histories of corps breakwater and jetty structures, Report 9, Southwest Division*. Technical Report REMR-CO-3. Vicksburg, MS: U.S. Army Engineer Waterways Experiment Station, Coastal Engineering Research Center.

Scheffner, N. W., F. C. Carson, J. P. Rhee, and D. J. Mark. 2002. Coastal erosion study for the open coast from Sabine to San Luis Pass, Texas, Tropical storm surge frequency analysis. Unpublished report. Vicksburg, MS: U.S. Army Engineer Research and Development Center, Coastal and Hydraulics Laboratory.

Scheffner, N. W., and D. J. Mark. 1994. *ADCIRC: An advanced three-dimensional circulation model for shelves, coasts, and estuaries. Report 5, A tropical storm database for the east and Gulf of Mexico coasts of the United States*. Technical Report DRP-92-6. Vicksburg, MS: U.S. Army Engineer Waterways Experiment Station, Coastal Engineering Research Center.

Schneider, D. 1981. *The Littoral Environment Observation (LEO) data collection program*. Coastal Engineering Technical Aid CETA 81-5. Vicksburg, MS: U.S. Army Engineer Waterways Experiment Station.

Seelig, W. N., and R. M. Sorensen. 1973. *Historical shoreline changes in Texas*. Report TAMU-SG-73-206. College Station, TX: Texas A&M University.

Shiner Moseley and Associates, Inc. 2004. *Monitoring Geotextile-Tube Core Dunes in Galveston County, Texas, Spring 2003 to Spring 2004*. J200.20320. Corpus Christi, TX.

Simmons, H. B., and R. A. Boland, Jr. 1969 *Model study of Galveston Harbor Entrance, Texas*. Technical Report H-69-2. Vicksburg, MS: U.S. Army Engineer Waterways Experiment Station.

Slingluff, F. P. 1948. Sedimentation and shore processes of southwestern Galveston Island, Galveston City, Texas. MS thesis. Austin, TX: University of Texas.

Smith, J. M. 2001. *Modeling nearshore transformation with STWAVE*. Coastal and Hydraulics Engineering Technical Note CHETN I-64. Vicksburg, MS: U.S. Army Engineer Research and Development Center, Coastal and Hydraulics Laboratory.

Stern, T. W. 1948. Sedimentation and shore processes on the northeastern portion of Galveston Island, Texas. MS thesis. Austin, TX: University of Texas.

Thomas, L. J. 1994. *User's guide for the littoral environment observation (LEO) PC data retrieval and analysis system*. Instruction Report CERC-94-2. Vicksburg, MS: U.S. Army Engineer Waterways Experiment Station.

Tracy, B. 2002. *Gulf of Mexico 1990-1999 wave hindcast and Galveston hurricane hindcasts.* Draft Technical Note. Vicksburg, MS: U.S. Army Engineer Research and Development Center, Coastal and Hydraulics Laboratory.

Tubman, M. W., and J. N. Suhayda. 1976. Wave action and bottom movements in fine sediments. *Proceedings of the 15th Coastal Engineering Conference, Honolulu.* New York: ASCE, 1168-1183.

U.S. Army Corps of Engineers. 1874. *Survey and improvement of Galveston Harbor and entrance, Texas*. House Exec. Doc. 1, 43rd Congress, 2nd Session, Vol 2(1), 722-740.

U.S. Army Corps of Engineers. 1882. *Survey of Sabine Pass, Texas*. House Exec. Doc. 147, 47th Congress, 1st Session.

U.S. Army Corps of Engineers. 1959. *Gulf shore of Bolivar Peninsula in the vicinity of Rollover Fish Pass, Texas*. House Doc. 286, 86th Congress, 2nd Session.

U.S. Army Corps of Engineers. 1971. *Texas coast shores regional inventory report*. Galveston, TX: U.S. Army Corps of Engineers, Galveston District.

U.S. Army Corps of Engineers. 1976. *Texas coast inlet studies; Beach profiles, jetty condition surveys and mid-point surveys*. Galveston, TX: U.S. Army Corps of Engineers, Galveston District.

U.S. Army Corps of Engineers. 1981. *Texas coast inlet studies; Beach profiles, jetty contitiion surveys and mid-point surveys, 1979-1980*. Galveston, TX: U.S. Army Corps of Engineers, Galveston District.

U.S. Army Corps of Engineers. 1979. *Feasibility Report, Texas coast hurricane study, Volume I, Main report, and Volume II, Galveston Bay study segment*. Galveston, TX: U.S. Army Corps of Engineers, Galveston District.

U.S. Army Corps of Engineers. 1981. *Galveston's bulkwark against the sea, History of the Galveston seawall*. Galveston, TX: U.S. Army Corps of Engineers, Galveston District.

U.S. Army Corps of Engineers. 1983. *Galveston County shore erosion study, Feasibility report on beach erosion control, Volume 2, Gulf shoreline study site report*. Galveston, TX: U.S. Army Corps of Engineers, Galveston District.

U.S. Army Corps of Engineers. 1984. *Shore protection manual.* 4th ed., 2 Vols. Vicksburg, MS: U.S. Army Engineer Waterways Experiment Station, Coastal Engineering Research Center.

U.S. Army Corps of Engineers. 1995. *Jefferson County, Texas, Reconnaissance Report*. Galveston, TX: U.S. Army Corps of Engineers, Galveston District.

U.S. Army Corps of Engineers. 2000. *Sabine Pass to Galveston Bay, Texas, Shoreline erosion reconnaissance report, Section 905(b) analysis*. Galveston, TX: U.S. Army Corps of Engineers, Galveston District.

U.S. Army Corps of Engineers. 2002. *Coastal Engineering Manual*. Engineer Manual 1110-2-1100. Washington, DC: U.S. Army Corps of Engineers (in 6 volumes).

Van Andel, T. H., and D. M. Poole. 1960. Sources of recent sediments in the northern Gulf of Mexico. *Journal of Sedimentary Petrology* 30: 91-123.

Wamsley, T. V. 2000. Shoreline monitoring program on the upper Texas coast utilizing a real-time kinematic differential global positioning system. MS thesis. College Station, TX: Texas A&M University.

Wamsley, T. V., and B. L. Edge. 2001. Shoreline monitoring program on the Texas coast by real-time kinematic differential global positioning system. *Shore and Beach* 69(4): 25-31.

Wells, J. T., and G. P. Kemp. 1986. Interaction of surface waves and cohesive sediments: Field observations and geological significance. *Estuarine Cohesive Sediment Dynamics*, A. J. Mehta, ed., New York: Springer-Verlag. 43-65.

White, W. A., T. R. Calnan, R. A. Morton, R. S. Kimble, T. G. Littleton, J. H. McGowen, H. S. Nance, and K. E. Schmedes. 1985. *Submerged lands of Texas, Galveston-Houston area: Sediments, geochemistry, benthic marcoinvertebrates, and associated wetlands*. Austin, TX: University of Texas, Bureau of Economic Geology.

White, W. A., T. R. Calnan, R. A. Morton, R. S. Kimble, T. G. Littleton, J. H. McGowen, H. S. Nance, and K. E. Schmedes. 1987. *Submerged lands of Texas, Beaumont-Port Arthur area: Sediments, geochemistry, benthic marcoinvertebrates, and associated wetlands*. Austin, TX: University of Texas, Bureau of Economic Geology.

Wise, R. A., S. J. Smith, and M. Larson. 1996. *SBEACH: Numerical model for simulating storm-induced beach change, Report 4, Cross-shore transport under random waves and model validation with SUPERTANK and field data*. Technical Report CERC-89-9. Vicksburg, MS: U.S. Army Engineer Waterways Experiment Station, Coastal Engineering Research Center.

Zheng, J., and R. G. Dean. 1995. *Evaluation study and comparison of erosion models and effects of seawalls for coastal construction control line; Task 1D: Compare models with results from Hurricane Eloise and other data*. UFL/COEL-95/006. Gainesville, FL: University of Florida, Coastal and Oceanographic Engineering Department.

Appendix A: Wave Height, Period, and Angle Definitions

The 2-D WIS spectra have 20 frequency bins with values from 0.03 to 0.3 Hz and 16 angle bins at 22.5 deg intervals that cover all directions from 0 deg to 360 deg. To input these spectra into STWAVE, it is necessary to re-bin the wave angles into 35 five-degree angle bins that are oriented between ±85 deg of shore-normal. The energy outside this arc (the offshore-directed energy) is discarded. Examples of these STWAVE spectra are given in Figures 37 and 38. The following wave height, period, and angle calculations are made using these onshore-directed spectra, either before or after transformation.

Significant wave height

The energy density in each frequency/angle bin is multiplied by the frequency and angle bin widths and then summed to obtain the total energy in the spectrum. The significant wave height (H_{mo}) is four times the square root of the total energy.

Mean wave period

The total energy in the spectrum is calculated by multiplying the energy density in each frequency/angle bin by its frequency bin width and angle bin width, and then summing the resulting values. This is the zeroth moment. The 1st moment is calculated by multiplying the energy density in each frequency/angle bin by its frequency bin width and angle bin width and by the frequency of the band, and then summing these resulting values. The 1st moment is divided by the zeroth moment to obtain the mean frequency. The Mean Wave Period is the inverse of the mean frequency.

Peak wave period, discrete

The energy density in each frequency band is summed over all angles; the band with the maximum is the peak (discrete) frequency. The peak wave period, discrete is the inverse of that frequency. Thus, this parameter is constrained to be one of 20 values. References to the peak wave period in this report refer to this parameter.

Peak wave period, parabolic fit

The peak wave period, discrete is calculated as above. A parabola is fit to the values of the energy density in that peak period band and to the values of the first adjacent bands on either side (three points). The peak of the parabola is the peak wave period, parabolic fit. If the peak band is the shortest or longest wave period in the spectrum, the parabola is passed through the three shortest or longest bands, respectively; however, the peak period is not allowed to be less than the shortest period or greater than the longest period in the spectrum.

Vector mean wave angle

The energy density in each frequency/angle bin is multiplied by the frequency and angle bin widths and by the sine of the angle, and these values are summed. Separately the energy density in each bin is multiplied by the frequency and angle bin widths and by the cosine of the angle, and these values are summed. The vector mean wave angle is the arctangent of the summed sine values divided by the summed cosine values. Most references in the literature to mean wave angle refer to this parameter (e.g., Permanent International Association of Navigation Congresses (PIANC) 1986)[1] as do references to mean wave angle in this report.

Moment mean wave angle

The energy density in each frequency/angle bin is multiplied by the frequency and angle bin widths and then summed to obtain the total energy in the spectrum (the zeroth moment). Separately, the energy density in each bin is multiplied by the frequency and angle bin width and by the angle, and these values are summed (the 1st angle moment). This 1st moment is divided by the total energy to obtain the moment mean wave angle. Note: special care must be taken when using this parameter with a full 360-deg spectrum to deal with the numerical discontinuity of going from 360 deg to 0 deg. This was not a problem in this report as wave angles in the spectra only ranged between $\pm$85 deg.

Energy flux mean wave angle

The wave group speed is calculated for each frequency. Then for each bin the energy density times the angle and frequency bin width is multiplied by the group speed times the sine of twice the angle, and these values are summed. Separately for each bin the energy density times the angle and

[1] References cited in this appendix are located at the end of the main text.

frequency bin width is multiplied by the group speed, and these values are summed. The energy flux mean wave angle is half the arc sine of the first sum divided by the second. This is a non-standard wave angle parameter based upon the conservation of longshore wave energy flux.

Energy vector mean wave angle

The energy density in each bin is raised to the 1.25 power. Then the same steps are taken as in the calculation of the vector mean wave angle described above to obtain the energy vector mean wave angle. This non-standard parameter is based upon the fact that wave heights are raised to the 2.5 power in the transport relationship (CERC formula), which is equivalent to energy raised to the 1.25 power.

Vector mean of the peak frequency wave angle

The peak period band, discrete is determined as described above. Then the calculations for the vector mean wave angle, described above were made using only the energy density values in each bin in this band to obtain the vector mean of the peak frequency wave angle. References to mean of the peak wave angle in this report refer to this parameter.

Moment mean of the peak frequency wave angle

The peak period band, discrete is determined as described above. Then the calculations for the moment mean wave angle, described above were made using only the energy density values in each bin in this band to obtain the moment mean of the peak frequency wave angle.

Peak band wave angle, discrete

The energy density in each angle band is summed over all periods; the band with the maximum is the peak band wave angle, discrete. Thus, this parameter is constrained to be one of 35 values. This non-standard parameter has a definition analogous to that of the peak wave period, discrete.

Peak of the peak wave angle, discrete

The peak period band, discrete is determined as described above. Within this band, the angle having the greatest energy density is the peak of the peak wave angle, discrete. Thus, this parameter is constrained to be one of 35 values.

Appendix B: Derivation of Longshore Transport Formula with Wind-Driven Surf Zone Current

Local winds can modify the longshore sediment transport rate by directly increasing or decreasing the longshore current within the surf zone. These effects can be modeled by making modifications to the CERC formula, which is the core of the sediment transport model within GENESIS.

The classical CERC formula for the prediction of the longshore sediment transport rate is

$$I_l = \left(EC_g\right)_b K_1 \sin\alpha_b \cos\alpha_b \tag{B-1}$$

where:

I_l = the immersed weight sediment transport rate in newtons per second
E = the wave energy density at breaking in newtons per meter
C_g = wave group speed at breaking in meters per second
K_1 = a dimensionless empirical coefficient
α_b = angle of the breaking waves relative to the shoreline

The breaking wave energy density can be expressed as

$$E_b = \frac{1}{8}\rho g\left(\frac{H_b}{1.416}\right)^2 \tag{B-2}$$

where:

ρ = the density of water in kilograms per cubic meter
g = the acceleration of gravity in meters per second per second
H_b = the significant breaking wave height in meters. The factor 1.416 is used to convert from significant wave height to RMS wave height.

At breaking, the wave group velocity is equivalent to the wave phase velocity, C_b. The shallow water approximation for C_{gb} is

$$C_{gb} \approx C_b \approx \sqrt{gh_b} = \sqrt{\frac{gH_b}{1.416\gamma}} \tag{B-3}$$

where:

h_b = the breaker depth
γ = the breaker index ≈ 0.78

The volume longshore sediment transport rate, Q, is related to I_l as

$$Q = \frac{I_l}{(\rho_s - \rho) g (1-p)} \tag{B-4}$$

where:

ρ_s = the density of the sediment in kilograms per cubic meter
p = the porosity of the sediment, the ratio of the void spaces to the total (void plus sand) volume

Substituting Equations B-1, B-2, and B-3 into Equation B-4 yields a different form of the CERC equation:

$$Q = \frac{K_1}{16\left(\frac{\rho_s}{\rho} - 1\right)(1-p)} * \sqrt{\frac{g}{\gamma}} * \left(\frac{H_b}{1.416}\right)^{2.5} * \sin(2\alpha_b) \tag{B-5}$$

An additional term is added to Equation B-1 in the GENESIS formulation of the longshore sediment transport rate equation to allow for the potential for steep longshore gradients in wave height:

$$I_l = \left(EC_g\right)_b \left(K_1 \sin\alpha_b \cos\alpha_b - K_2 \frac{\cos\alpha_b}{\tan\beta} \frac{\partial H_b}{\partial x} \right) \tag{B-6}$$

where:

K_2 = a second dimensionless empirical coefficient
$\tan\beta$ = the dimensionless average bottom slope from the shoreline to the limiting depth of longshore transport
x = the distance in the longshore direction in meters

The nominal value of K_1 is 0.77, whereas there is no corresponding value of K_2. As a rule of thumb, based on modeling experience, Hanson and Kraus (1989)[1] recommend $0.5K_1 < K_2 < 1.5K_1$.

The Bagnold (1963) original longshore transport rate formulation, from which the CERC formula is derived, explicitly included the longshore current as

$$I_l = K_3' \left(EC_g\right)_b \cos\alpha_b \frac{\bar{v}_l}{u_m} \tag{B-7}$$

where:

K_3' = a third dimensionless coefficient (the symbol, K_3, (no prime) is reserved for later use)

$\bar{v}_l$ = the average longshore current in the surf zone in meters per second

u_m = the maximum wave-induced near-bottom horizontal velocity at wave breaking in meters per second

The maximum wave-induced near-bottom horizontal velocity at wave breaking may be expressed as

$$u_m = \left(\frac{2E_b}{\rho h_b}\right)^{1/2} = \left(\frac{\gamma g H_b}{4 \cdot 1.416}\right)^{1/2} \tag{B-8}$$

If the mean longshore current in Equation B-7 is generated by forces in addition to those caused by breaking waves, to first order, the total longshore current can be expressed as

$$\bar{v}_l = \bar{v}_b + \bar{v}_t + \bar{v}_w \tag{B-9}$$

where:

$\bar{v}_b$ = the breaking wave component

$\bar{v}_t$ = the tidal induced component

$\bar{v}_w$ = the wind-induced component

All currents are in units of meters per second.

[1] References cited in this appendix are located at the end of the main text.

In this report, an expression for the breaking wave and wind-induced components is presented. An expression for the tidal induced component will not be derived ($\overline{v}_t$ is assumed = 0.) However, a tidally induced or other forcing component could be included in the longshore transport rate formula in the same manner as will be done for the wind-induced component.

Longuet-Higgins (1970) and Komar and Inman (1970) developed an expression for the breaking-wave induced component of the longshore current as

$$\overline{v}_b = K_4 u_m \sin\alpha_b \tag{B-10}$$

where K_4 is a fourth dimensionless empirical coefficient. Komar and Inman (1970) suggested K_4 = 2.7. Assuming that the longshore current is only derived from breaking waves, the CERC formula, Equation B-1, is obtained if Equations B-7 and B-10 are combined, yielding a value for K_3' of

$$K_3' = K_1/K_4 = 0.28 \tag{B-11}$$

Likewise the GENESIS longshore transport equation can be obtained if the breaking wave longshore current is defined as

$$\overline{v_b} = K_4 u_m \sin\alpha_b - K_5 \frac{4}{\gamma g} u_m \frac{\partial(u_m^2)}{\partial x} \frac{1}{\tan\beta} \tag{B-12}$$

where K_5 is a fifth dimensionless empirical coefficient (= K_2/K_3').

The following development for a wind-driven longshore surf zone current follows Kraus and Larson (1991). Wind, blowing over a water surface, will produce a stress of the form

$$\tau_a = C_a \rho_a W^2 \tag{B-13}$$

where:

τ_a = the shear stress at the air-water interface in newtons per square meter
C_a = the dimensionless drag coefficient at the air-water interface
ρ_a = the density of air in kilograms per cubic meter

W = the wind speed in meters per second

The longshore component of this stress is

$$\tau_{la} = C_a \rho_a (W \sin\theta)^2 \tag{B-14}$$

where θ is the wind direction with respect to shore normal. This stress not only produces waves, but also a current. In the surf zone this wind-induced longshore current will be balanced by a retarding bottom stress:

$$\tau_{lb} = C_b \rho \bar{v}_w^{\,2} \tag{B-15}$$

where C_b is the dimensionless longshore current drag coefficient at bottom.

Equating these two stresses and solving for the wind-induced longshore current yields

$$\bar{v}_w = \sqrt{\frac{C_a \rho_a}{C_b \rho}}\ W \sin\theta \tag{B-16}$$

The density of air, ρ_a, at sea level is ≅ 1.29 kg/m^3, and the density of seawater, ρ, is ≅ 1,025 kg/m^3, so $(\rho_a/\rho)^{0.5} \cong 0.035$. The ratio, $(C_a/C_b)^{0.5}$ is much less well understood. Long and Hubertz (1988) found wide scatter in C_a values reported in the literature; C_a values ranged from 0.0002 to 0.0064, though typical values were in the range of 0.001 to 0.003. Likewise there is substantial scatter in reported values of C_b, though typical values fall within the range of 0.003 to 0.01. Analyzing FRF data, Kraus and Larson (1991) reported a (C_a/C_b) value of 1.2, though they noted considerable scatter in their data. K_3 is now defined as

$$K_3 = \sqrt{\frac{C_a \rho_a}{C_b \rho}}\ K_3' \tag{B-17}$$

To obtain a sediment transport relationship, Equations B-9, B-12, B-16, and B-17 can be substituted into Equation B-7, and assuming $\bar{v}_t$ =0, the result is

$$I_l = \left(EC_g\right)_b \cos\alpha_b \left[K_1 \sin\alpha_b - \frac{K_2}{\tan\beta}\frac{\partial H_b}{\partial x} + K_3 \frac{W}{u_m}\sin\theta\right] \tag{B-18}$$

or, in terms of the wind driven longshore current

$$I_l = \left(EC_g\right)_b \cos\alpha_b \left[K_1 \sin\alpha_b - \frac{K_2}{\tan\beta}\frac{\partial H_b}{\partial x} + K'_3 \frac{\overline{v}_w}{u_m}\right] \tag{B-19}$$

Converting Equation B-18 to the volume transport rate, using Equation B-4 yields:

$$Q = \frac{\left(H_b / 1.416\right)^{2.5} \cos\alpha_b}{8\left(\frac{\rho_s}{\rho} - 1\right)(1-p)} \sqrt{\frac{g}{\gamma}} \left[K_1 \sin\alpha_b - \frac{K_2}{2\tan\beta}\frac{\partial H_b}{\partial x} + 2K_3 \sqrt{\frac{1.416}{H_b \gamma g}} W \sin\theta\right] \tag{B-20}$$

which is the goal of this exercise, an expression for the sediment transport rate that includes a wind-driven longshore current term.

It is noted that for the standard terms in the GENESIS formulation (the K_1 and K_2 terms), the wave height is raised to the 2.5 power, while it is only squared in the wind current term (the K_3 term). Thus, the influence of a wind-driven surf zone current would be expected to have greater relative importance at locations where the waves are generally small.

Appendix C: Comparison of Wave Data from NDBC Buoy 42035 and Co-Located WIS Hindcast

The WIS 1990-1999 Gulf of Mexico hindcast information is available from many stations other than those discussed in the main text, including stations that are co-located with NDBC wave buoys. The following text, excerpted from the unpublished WIS final report (Tracy 2002), gives detailed comparisons between data from NDBC Buoy 42035 (Lat 29.25 deg N, Long 94.41 deg W) (Figure 19) and the co-located WIS hindcast station. The comparison plots indicate excellent agreement between the hindcast results and the measurements.

Figure C1 shows a plot of the monthly bias for each month that had measurements available for wind speed, wave height, peak period, and mean period for NDBC 42035 and WIS from 1990 to 1999. A line connects each of these values, but notice that information is not available for all months. A positive bias indicates that the WIS value is greater than the measured value. Wind speed bias seems to average about 0.5 m/sec indicating very good agreement. Wave height bias at this location is always positive indicating that WIS wave heights are slightly higher than the measured wave heights. Maximum wave height biases tend to occur around January with these values being about 0.3 or 0.4 m. August bias values tend to be around 0.05 to 0.10 m indicating good agreement during the relative calm of this month. The peak period tends to show a positive bias when the wave height has a positive bias. This probably indicates a slight over-prediction in both wave height and peak period of some of the winter storm events. Mean period generally shows a positive bias with the average below 0.5 sec indicating very good agreement.

Figure C2 shows the scatter index for WIS and 42035 from 1990 to 1999. The scatter index is on a scale of 1 to 100 with 1 indicating very little scatter in the data and 100 indicating much scatter. Scatter index values in Figure C2 show a good scatter index of about 15 for the wind speeds. Scatter index for wave heights averages between 25 and 30 except for higher indices from 35 to 45 for January 1999, January and February 1997, and March 1994. Peak period shows a spike in the summer of 1995

probably from a problem with specification of the peak during a tropical event. Most of the rest of the scatter indices for peak period fall below 30 indicating good agreement. Mean period shows the same spike as the peak period, but most other values fall below 20 indicating very good agreement. Tropical Storm Dean had a path very close to this area at the end of July 1995, and Hurricane Erin made landfall on the Alabama coast around this same time.

Figures C3 through C6 show the regression results for WIS versus NDBC Buoy 42035. The mean wave heights shown with the magenta circles in Figure C3 show that most WIS wave heights at this location tend to be slightly high although all the 95 percent confidence bands incorporate the 45-deg line through the data. Points at 2.75 m and 3.0 m show that WIS wave heights are slightly low. These events could be attributed to tropical storms where WIS did not produce the peak wave of the event. It is possible that WIS missed some storm peaks since the WIS peak periods tend to be slightly low in the higher peak period range in Figure C4. This plot also depends on which peak is chosen in a two-peak situaation. The line of points at the lower end of the modeled axis stem from very low wave heights. Mean period results in Figure C5 show good agreement between WIS and NDBC Buoy 42035. WIS shows an over-prediction of mean period for WIS values above 12 sec. Directional results shown in Figure C6 show a consistent bias of about 20 deg for directions 60 to 240 deg. An example of this would be a WIS direction of 75 deg corresponds to 100 deg for NDBC Buoy 42035. Figure C6 shows the best agreement in wave directions that are coming from offshore.

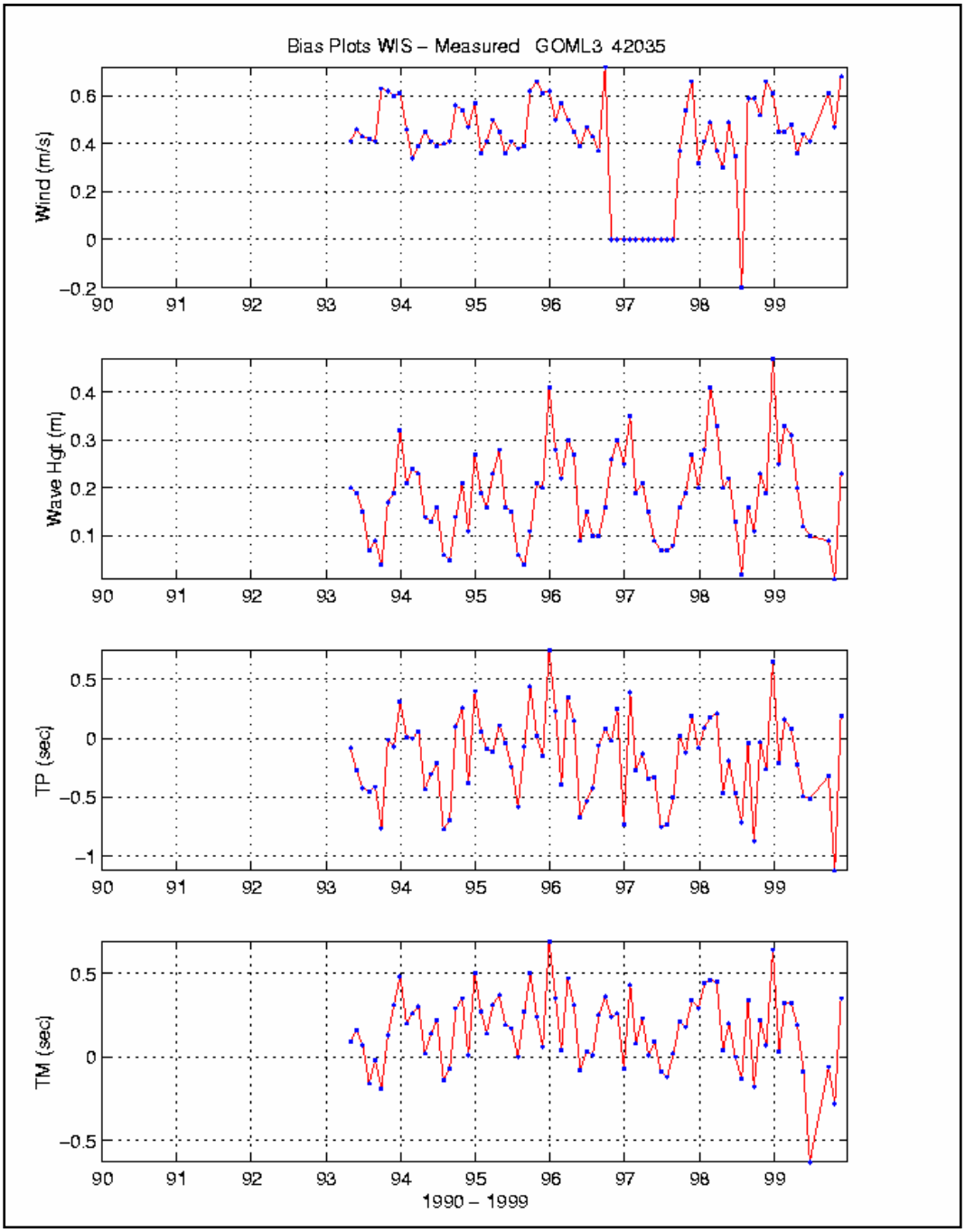

Figure C1. 1990-1999 monthly bias results for comparison of WIS and NDBC Buoy 42035.

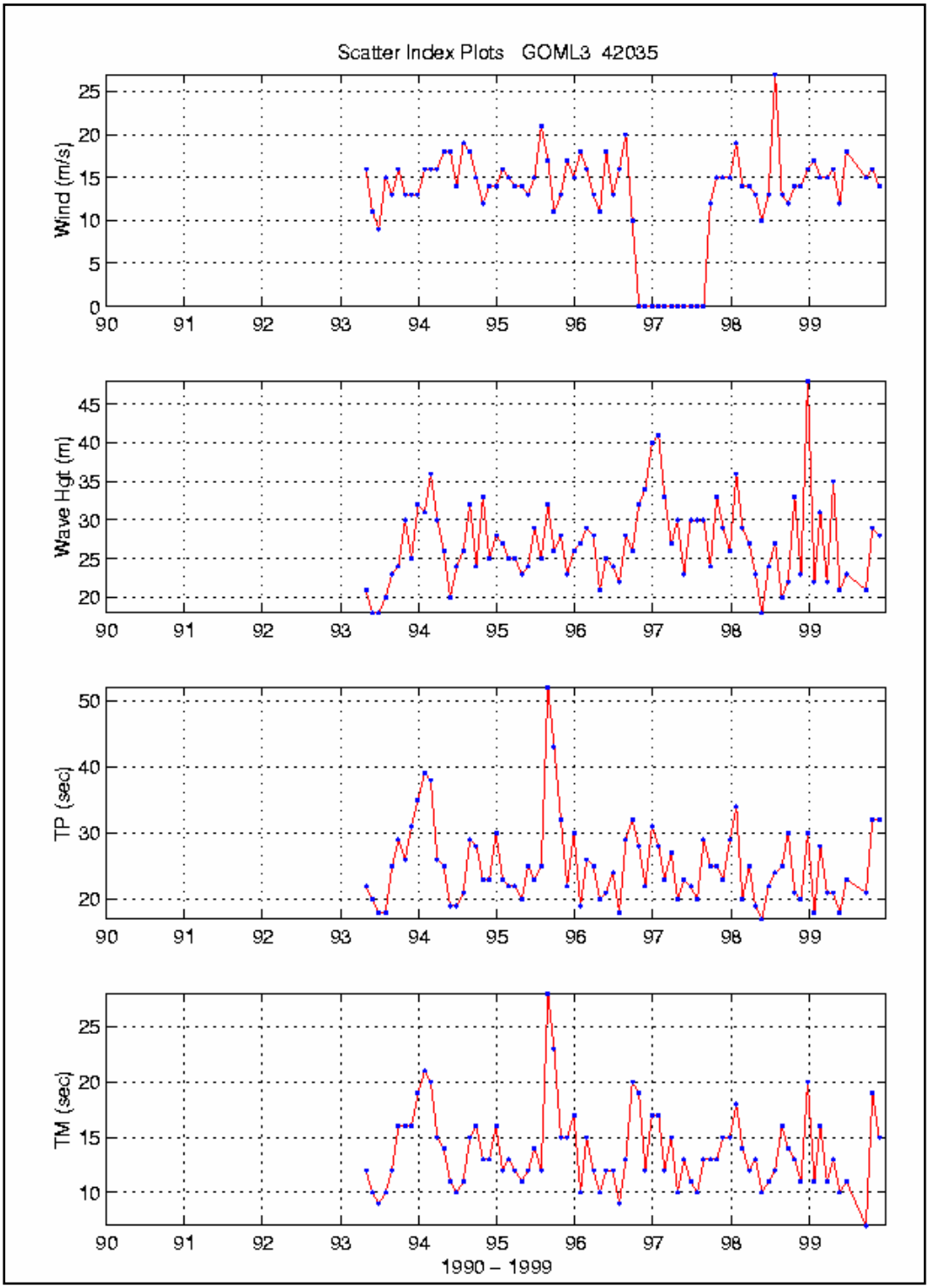

Figure C2. 1990-1999 monthly scatter index plots for comparison of WIS and NDBC Buoy 42035.

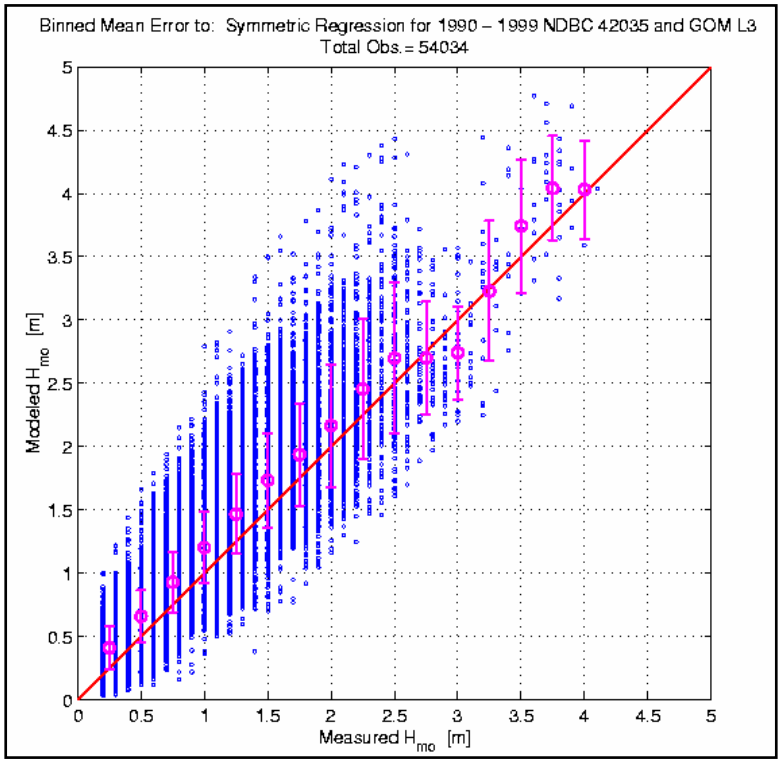

Figure C3. Symmetric regression for 1990-1999 WIS and NDBC Buoy 42035 wave heights.

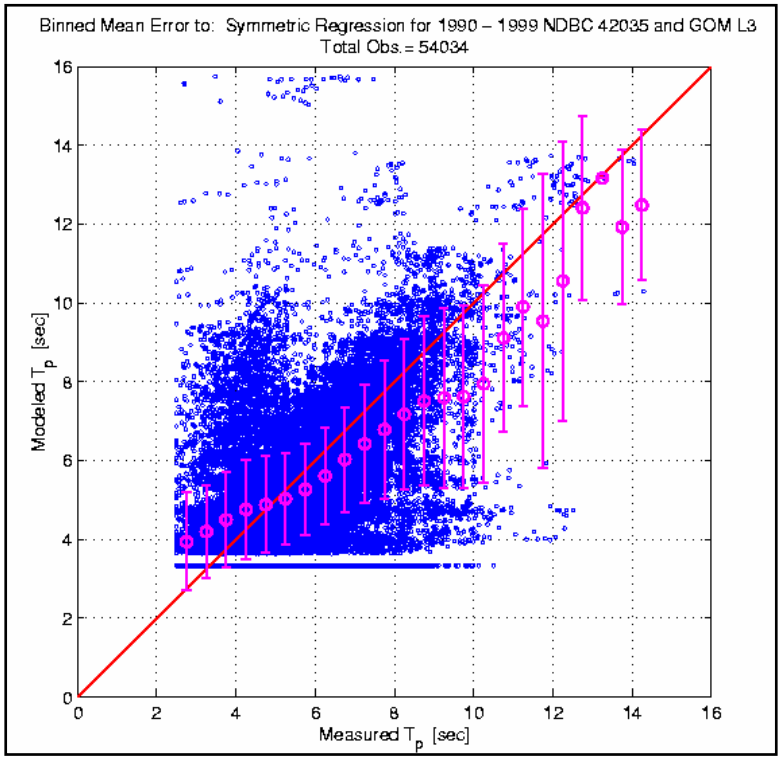

Figure C4. Symmetric regression for 1990-1999 WIS and NDBC Buoy 42035 peak periods.

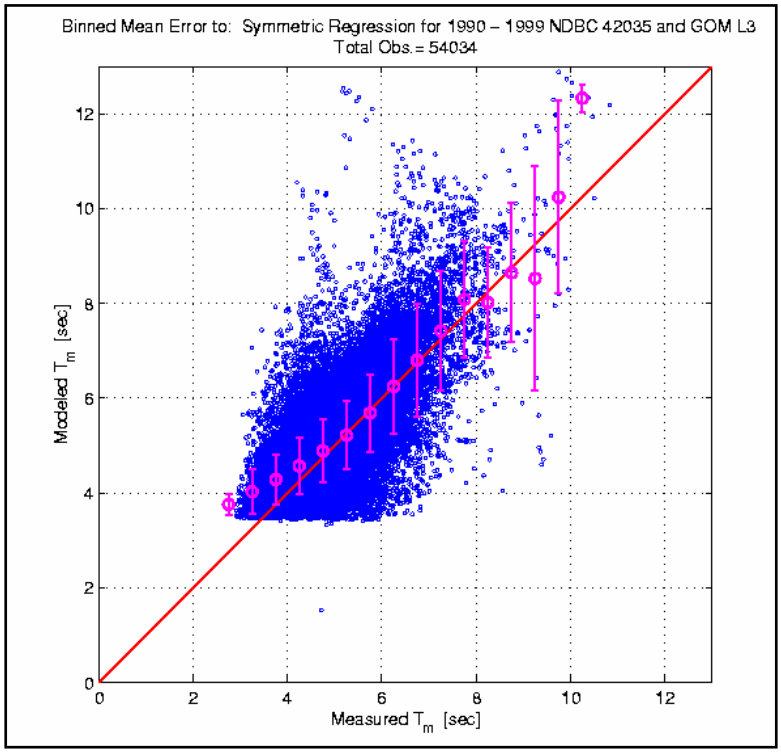

Figure C5. Symmetric regression for binned mean periods for WIS and NDBC Buoy 42035.

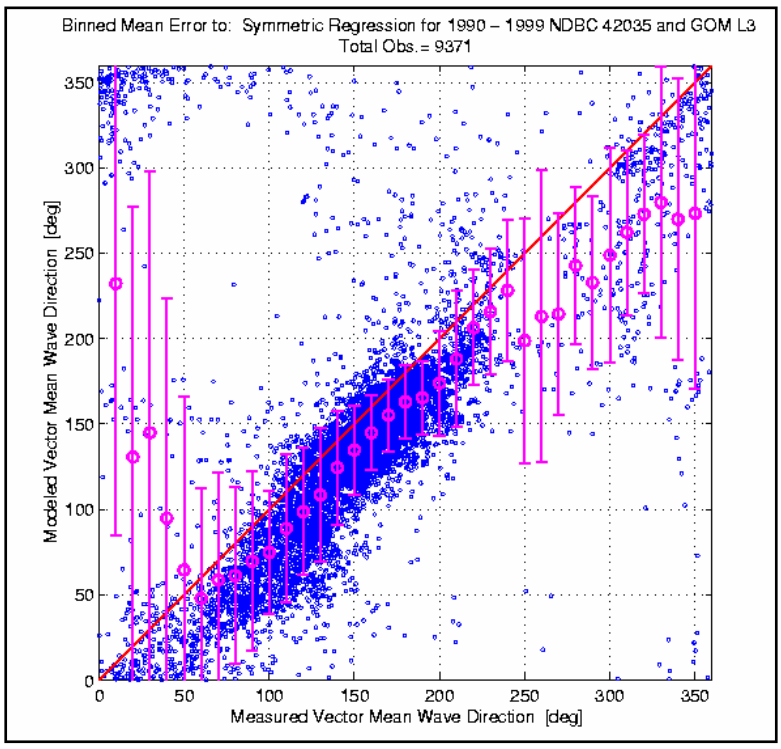

Figure C6. Binned mean error for comparison of WIS and NDBC Buoy 42035 vector mean wave direction for 1990-1999.

Figures C7 through C12 show the scatter plot comparisons of WIS mean wave direction at NDBC Buoy 42035. Figure C7 shows a scatter plot of mean wave directions for waves above 2m. Only 2.6 percent of the waves at this location fall in this category. Agreement is generally good with some waves in the 2- to 2.5-m category showing the most scatter. Larger waves tend to show excellent directional agreement. Figure C8 for waves greater 1.5 m but less than or equal to 2 m mean directions show excellent agreement from about 150 to 200 deg. In other cases, WIS results are generally about 20 deg more northerly than the buoy results. Figure C9 for mean wave directions for waves greater than 1 m but less than or equal to 1.5 m shows the same situations as Figure C8. Figures C10 and C11 also show similar behavior with more deviations in the northeast direction quadrant. This could indicate that WIS is not catching close to shore situations. The regression line summary plot in Figure C12 summarizes the results for mean wave direction for Figures C7 through C11. This shows the general trend for WIS results to be smaller (indicating more northerly WIS directions) than the NDBC Buoy 42035 mean direction results.

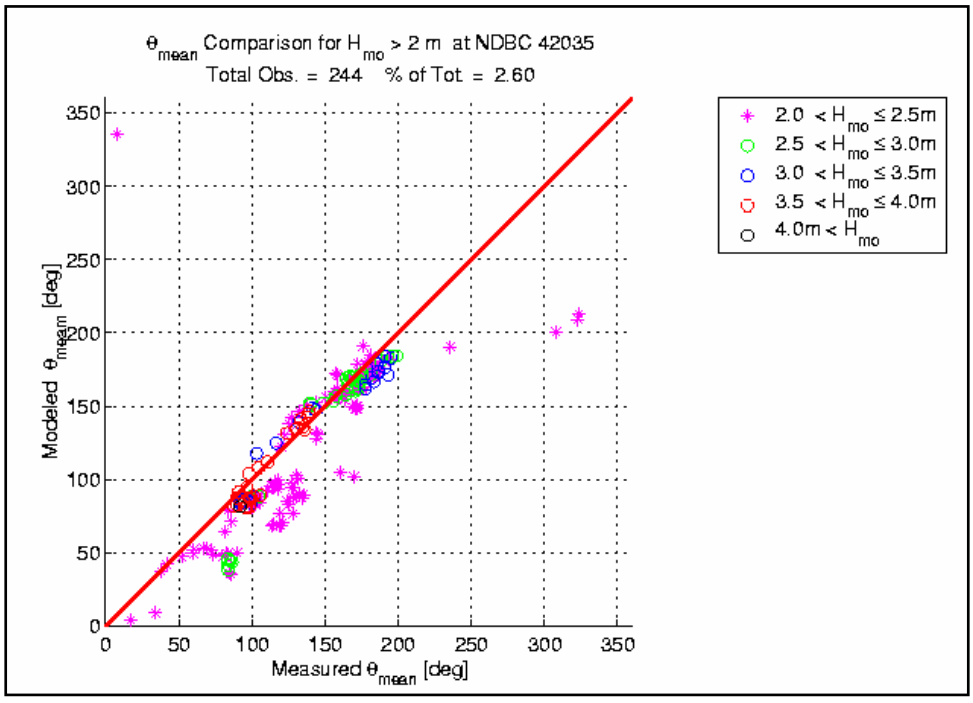

Figure C7. Scatter plot showing mean wave direction for waves above 2 m for NDBC Buoy 42035

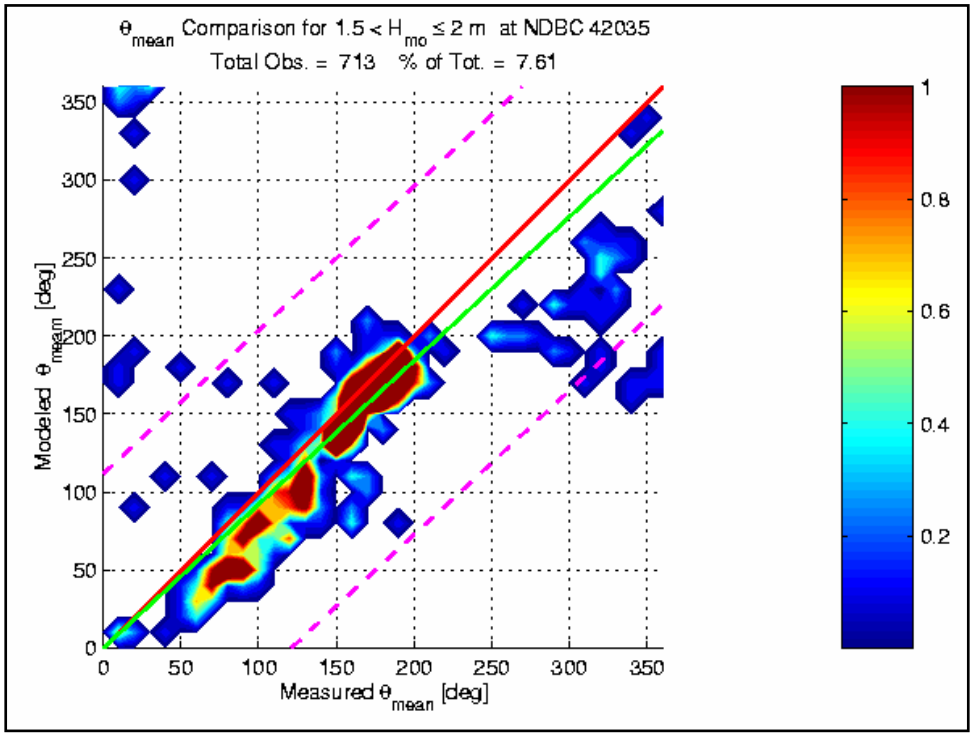

Figure C8. Mean wave direction contoured scatter plot for waves greater than 1.5 m but less than or equal to 2 m at NDBC Buoy 42035 and WIS.

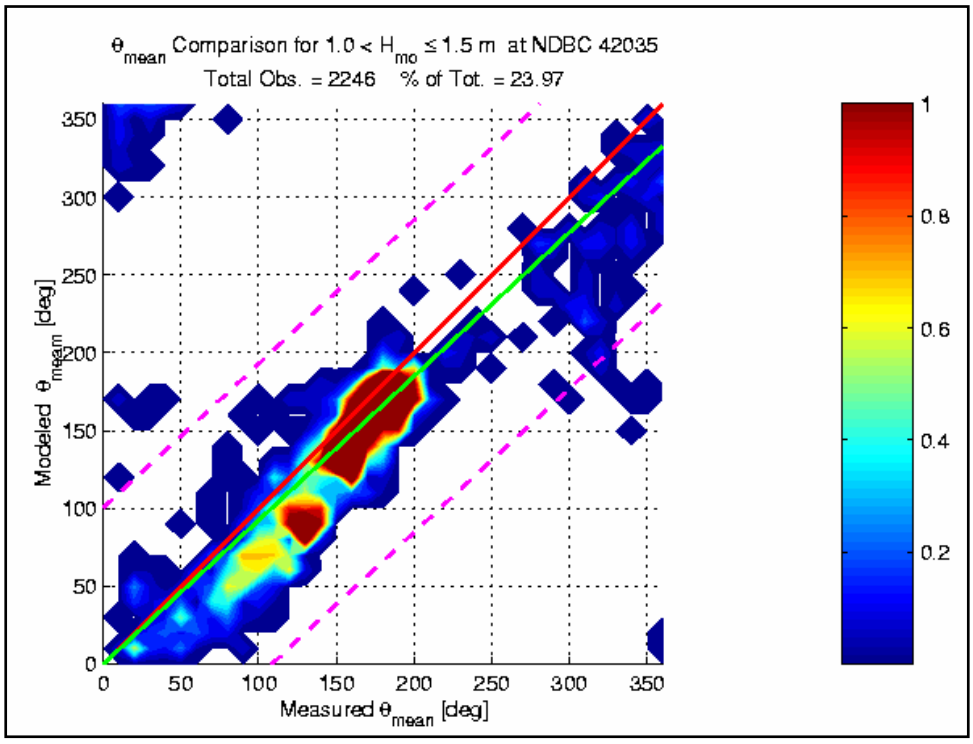

Figure C9. Contoured scatter plot comparison of mean wave direction for waves greater than 1 m but less than or equal to 1.5 m for NDBC Buoy 42035 and WIS.

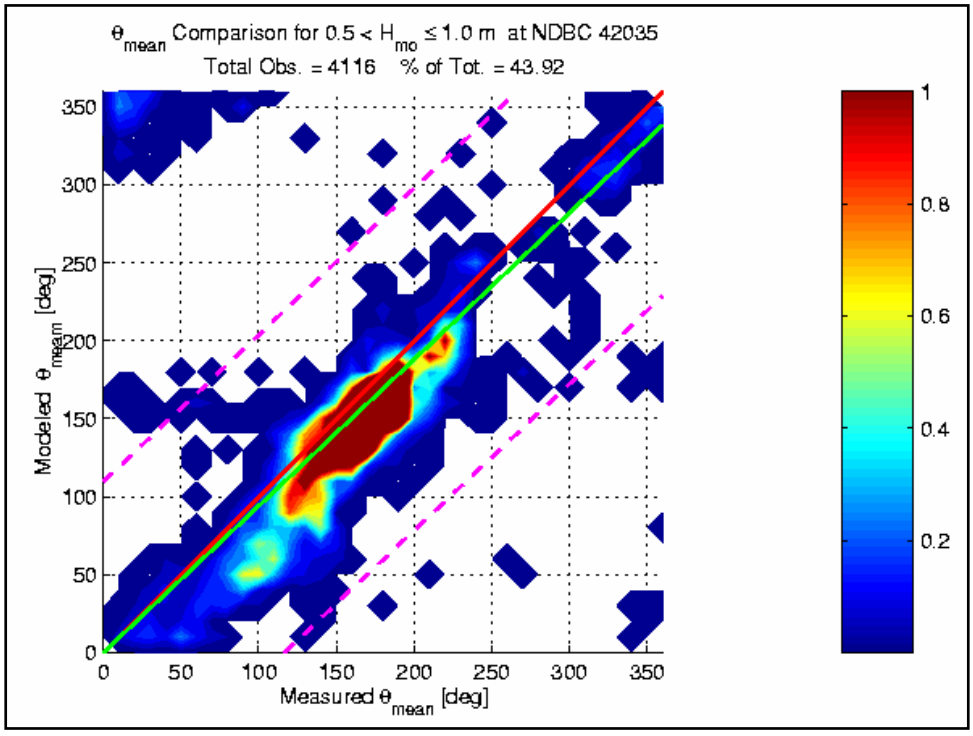

Figure C10. Contoured scatter plot of mean wave direction for waves greater than 0.5 m but less than or equal to 1 m for NDBC Buoy 42035 and WIS.

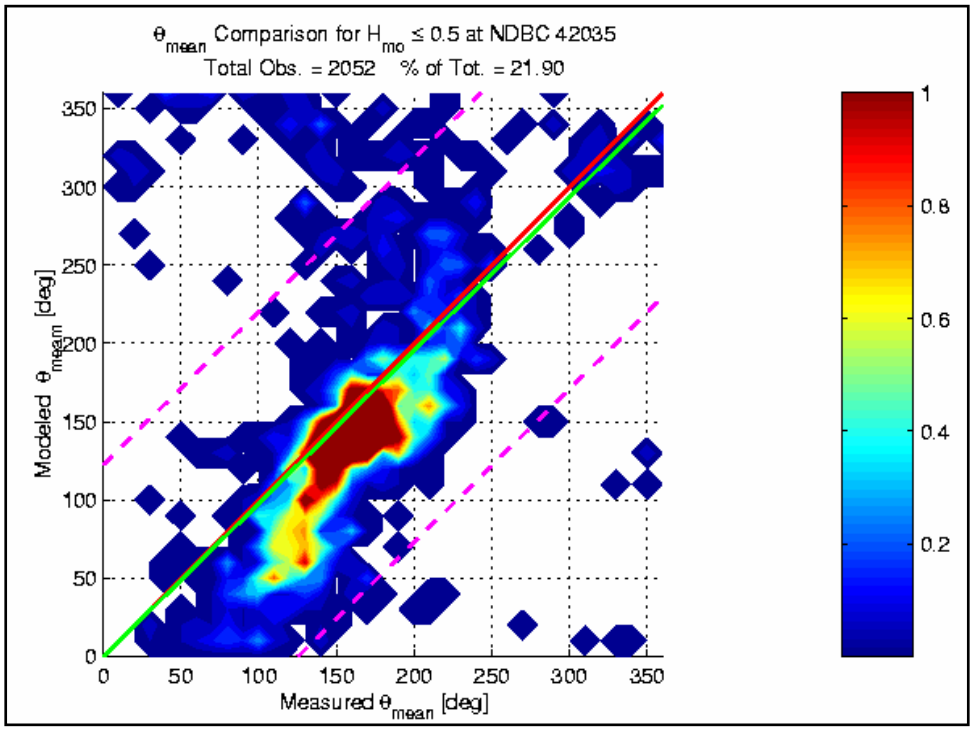

Figure C11. Contoured scatter plot for mean wave direction for waves less than or equal to 0.5 m for NDBC Buoy 42035 and WIS.

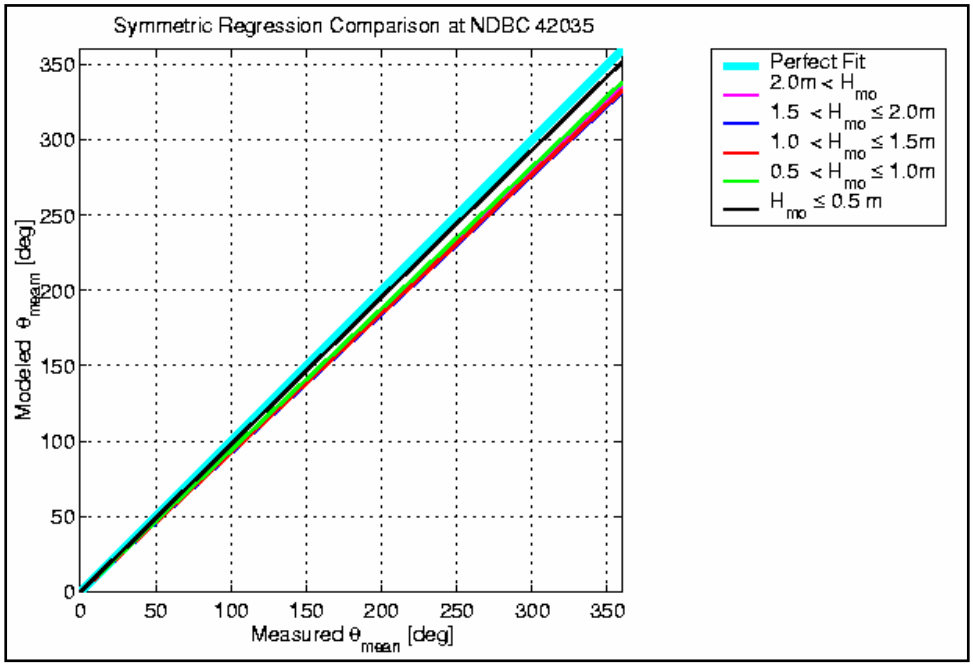

Figure C12. Symmetric regression lines for mean wave direction for NDBC Buoy 42035 and WIS using results from Figures C7 through Figure C11.

Figures C13 through C18 show the scatter plot results for peak period comparisons between WIS and NDBC Buoy 42035. These figures have the same format as the previous sets of scatter plots. Figure C13 showing peak period scatter for waves above 2 m shows excellent agreement. Only 2.08 percent of the waves fall into this category at this location. Figure C14 for waves above 1.5 m but less than or equal to 2 m shows a tendency for WIS peak period results to be a little less than a second high. Figure C15 for waves greater than 1 m but less than or equal to 1.5 m shows excellent agreement in peak period results. Waves above 0.5 m but less than or equal to 1 m in Figure C16 show that WIS results tend to be slightly low. This trend continues in Figure C17 for waves less than or equal to 0.5 m. Symmetric regression lines for Figures C13 through C17 showing peak period results for WIS and NDBC Buoy 42035 are summarized in Figure C18.

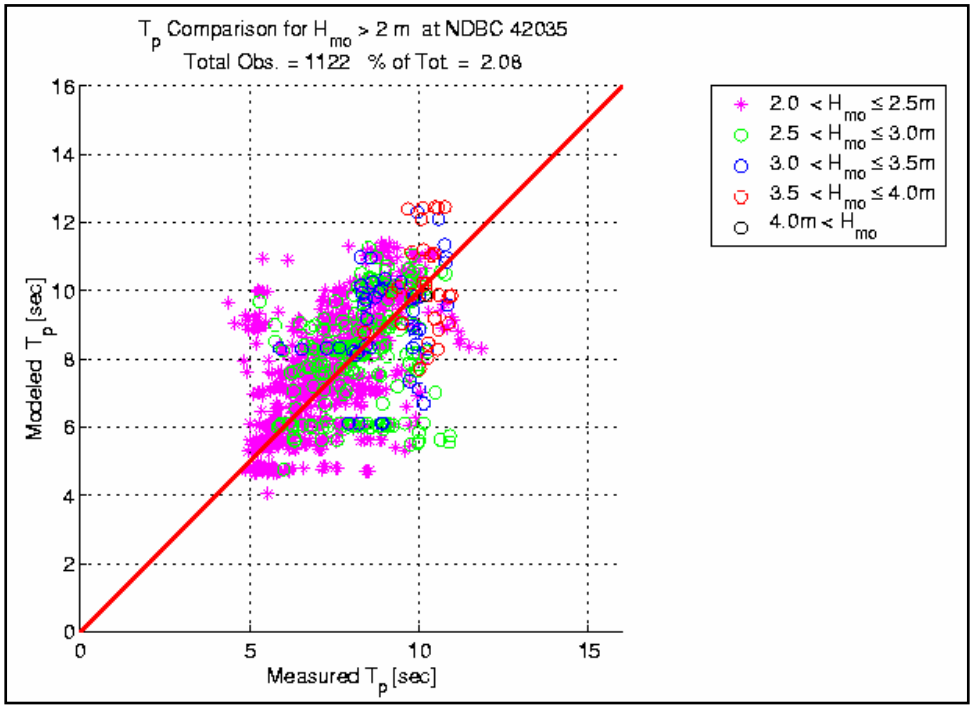

Figure C13. Scatter plot showing peak periods for waves above 2 m at NDBC Buoy 42035 and WIS.

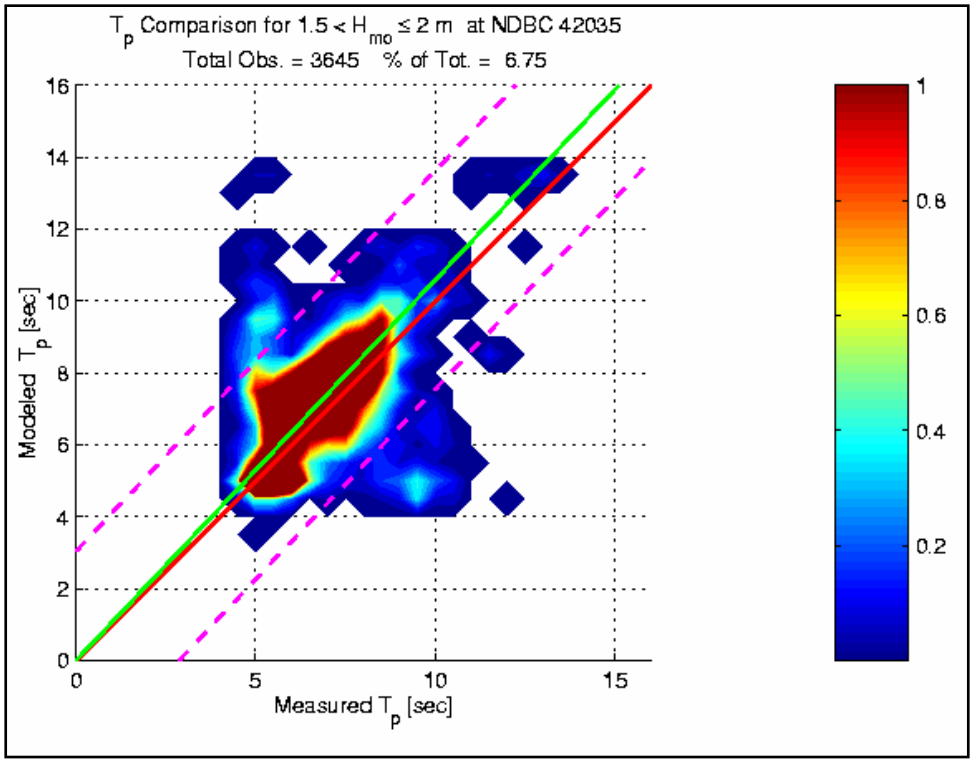

Figure C14. Contoured scatter plot showing peak periods for waves above 1.5 m but less than or equal to 2 m at NDBC Buoy 42035 and WIS.

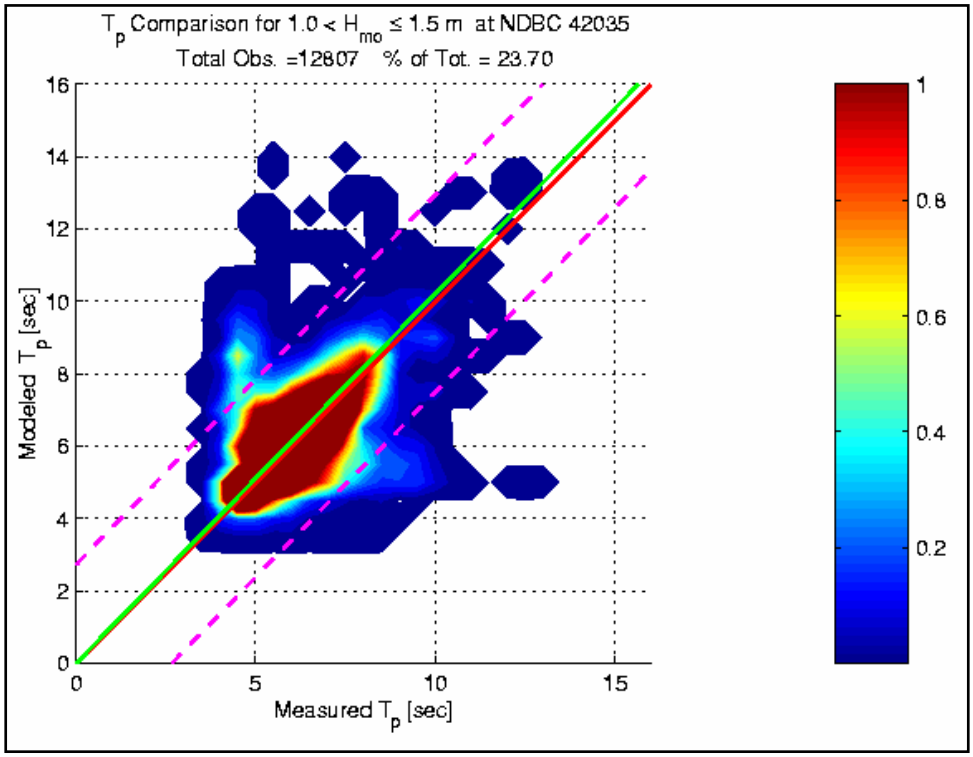

Figure C15. Peak period scatter plot for waves greater than 1 m but less than or equal to 1.5 m for NDBC Buoy 42035 and WIS.

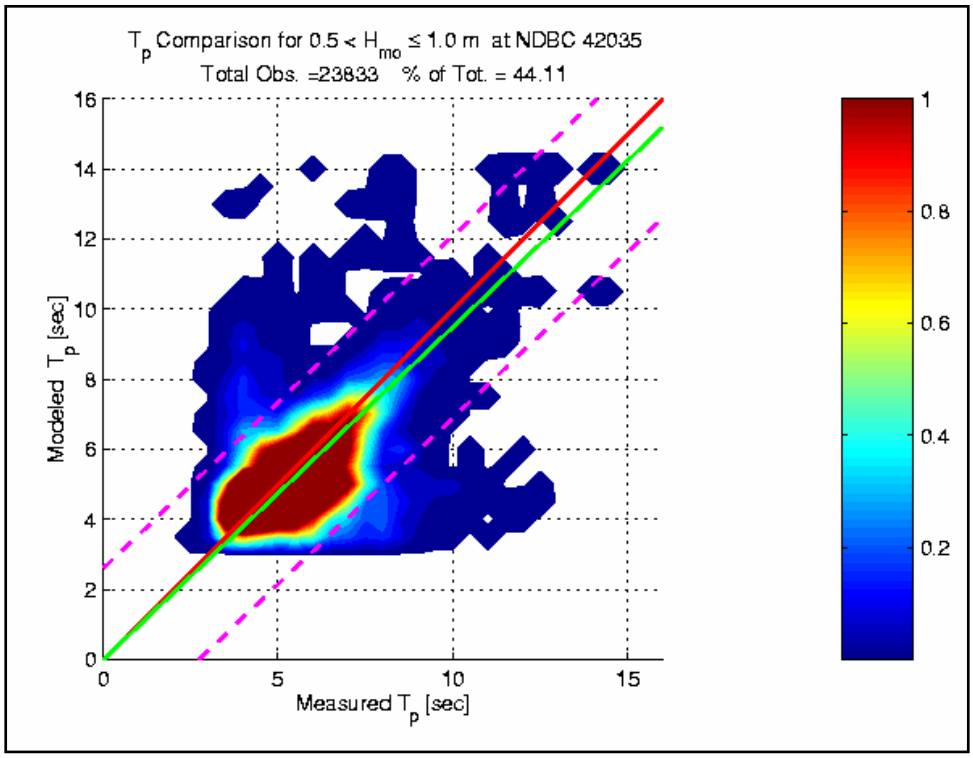

Figure C16. Peak period scatter plot for waves greater than 0.5 m but less than or equal to 1 m at NDBC Buoy 42035 and WIS.

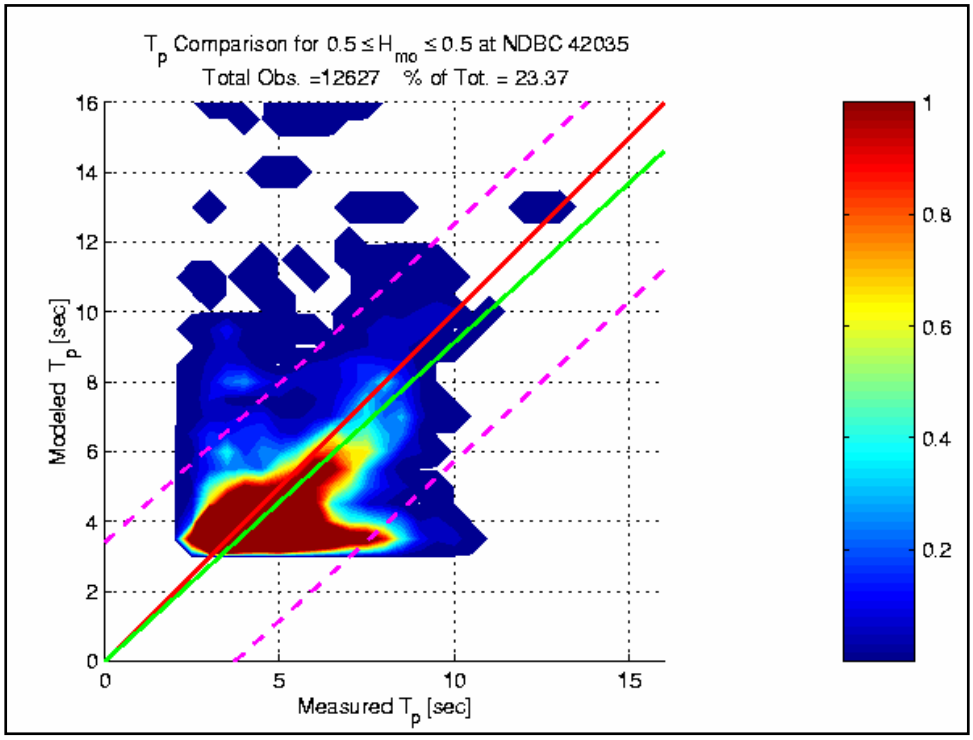

Figure C17. Contoured scatter plot for peak periods for waves greater than or equal to 0.5 m at NDBC Buoy 42035 and WIS.

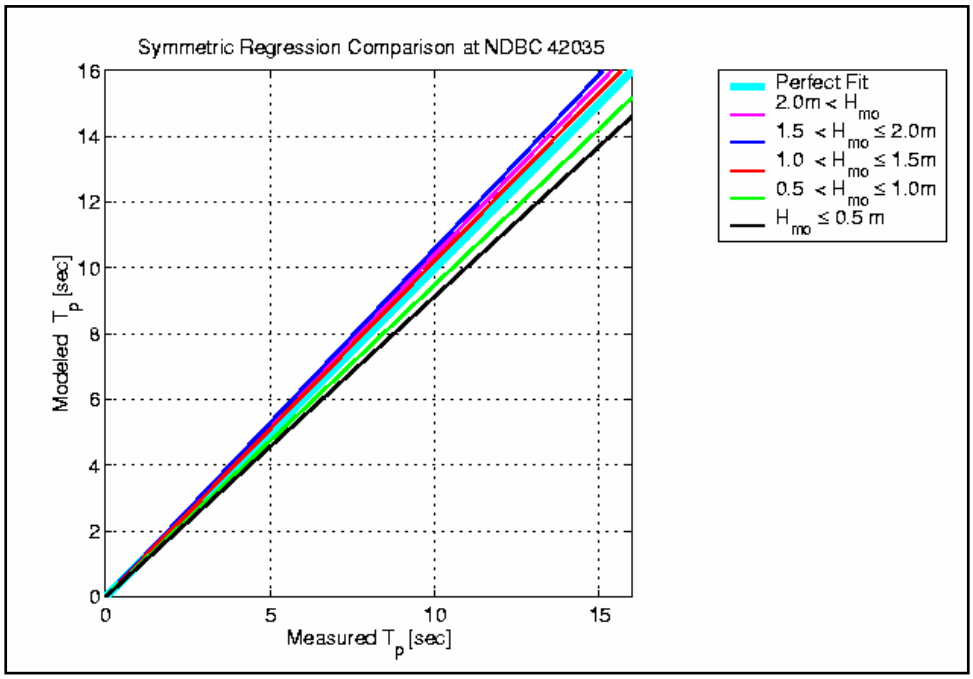

Figure C18. Symmetric regression lines for plots of peak period comparisons shown in Figures C13 through C17.

Figures C19 through C24 show the mean period scatter results for for WIS and NDBC Buoy 42035. Figure C19 showing mean period comparisons for waves above 2 m shows very good agreement. Waves in the 2- to 2.5-m category tend to show slightly higher mean periods than the buoy results. Again, only 2.08 percent of the waves at this location fall in this height category. Mean period results in Figures C20 and C21 show that WIS mean periods are slightly high. Figure C22 shows excellent agreement for waves greater than 0.5 m but less than or equal to 1 m. Figure C23 for waves less than or equal to 0.5 m also shows excellent agreement for mean periods. Figure C24 summarizes the mean period scatter regression lines for WIS and NDBC Buoy 42035 shown in Figures C19 through C23.

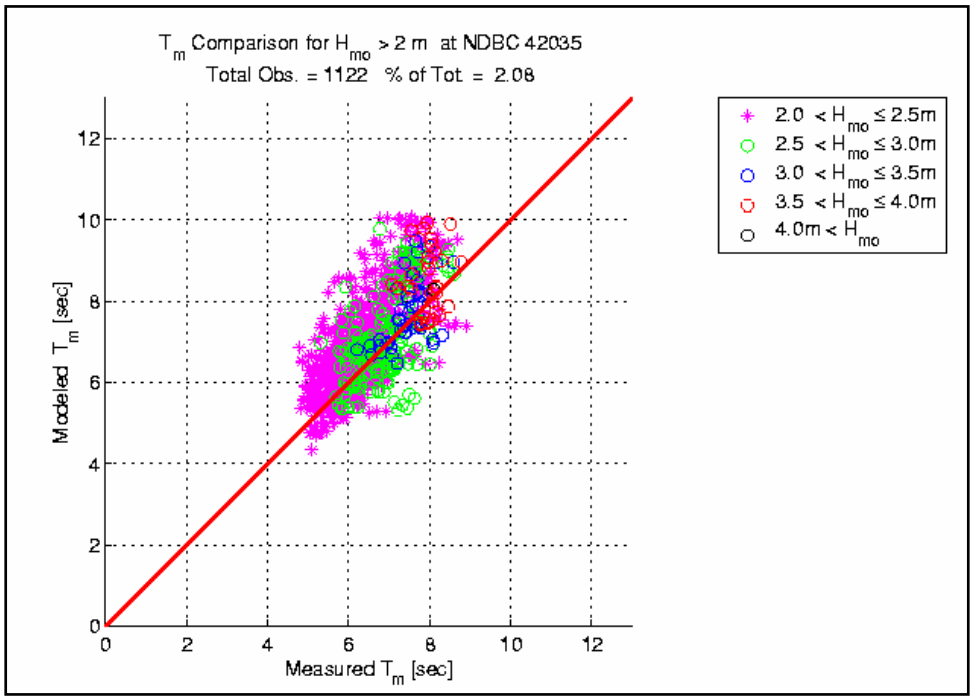

Figure C19. Mean period scatter plot for waves above 2 m at NDBC Buoy 42035 and WIS.

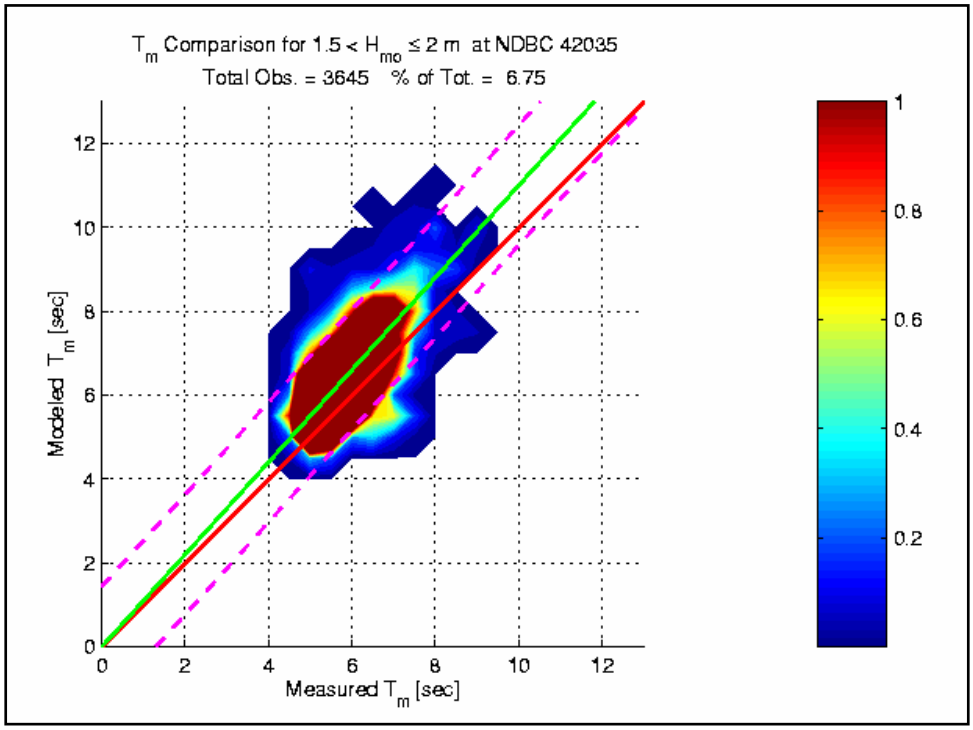

Figure C20. Contoured scatter plot of mean periods for waves less than or equal to 2 m but greater than 1.5 m for NDBC Buoy 42035 and WIS.

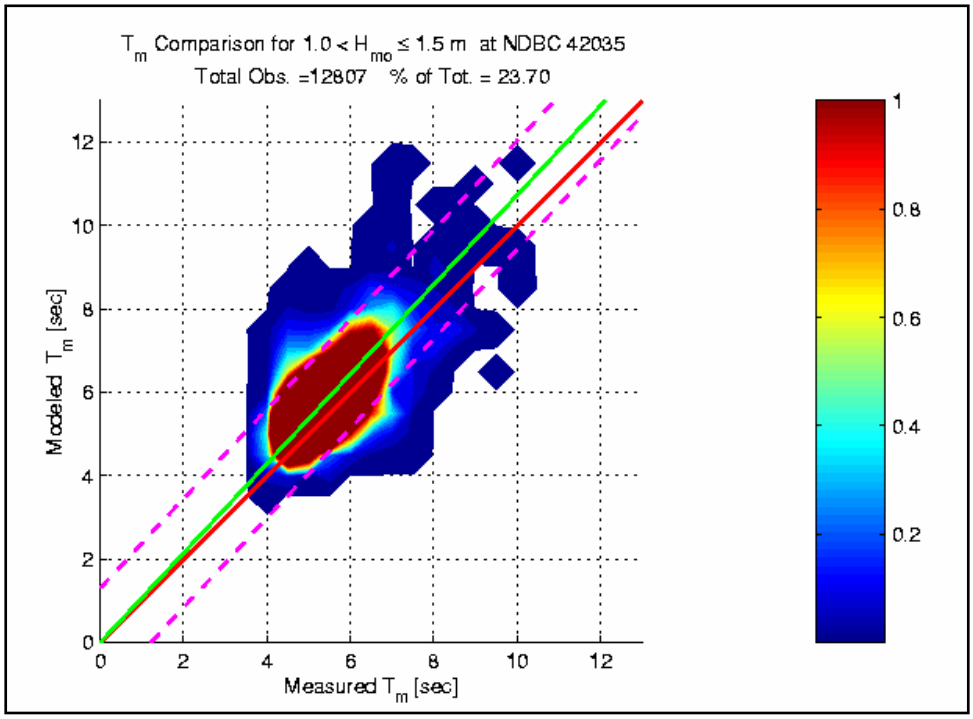

Figure C21. Contoured scatter plot for mean periods for waves above 1 m but less than or equal to 1.5 m for NDBC Buoy 42035 and WIS.

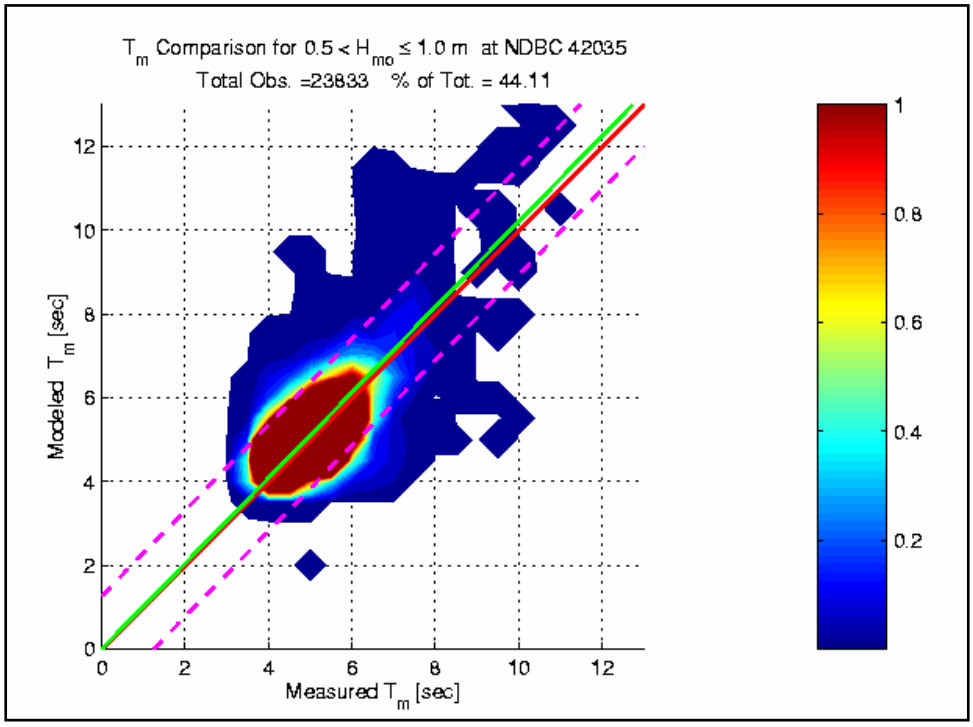

Figure C22. Contoured scatter plot for mean periods for waves greater than 0.5 m but less than or equal to 1 m for NDBC Buoy 42035 and WIS.

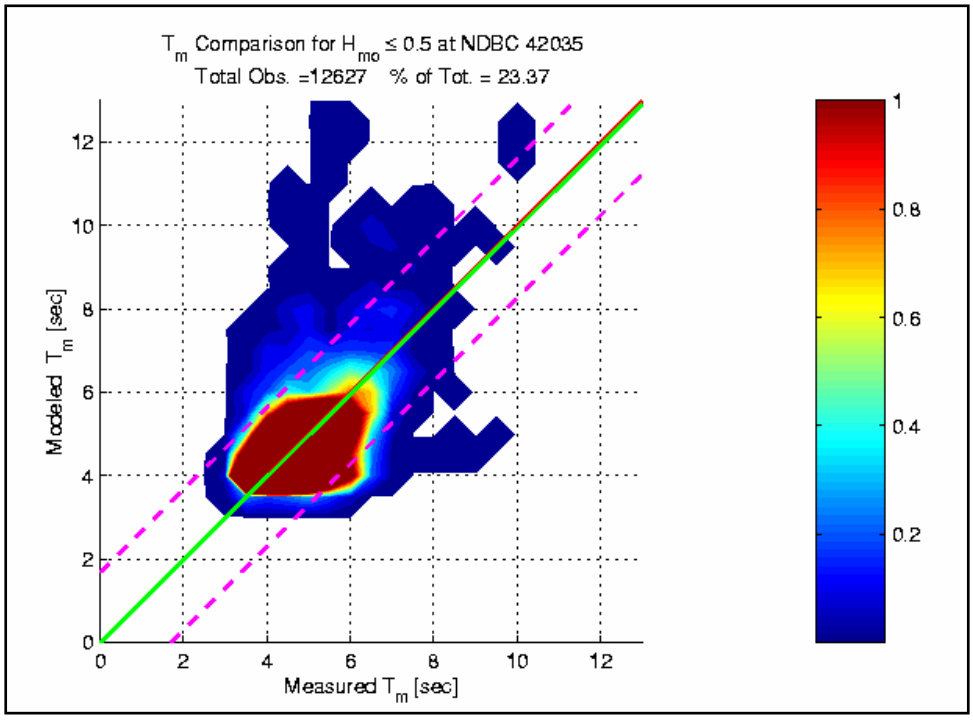

Figure C23. Contoured scatter plot for mean periods for wave less than or equal to 0.5 m for NDBC Buoy 42035 and WIS.

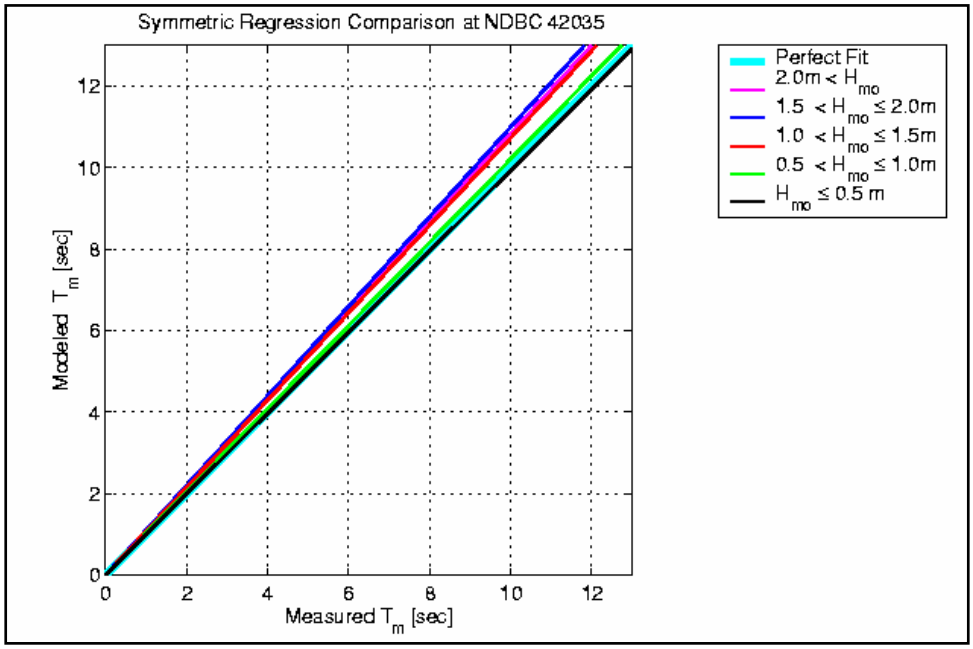

Figure C24. Symmetric regression lines for mean period scatter plots shown in Figures C19 through C23 for NDBC Buoy 42035 and WIS.

Appendix D: SBEACH Calibration Plots

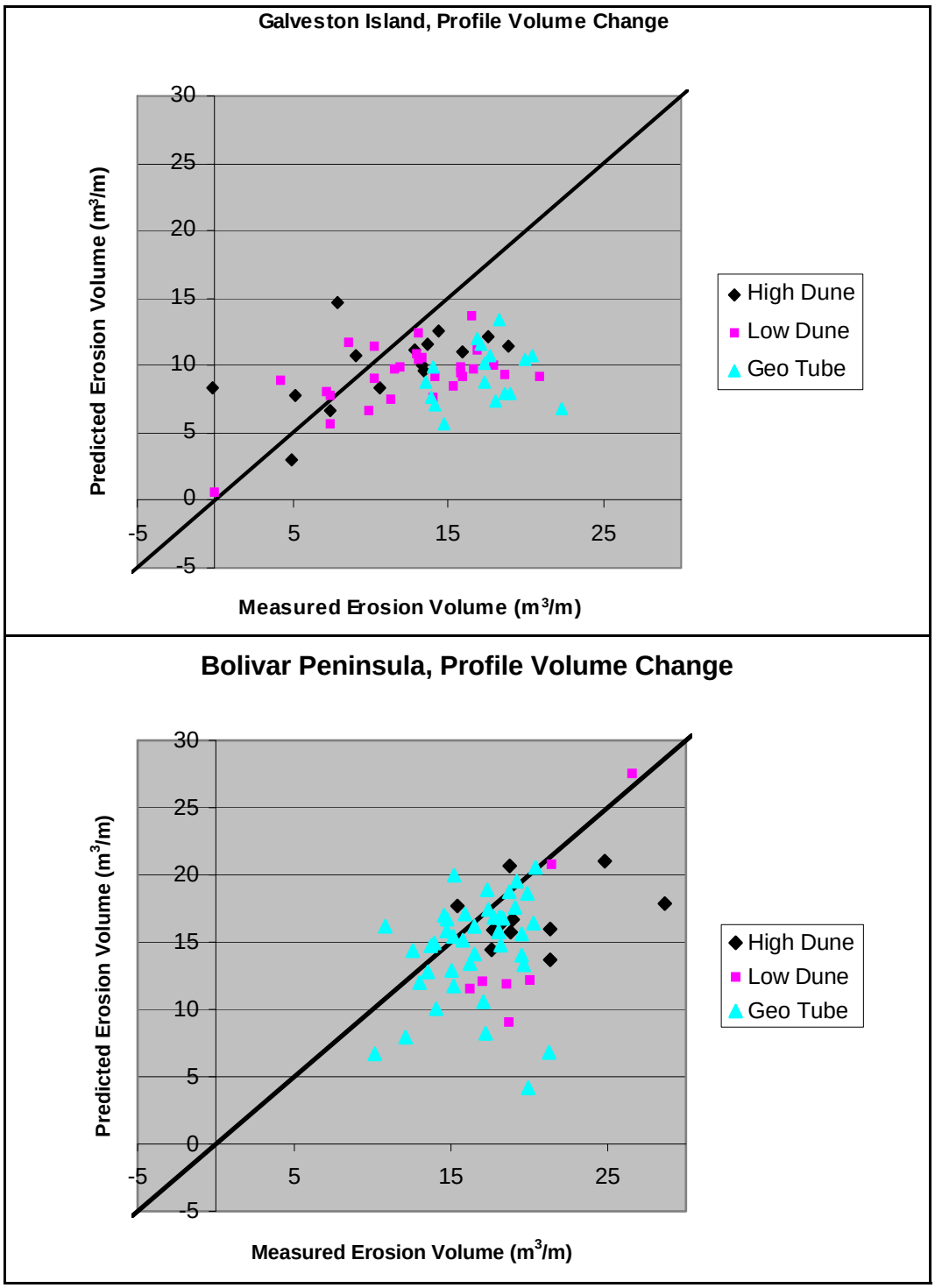

Figure D1. Scatterplot of profile volume changes for Galveston Island (top) and Bolivar Peninsula (bottom).

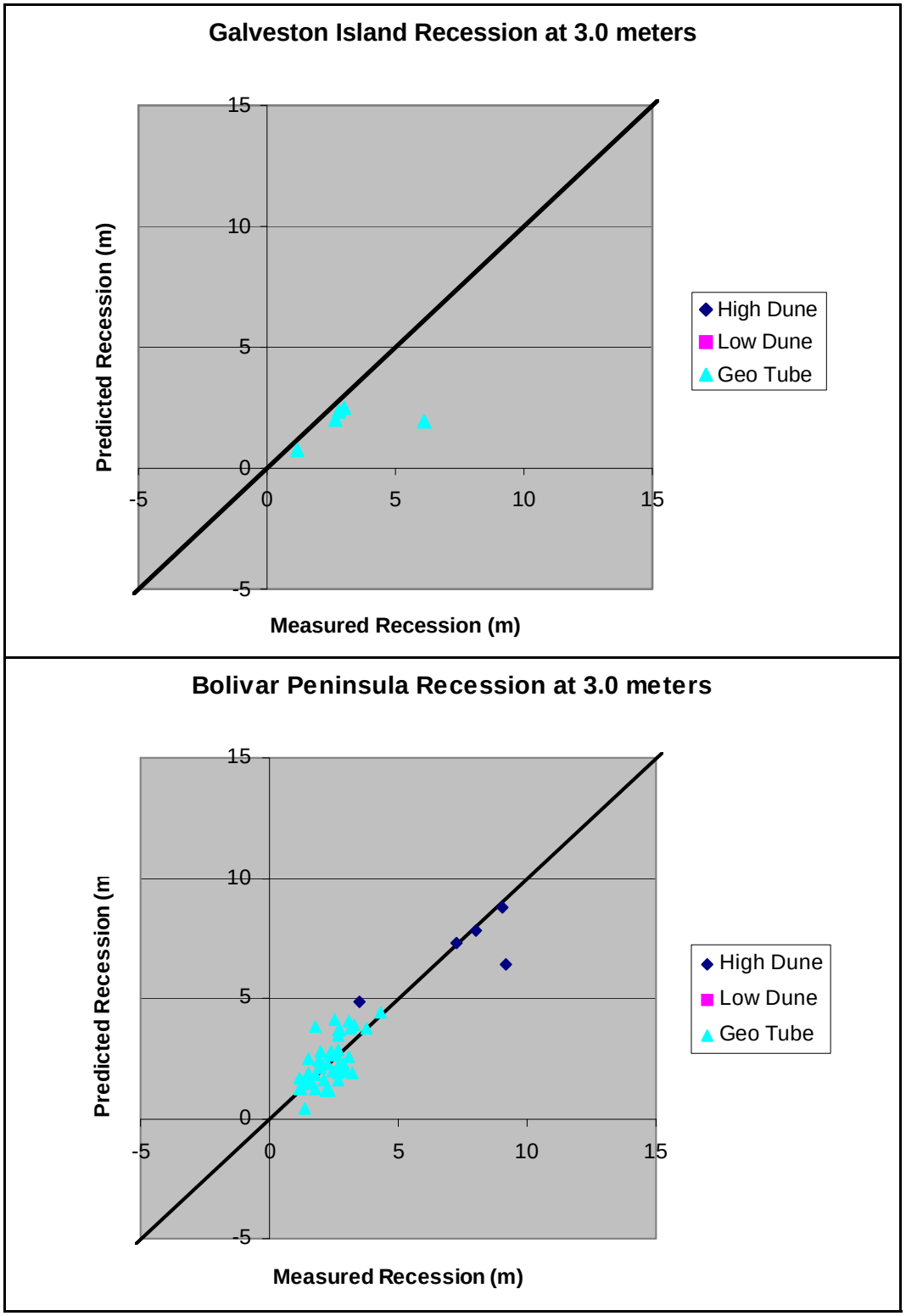

Figure D2. Scatterplot of 3-meter elevation erosion distances for Galveston Island (top) and Bolivar Peninsula (bottom).

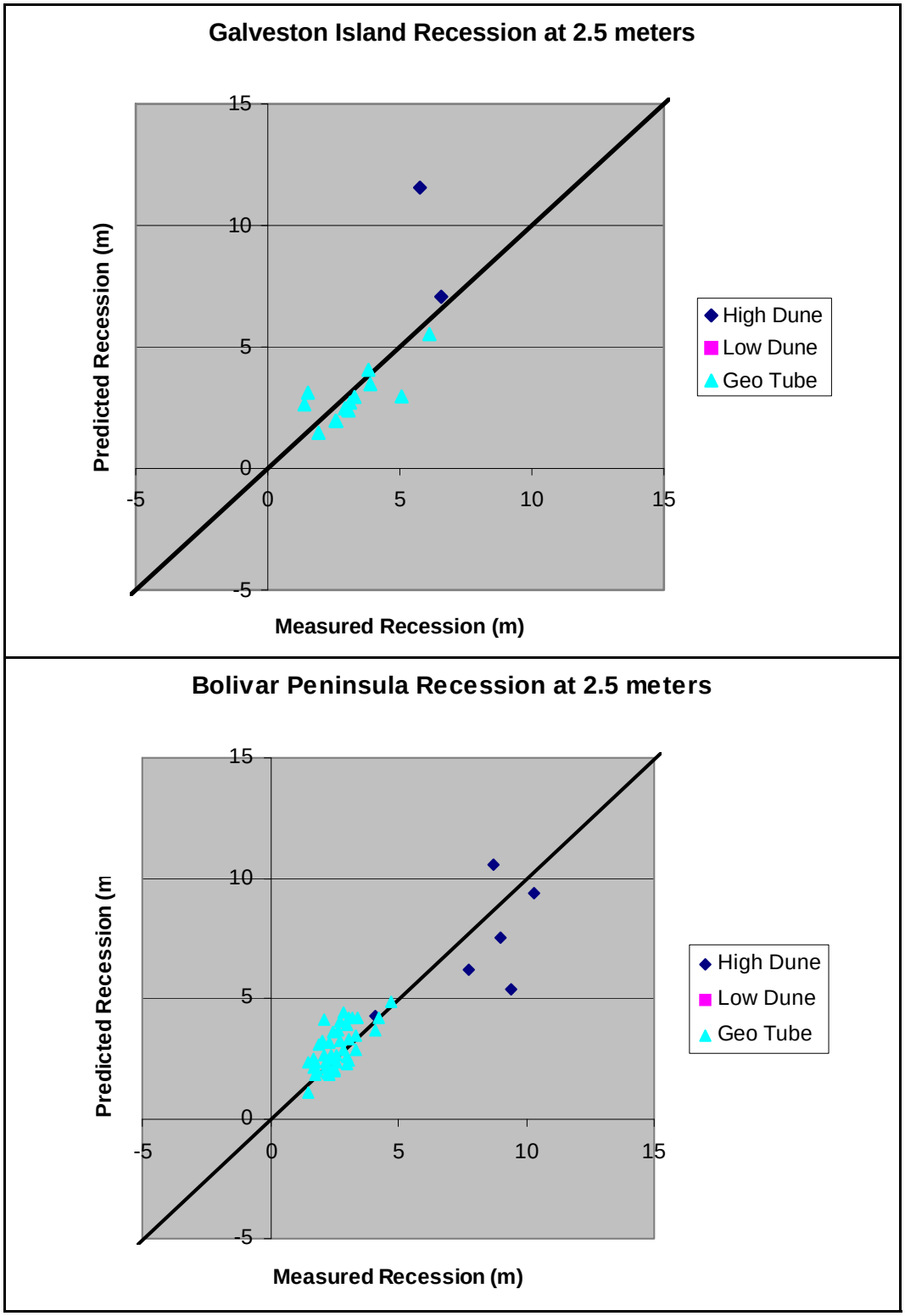

Figure D3. Scatterplot of 2.5-meter elevation erosion distances for Galveston Island (top) and Bolivar Peninsula (bottom).

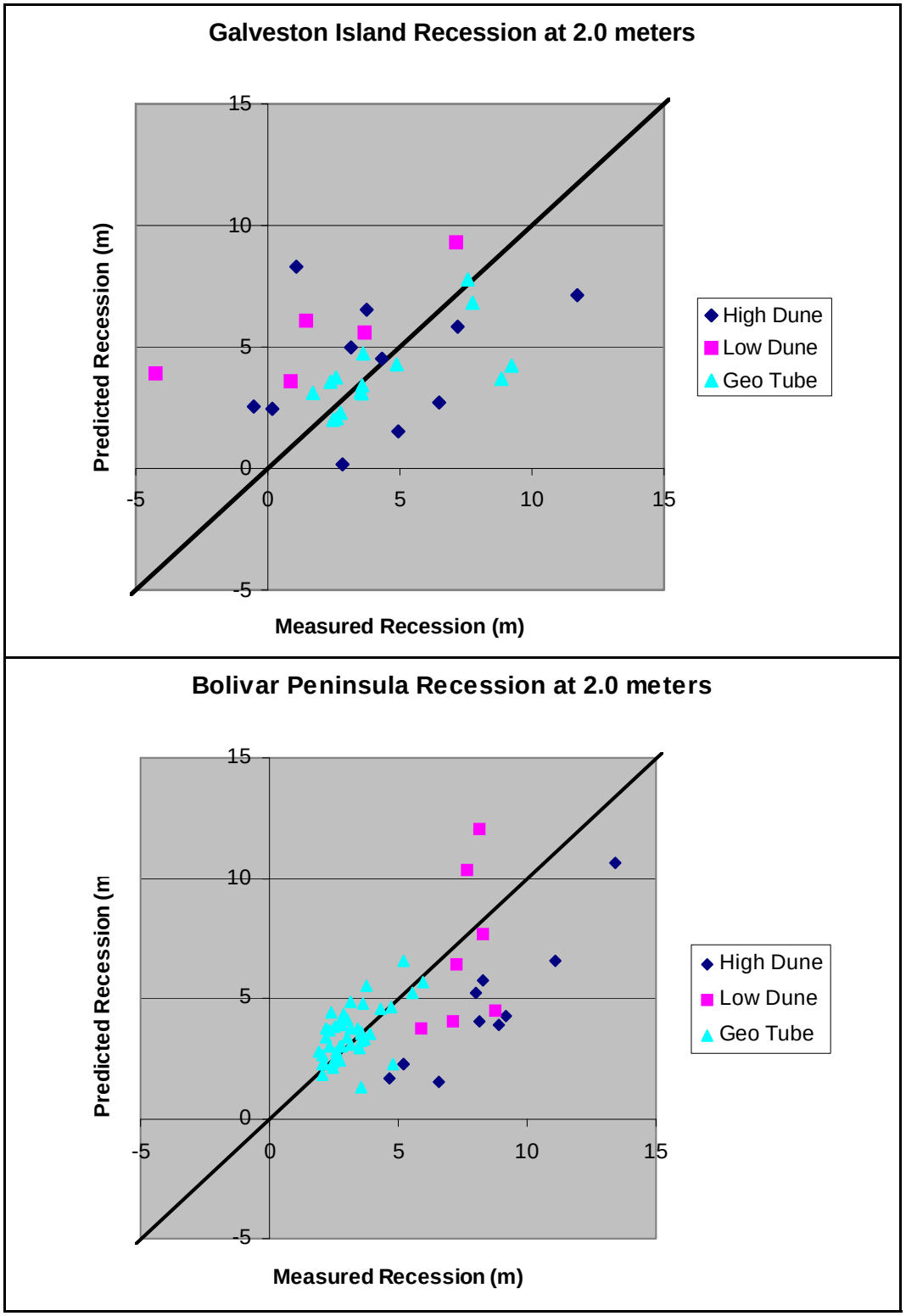

Figure D4. Scatterplot of 2-meter elevation erosion distances for Galveston Island (top) and Bolivar Peninsula (bottom).

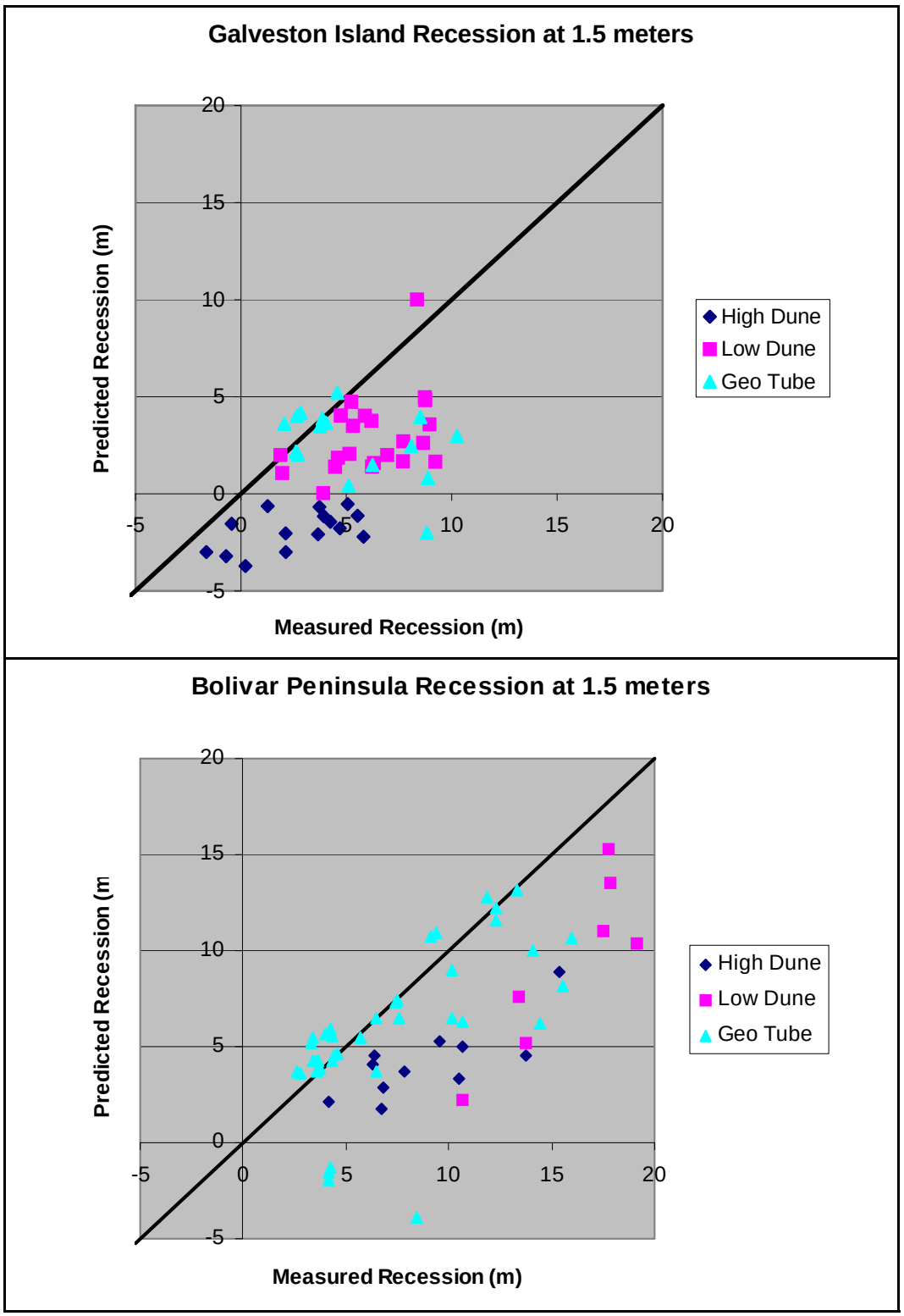

Figure D5. Scatterplot of 1.5-meter elevation erosion distances for Galveston Island (top) and Bolivar Peninsula (bottom).

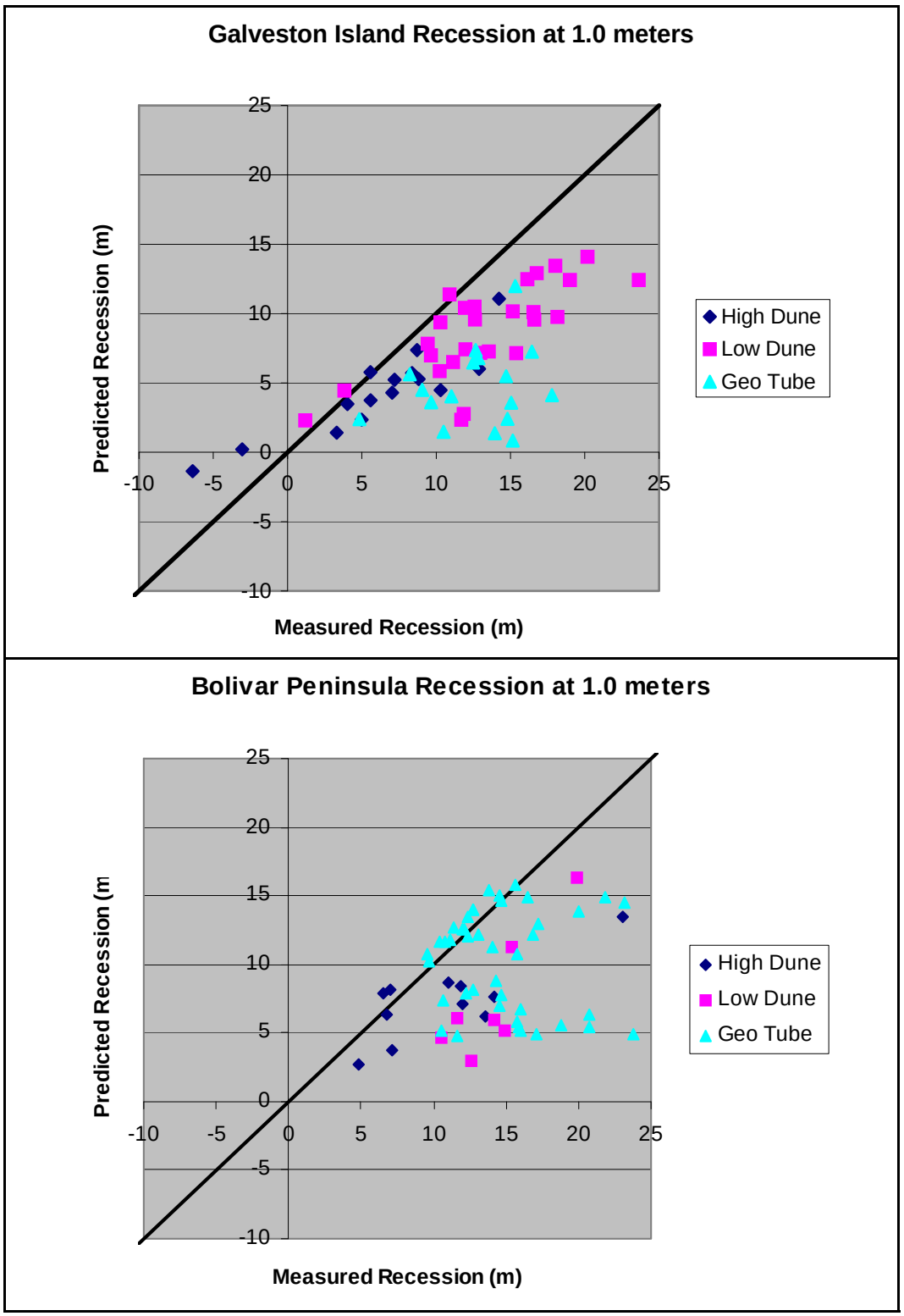

Figure D6. Scatterplot of 1-meter elevation erosion distances for Galveston Island (top) and Bolivar Peninsula (bottom).

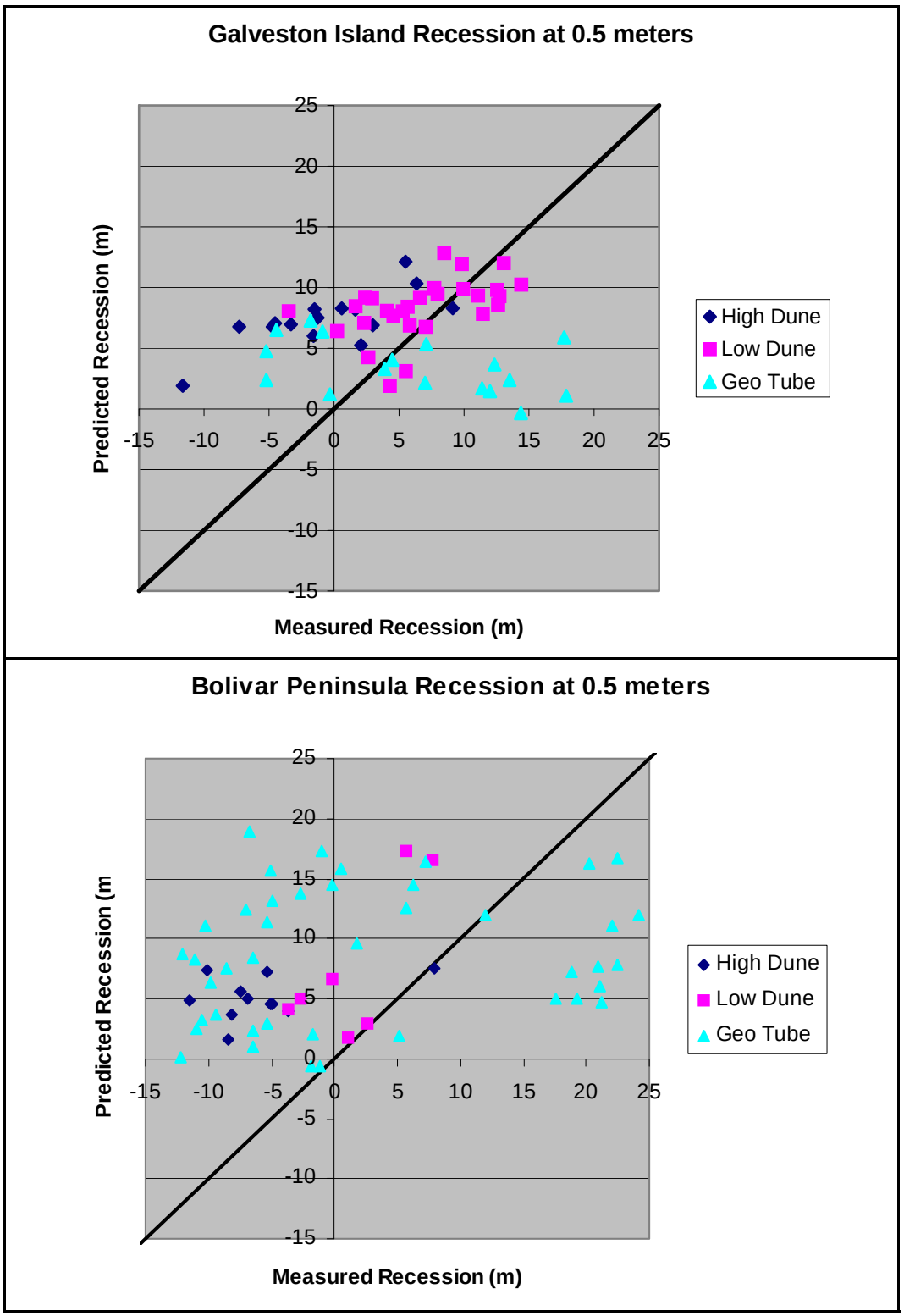

Figure D7. Scatterplot of 0.5-meter elevation erosion distances for Galveston Island (top) and Bolivar Peninsula (bottom).

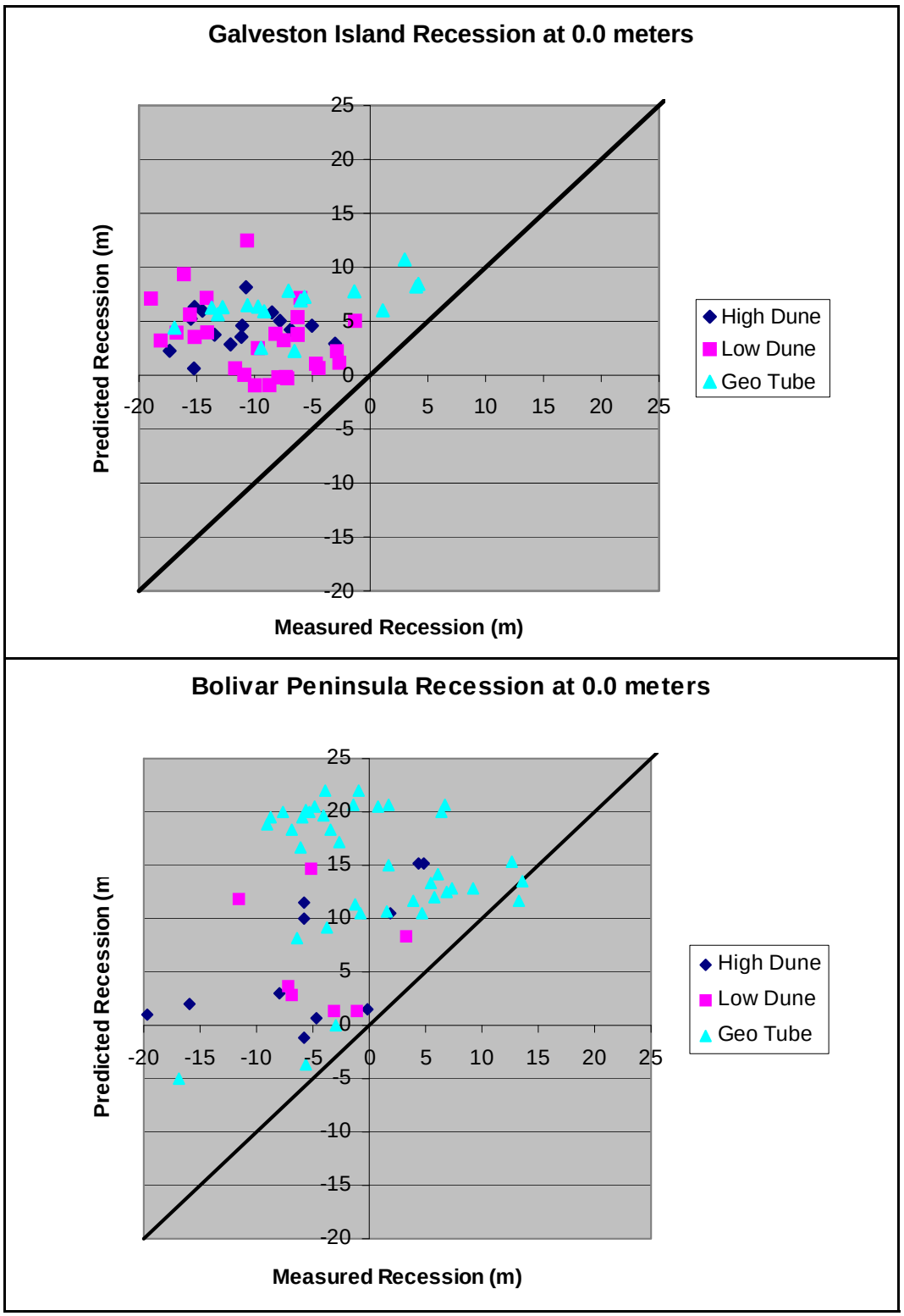

Figure D8. Scatterplot of 0.0-meter elevation erosion distances for Galveston Island (top) and Bolivar Peninsula (bottom).

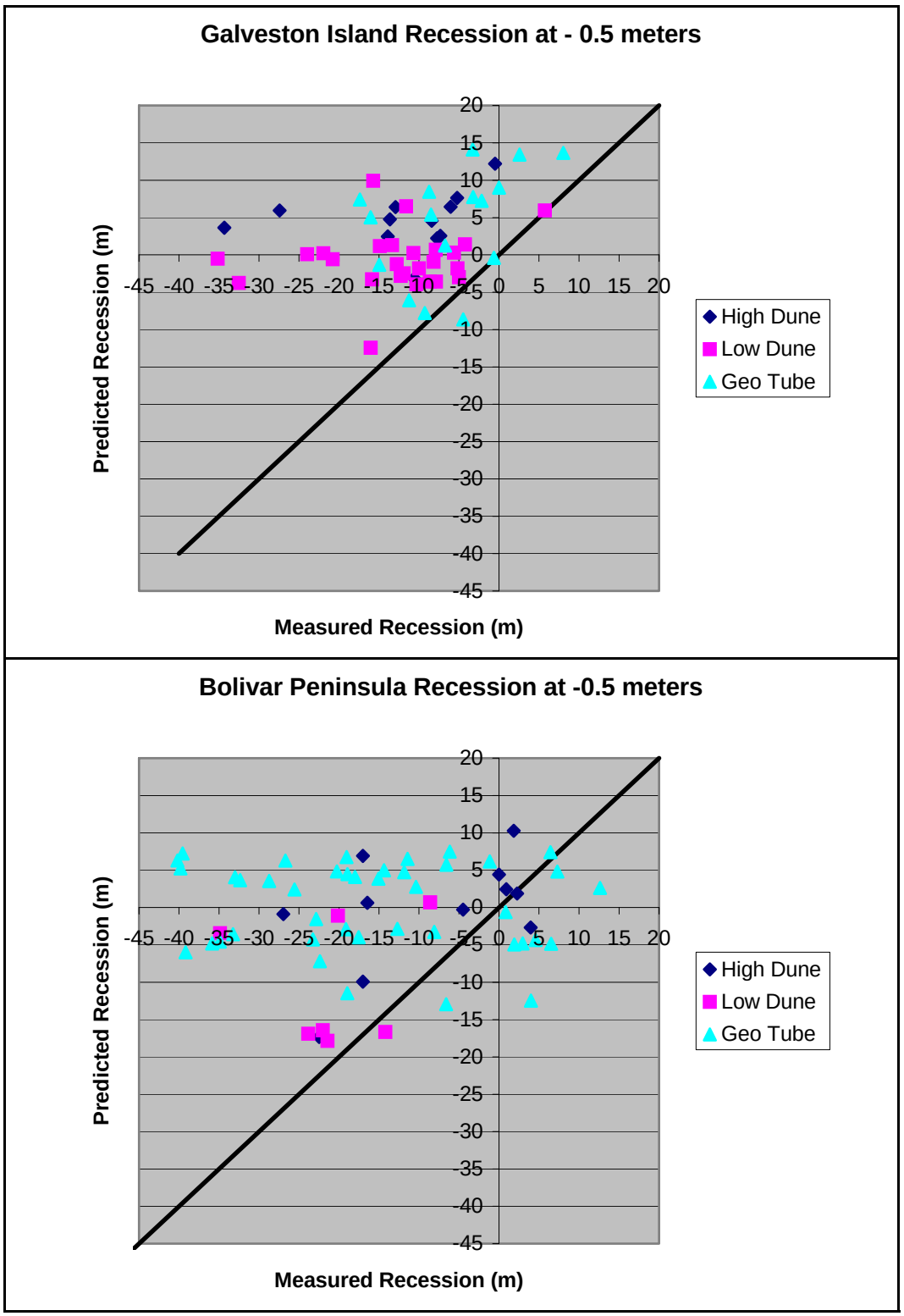

Figure D9. Scatterplot of –0.5-meter elevation erosion distances for Galveston Island (top) and Bolivar Peninsula (bottom).

REPORT DOCUMENTATION PAGE

Form Approved
OMB No. 0704-0188

1. REPORT DATE *(DD-MM-YYYY)*	2. REPORT TYPE	3. DATES COVERED *(From - To)*
August 2007	Final report	

4. TITLE AND SUBTITLE

Wave and Beach Processes Modeling for Sabine Pass to Galveston Bay, Texas, Shoreline Erosion Feasibility Study

5a. CONTRACT NUMBER

5b. GRANT NUMBER

5c. PROGRAM ELEMENT NUMBER

6. AUTHOR(S)

David B. King Jr.

5d. PROJECT NUMBER

5e. TASK NUMBER

5f. WORK UNIT NUMBER

7. PERFORMING ORGANIZATION NAME(S) AND ADDRESS(ES)

Coastal and Hydraulics Laboratory
U.S. Army Engineer Research and Development Center
3909 Halls Ferry Road
Vicksburg, MS 39180-6199

8. PERFORMING ORGANIZATION REPORT NUMBER

ERDC/CHL TR-07-6

9. SPONSORING / MONITORING AGENCY NAME(S) AND ADDRESS(ES)

U.S. Army Engineer District, Galveston
2000 Fort Point Road, Galveston, TX 77553

10. SPONSOR/MONITOR'S ACRONYM(S)

11. SPONSOR/MONITOR'S REPORT NUMBER(S)

12. DISTRIBUTION / AVAILABILITY STATEMENT

Approved for public release; distribution is unlimited.

13. SUPPLEMENTARY NOTES

14. ABSTRACT

This report describes the STWAVE/GENESIS modeling, the SBEACH modeling, and the related technical analysis that the U.S. Army Engineer Research and Development Center's Coastal and Hydraulics Laboratory has provided the U.S. Army Engineer District, Galveston, in support of their feasibility project: "Sabine Pass to Galveston Bay, Texas – Shoreline Erosion Feasibility Study." The main goal of this effort has been to set up and calibrate the numerical models so that they can provide a predictive capability that will be used to objectively evaluate alternative measures for beach restoration/protection projects within the study area. The predictive capabilities address both long-term performance, evaluated using GENESIS, and short-term storm-induced performance, evaluated using SBEACH.

The setup of the GENESIS model proved to be particularly challenging. As had been found by previous researchers, the use of standard procedures led to the model's prediction of an unrealistic net sediment transport direction on Galveston Island. However, a careful analysis of the important forcing functions, particularly the effects of the local wind field, led to the development of an appropriate alternative procedure which produced GENESIS results in agreement with observations.

15. SUBJECT TERMS

See reverse.

16. SECURITY CLASSIFICATION OF:			17. LIMITATION OF ABSTRACT	18. NUMBER OF PAGES	19a. NAME OF RESPONSIBLE PERSON
a. REPORT	b. ABSTRACT	c. THIS PAGE			19b. TELEPHONE NUMBER *(include area code)*
UNCLASSIFIED	UNCLASSIFIED	UNCLASSIFIED		163	

15. SUBJECT TERMS
Beach erosion
Beach fill design
Bolivar Peninsula, TX, shoreline
Galveston County, TX, shoreline
Galveston Island, TX, shoreline
GENESIS
Jefferson County, TX, shoreline
Numerical modeling
SBEACH
Sediment transport
Shoreline change
STWAVE